

CREATION OF A MODEL FOR INTERACTION OF BOTTOM-FIXED WIND TURBINES WITH SURFACE ICE FOR USE WITH COMMON SIMULATION CODES AWARD NO. DE-EE0005477

Ice Load Project Final Technical Report

U.S. Department of Energy

Document No.: DDRP0133

Date: 30 October 2014



IMPORTANT NOTICES AND DISCLAIMERS

1. Acknowledgment: "This report is based upon work supported by the U.S. Department of Energy under Award No. DE-EE0005477."
2. Disclaimer: "Any findings, opinions, and conclusions or recommendations expressed in this report are those of the author(s) and do not necessarily reflect the views of the Department of Energy"
3. Proprietary Data Notice: If there is any patentable material or protected data in the report, the recipient, consistent with the data protection provisions of the award, must mark the appropriate block in Section K of the DOE F 241.3, clearly specify it here, and identify them on appropriate pages of the report. Other than patentable material or protected data, reports must not contain any proprietary data (limited rights data), classified information, information subject to export control classification, or other information not subject to release. Protected data are specific technical data, first produced in the performance of the award, which are protected from public release for a period of time by the terms of the award agreement. Reports delivered without such notice may be deemed to have been furnished with unlimited rights, and the Government assumes no liability for the disclosure, reproduction, or use of such reports.
4. This document is intended for the sole use of the Customer as detailed on the front page of this document to whom the document is addressed and who has entered into a written agreement with the DNV GL entity issuing this document ("DNV GL"). To the extent permitted by law, neither DNV GL nor any group company (the "Group") assumes any responsibility whether in contract, tort including without limitation negligence, or otherwise howsoever, to third parties (being persons other than the Customer), and no company in the Group other than DNV GL shall be liable for any loss or damage whatsoever suffered by virtue of any act, omission or default (whether arising by negligence or otherwise) by DNV GL, the Group or any of its or their servants, subcontractors or agents. This document must be read in its entirety and is subject to any assumptions and qualifications expressed therein as well as in any other relevant communications in connection with it. This document may contain detailed technical data which is intended for use only by persons possessing requisite expertise in its subject matter.
5. This document is protected by copyright and may only be reproduced and circulated in accordance with the Document Classification and associated conditions stipulated or referred to in this document and/or in DNV GL's written agreement with the Customer. No part of this document may be disclosed in any public offering memorandum, prospectus or stock exchange listing, circular or announcement without the express and prior written consent of DNV GL. A Document Classification permitting the Customer to redistribute this document shall not thereby imply that DNV GL has any liability to any recipient other than the Customer.
6. This document has been produced from information relating to dates and periods referred to in this document. This document does not imply that any information is not subject to change. Except and to the extent that checking or verification of information or data is expressly agreed within the written scope of its services, DNV GL shall not be responsible in any way in connection with erroneous information or data provided to it by the Customer or any third party, or for the effects of any such erroneous information or data whether or not contained or referred to in this document.
7. Any energy forecasts estimates or predictions are subject to factors not all of which are within the scope of the probability and uncertainties contained or referred to in this document and nothing in this document guarantees any particular wind speed or energy output.

KEY TO DOCUMENT CLASSIFICATION

Strictly Confidential	:	For disclosure only to named individuals within the Customer's organisation.
Private and Confidential	:	For disclosure only to individuals directly concerned with the subject matter of the document within the Customer's organisation.
Commercial in Confidence	:	Not to be disclosed outside the Customer's organisation.
DNV GL only	:	Not to be disclosed to non-DNV GL staff
Customer's Discretion	:	Distribution for information only at the discretion of the Customer (subject to the above Important Notice and Disclaimer and the terms of DNV GL's written agreement with the Customer).
Published	:	Available for information only to the general public (subject to the above Important Notice and Disclaimer).

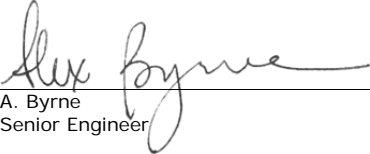
Project name: Creation of a model for interaction of bottom-fixed wind turbines with surface ice for use with common simulation codes Award No. DE-EE0005477 DNV GL - Energy Renewables Advisory 1501 4th Avenue, Suite900 Seattle, WA 98101
 Report title: Ice Load Project Final Technical Report
 Customer: U.S. Department of Energy - Golden Field Office 1617 Cole Boulevard, Golden, Colorado 80401-3393 Tel: 206-387-4200 Enterprise No.: 26-253197
 Contact person: DOE/CNJV Project Monitor – Erik Mauer
 Date of issue: 30 October 2014
 Project No.: 84230955
 Document No.: DDRP0133-A

Task and objective:

Prepared by:


 T. McCoy
 Senior Engineer

Verified and approved by:


 A. Byrne
 Senior Engineer

- Strictly Confidential
- Private and Confidential
- Commercial in Confidence
- DNV GL only
- Customer's Discretion
- Published

Keywords:

Ice loading, offshore, wind energy

© DNV KEMA Renewables, Inc.. All rights reserved.

Reference to part of this report which may lead to misinterpretation is not permissible.

Version	Date	Reason for Issue	Prepared by	Verified by	Approved by
A	30 October 2014	Initial draft for review	T. McCoy	A. Byrne	A. Byrne



Table of contents

EXECUTIVE SUMMARY	1
1 INTRODUCTION.....	2
1.1 Project goals and objectives	2
1.2 Project approach and history	3
2 ICE LOADING BACKGROUND	5
2.1 Theory introduction.....	6
2.2 Ice models.....	6
2.3 IceFloe subroutine description	7
3 VERIFICATION	8
4 ICEFLOE WITH FAST	14
4.1 Initial verification.....	14
4.2 Simulations with turbine operation in turbulence	17
5 ICEFLOE WITH OTHER CODES	20
5.1 HAWC2	20
5.2 Bladed	21
5.3 ADAMS.....	23
6 CONCLUSIONS	25
7 RECOMMENDATIONS.....	26
8 REFERENCES.....	27

Appendices

APPENDIX A – THEORY OF ICE FORCES ON OFFSHORE WIND TURBINE PIERS

APPENDIX B – ICEFLOE USER MANUAL

APPENDIX C – EXAMPLE ICEFLOE INPUT FILE

APPENDIX D – EXAMPLE ICEFLOE OUTPUT FILE

List of tables

Table 1-1 Review of project goals	3
Table 2-1 Ice load models in IceFloe.....	7
Table 3-1 Ice properties used for initial phase of verification	8
Table 3-2 Tower configurations for initial phase of verification	9
Table 3-3 Limit crushing loads with the ISO algorithm.....	9
Table 3-4 Limit crushing loads with the IEC algorithm	9
Table 3-5 Limit flexural loads with the ISO algorithm	9
Table 3-6 Limit flexural loads with the IEC algorithm	10
Table 3-7 Ice properties used for verification of parameter range – Baltic Sea	12
Table 3-8 Ice properties used for verification of parameter range – Great Lakes.....	12
Table 3-9 Structure properties used for verification of parameter range	13

List of figures

Figure 3-1 Spectrum of ice forces compared to analytical basis.....	10
Figure 3-2 Check of coupled crushing strength curve	11
Figure 3-3 Example verification set	13
Figure 4-1 Ice load and base reaction force in FAST for IEC crushing.....	14
Figure 4-2 Ice load and base reaction force in FAST for ISO flexural failure	15
Figure 4-3 Applied ice load and base reaction force in FAST for random crushing	15
Figure 4-4 Check of applied ice loads on a multi-leg structure	16
Figure 4-5 Check of base reaction loads in FAST on a multi-leg structure	17
Figure 4-6 Time series of base reaction moments in 16 m/s turbulent wind in FAST.....	18
Figure 4-7 Mean base reaction moments vs. wind speed.....	18
Figure 4-8 Peak base reaction moment vs. wind speed.....	19
Figure 4-9 Base reaction moment DEL (N=600, m=3.5) vs. wind speed.....	19
Figure 5-1 Check of ice force and base reaction loads in HAWC2.....	20
Figure 5-2 Time series of base reaction moments in 16 m/s turbulent wind in HAWC2	21
Figure 5-3 Check of ice force and base reaction loads in Bladed.....	22
Figure 5-4 Time series of base reaction moments in 16 m/s turbulence in Bladed.....	22
Figure 5-5 Check of ice force and base reaction loads in ADAMS	23
Figure 5-6 Time series of base reaction moments in 16 m/s turbulence in ADAMS	24



List of abbreviations

Abbreviation	Meaning
dll	dynamic link library
DEL	Damage Equivalent Load
DNV	Det Norske Veritas
DNV GL	DNV KEMA Renewables, Inc.
DTU	Danmarks Tekniske Universitet (a.k.a. Technical University of Denmark)
ISO	International Organization for Standardization
IEC	International Electrotechnical Commission
NREL	National Renewable Energy Laboratory
NWTC	National Wind Technology Center

EXECUTIVE SUMMARY

The U.S. Department of Energy (DOE) awarded DNV KEMA Renewables, Inc. (DNV GL) a project entitled *Creation of a Model for Interaction of Bottom-Fixed Wind Turbines with Surface Ice for Use with Common Simulation Codes*, Award No. DE-EE0005477.

As interest and investment in offshore wind projects increase worldwide, some turbines will be installed in locations where ice of significant thickness forms on the water surface. This ice moves under the driving forces of wind, current, and thermal effects and may result in substantial forces on bottom-fixed support structures. The North and Baltic Seas in Europe have begun to see significant wind energy development and the Great Lakes of the United States and Canada may host wind energy development in the near future. Design of the support structures for these projects is best performed through the use of an integrated tool that can calculate the cumulative effects of forces due to turbine operations, wind, waves, and floating ice. The dynamic nature of ice forces requires that these forces be included in the design simulations, rather than added as static forces to simulation results.

The International Electrotechnical Commission (IEC) standard [2] for offshore wind turbine design and the International Organization for Standardization (ISO) standard [3] for offshore structures provide requirements and algorithms for the calculation of forces induced by surface ice; however, currently none of the major wind turbine dynamic simulation codes provides the ability to model ice loads. The scope of work of the project described in this report includes the development of a suite of subroutines, collectively named *IceFloe*, that meet the requirements of the IEC and ISO standards and couples with four of the major wind turbine dynamic simulation codes.

The mechanisms by which ice forces impinge on offshore structures generally include the forces required for crushing of the ice against vertical-sided structures and the forces required to fracture the ice as it rides up on conical-sided structures. Within these two broad categories, the dynamic character of the forces with respect to time is also dependent on other factors such as the velocity and thickness of the moving ice and the response of the structure. In some cases, the dynamic effects are random and in other cases they are deterministic, such as the effect of structural resonance and coupling of the ice forces with the deflection of the support structure. The initial versions of the IceFloe routines incorporate modules that address these varied force and dynamic phenomena with seven alternative algorithms that can be specified by the user.

The IceFloe routines have been linked and tested with four major wind turbine aeroelastic simulation codes: FAST, a tool developed under the management of the National Renewable Energy Laboratory (NREL) and available free of charge from its web site; Bladed [4], a widely-used commercial package available from DNV GL; ADAMS [5], a general purpose multi-body simulation code used in the wind industry and available from MSC Software; and HAWC2[6], a code developed by and available for purchase from Danmarks Tekniske Universitet (DTU). Interface routines have been developed and tested with full wind turbine simulations for each of these codes and the source code and example inputs and outputs are available from the NREL website.



1 INTRODUCTION

The U.S. Department of Energy (DOE) awarded DNV KEMA Renewables, Inc. (DNV GL) a project entitled *Creation of a Model for Interaction of Bottom-Fixed Wind Turbines with Surface Ice for Use with Common Simulation Codes*, Award No. DE-EE0005477. This report presents the background, theory and accomplishments of the work completed under the award.

As interest and investment in offshore wind projects increase worldwide, some turbines will be installed in locations where ice of significant thickness forms on the water surface. This ice moves under the driving forces of wind, current, and thermal effects and may result in substantial forces on bottom-fixed support structures. The North and Baltic Seas in Europe have begun to see significant wind energy development and the Great Lakes of the United States and Canada may host wind energy development in the near future. Design of the support structures for these projects will require an integrated tool that can calculate the cumulative effects of forces due to turbine operations, wind, waves, and floating ice, although ice and wave loads are most often mutually exclusive. The dynamic nature of ice forces requires that these forces be included in design simulations, rather than added as static forces to simulation results.

1.1 Project goals and objectives

A number of goals were set for this project; the primary focus being the provision of suitable tools in the form of subroutines for aeroelastic simulations for use in the design of offshore support structures in ice-prone regions. The project goals and associated accomplishments are summarized in Table 1-1.

Table 1-1 Review of project goals

Project Goal	Accomplishment
Enable the wind energy industry to develop opportunities offshore in cold regions with greater confidence.	Subroutines that can be used with multiple wind turbine aeroelastic simulations have been developed and are available to the public.
Include both slow-moving and dynamic ice-structure interaction.	Models for multiple types of ice phenomenology are included in the subroutines, including ice crushing, flexural ice failure, and coupled crushing.
Consider the possible range of offshore wind turbine tower designs, including single tube, multiple tube, and "jacket" (truss) structures.	Support structure types that can be modeled are: vertical-sided monopoles, conical-sided monopoles, and multi-leg structures with three or four legs.
Design the code to interface with common wind turbine simulation codes that simultaneously consider aerodynamic, hydrodynamic, and structural interactions. Test the code with several common simulation codes.	Interface routines have been developed and tested for FAST, Bladed, ADAMS, and HAWC2.
Disseminate the work and application to the wind energy industry.	This report is available to the public, and includes as appendices thorough theory and user manuals. Presentation at relevant conferences is underway including possibly: AWEA Offshore, EWEA Offshore, AWEA, and AIAA/ASME Wind Symposium.
Identify the most current and appropriate algorithms to describe ice loading on the towers of offshore, floor-mounted, wind turbines.	Several algorithms are included in the subroutines including those suggested by IEC and ISO offshore design standards.
Consider the possible range of sea and lake environments for wind turbines in the coming decades.	The subroutines have been run with a range of ice conditions typical of the Great Lakes and Baltic Sea.
Create a code written in a common, modern language which will be made available to the public.	The subroutines are written in Fortran and will be available on the NREL website.
Make the results of test cases available to the public.	Included in the distribution of the code are test case examples with inputs and results.

1.2 Project approach and history

The project was managed and the majority of the work was carried out in the Seattle office of DNV GL's Renewables Advisory Group.

In order to achieve the project goals, an expert in ice loading of offshore structures was brought under subcontract. Dr. Thomas Brown, professor emeritus from the University of Calgary in Alberta, Canada and current president of IFC Engineering, is an internationally recognized expert in the field. Dr. Brown has led research in ice mechanics within the civil engineering department for many years and is also a member of several international organizations and committees related to ice loading. Dr. Brown is responsible for the identification, development, and verification of the ice load algorithms used in the subroutines. He also authored the theory manual included as Appendix A.

Other partners in the project included the DNV GL certification group headquartered in Hamburg, Germany, and NREL's National Wind Technology Center (NWTC) in Colorado. The DNV GL certification group was tasked with integrating and testing the ice load subroutines in the HAWC2 wind turbine aeroelastic simulation code. The HAWC2 software is a widely-used design tool in the wind industry and is developed by and available from DTU. HAWC2 is used by DNV GL to verify loads calculations as part of the certification process. The DNV GL office in Seattle executed this task because it had more available resources than the



DTU certification group at the time. DNV GL gratefully acknowledges the assistance of DTU in providing a copy of the HAWC2 code for this work.

NREL was tasked with integrating the ice load routines into the FAST framework. The FAST framework is undergoing concurrent development of a variety of enhancements, including many features specific to the analysis of offshore wind turbines [1].

The planned approach to development of a suite of subroutines was as follows:

- Identify and specify appropriate algorithms;
- Code and test the algorithms in subroutines in C++;
- Integrate the resulting subroutines with the FAST and HAWC2 simulation software;
- Test the integrated software;
- Write theory and user manuals for the subroutines; and
- Publish the subroutines and integration source code via the NREL website.

While the goals for the project have all been met or exceeded, there were some changes made during the course of the project. Primarily after some personnel changes occurred and a more careful review of the requirements for integrating with FAST was made, a decision was made to switch from C++ to Fortran for the subroutine development. This decision was made after consultation internally and with the engineers at NREL and the program administrators at DOE. Fortunately, most of the development in C++ was in coding the initially specified algorithms and much of the learning from that effort was leveraged into rewriting the code in Fortran. Further, the effort to integrate with the FAST software, itself written in Fortran, was considerably reduced as a result of this change, allowing more effort to be put into algorithm development, verification, and testing.

As noted above, the task of integrating and testing the ice load routines with the HAWC2 software was moved from the DNV GL certification group in Copenhagen to the DNV GL advisory group in Seattle. The combination of the switch to Fortran and the switch in responsibility for HAWC2 enabled the project to leverage the experience gained in Seattle with the ADAMS software and the availability of the Bladed software due to the merger of DNV and GL. As a result, both the ADAMS and Bladed tools were added to the list of software that was integrated and tested for use with the ice load routines.

2 ICE LOADING BACKGROUND

2.1 Wind turbine loads simulation

Wind turbine design relies largely on the use of computer modeling to simulate the dynamic effects of wind, waves, and turbine structural response, operation and controls to predict load levels. There are many models used by designers and researchers around the world with a few in common use in North America and Europe: FAST, Bladed, ADAMS, HAWC2, and Flex5 among the most well-known. This project is largely focused on using FAST although many of the descriptions here are analogous to the other models.

The FAST computer model for wind turbine aeroelastic simulations has been in development and use by researchers and designers for over 20 years. Recently a team of developers composed of engineers from the NWTC, universities, laboratories, and private companies has embarked on a project to improve the capability of the FAST model by making it more modular in general and improving or adding modules with specific capabilities for inflow, aerodynamics, wave loading, and fixed and floating support substructures among others. This project is part of the FAST framework development with the aim of providing the capability of integrating ice forces into the dynamic modeling. A conceptual overview of the FAST framework is shown in Figure 2-1. Note that this figure depicts a floating platform the IceFloe model is intended for use with fixed bottom structures only.

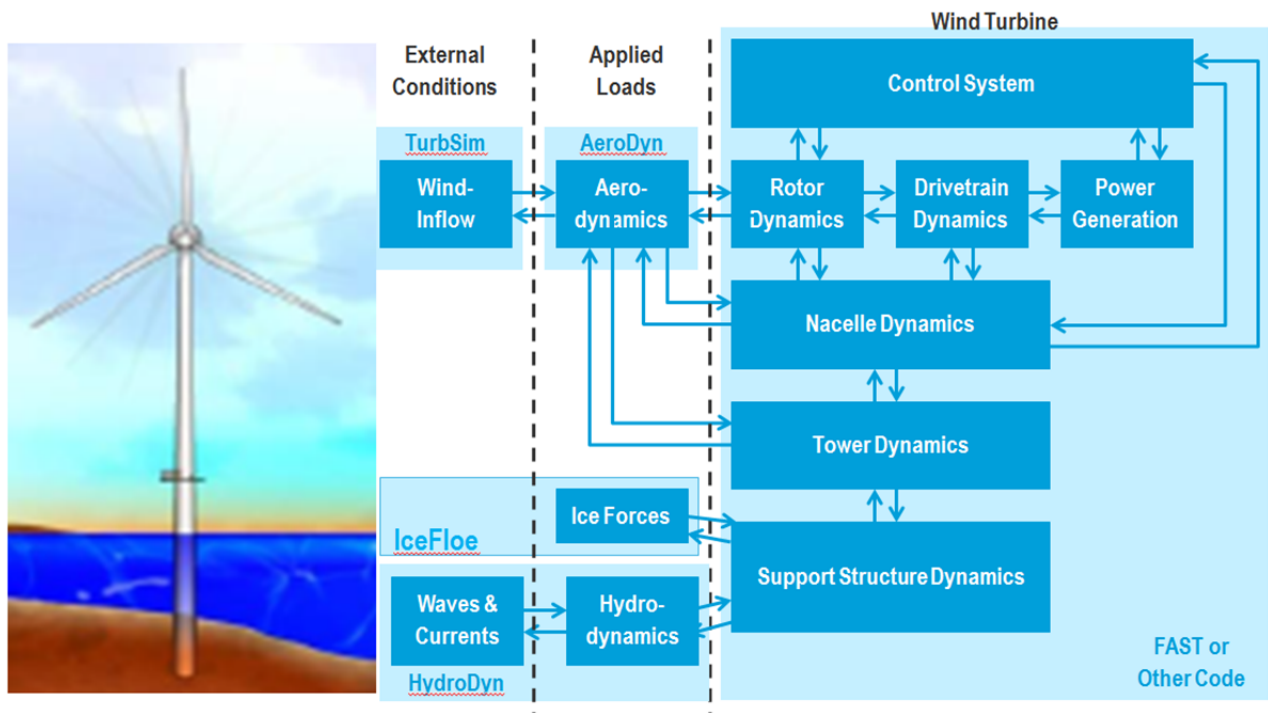


Figure 2-1 Graphic of FAST module interaction from ref [1]

2.2 Ice loading theory introduction

The theoretical basis for the calculation of ice loads is a combination of physics and empiricism. Because the phenomena are so complex and varied, a comprehensive theoretical framework is not feasible. As a result, engineers use models that are derived from physical principles but are substantially informed by empirical results. These results are based on laboratory and field measurements including visual observation of the behavior of ice impingement on structures.

The mechanism by which ice applies load to a structure has to do with the failure modes of the ice itself. These failure modes depend on the thickness and mechanical properties of the ice, its velocity, and the width of the structure that it is pushing on as it moves. For example, for thick, slow-moving ice impinging against a vertically-sided structure, the ice crushes itself against the structure. The force imparted to the structure is a function of the ice strength in ductile crushing. Alternatively, if the ice is thin and/or moving rapidly, it fails in a brittle fashion and the force applied to the structure is related to the strength of the ice in buckling.

Yet another failure mode occurs when the structure has sufficiently angled conical sides. In this case the force imparted on the structure is that which is required to break the ice in bending. The ice breaks in bending as it moves and is forced upward (or downward) against the structure. Thus, in this failure mode the force on the structure is a function of the flexural strength of the ice.

The dynamic behavior of these failure modes is also dependent on the properties of the ice and structure. The dynamics can range from periodic wave forms with nearly constant amplitude to wave forms where the periods and amplitudes are randomly distributed although bounded. In some cases, particularly for fast moving ice, the waveforms are quite stochastic and are best described with a frequency spectrum.

A comprehensive discussion of the theory of these various ice loading models is provided in Appendix A. The implementation of these models in the subroutines is discussed in a later section and in the user manual found in Appendix B.

2.3 Ice models

The choice of ice loading models incorporated in the subroutines was based on the following criteria:

- The ice model must have engineering relevance, specifically normative or informative in relevant design standards.
- The ice model must be well vetted by the ice research community.
- The ice model must be tractable from a software standpoint.

Based on these requirements several models were chosen as listed in Table 2-1. Detailed theoretical development, discussion, and guidance for the use of these models can be found in the theory and user manuals.

Table 2-1 Ice load models in IceFloe

Ice Load Model	Source
Continuous random crushing	ISO 19906[3], Karna[2] [6]
Intermittent crushing per ISO	ISO 19906 [3]
Lock-in crushing per ISO	ISO 19906 [3][2]
Lock-in crushing per IEC	IEC 61400-3 [2], Korzhavin [8]
Coupled crushing	Määttänen [11]
Flexural failure per ISO	ISO 19906 [3], Croasdale [9]
Flexural failure per IEC	IEC 61400-3 [2], Ralston [10]

IceFloe includes the option to apply loads from any of these models to a monopole structure or a multi-leg structure of either three or four legs of the same diameter. For multi-leg support structures, the ice loads are calculated independently for each leg; however, factors based on sheltering of one leg by another are also used, which can be automatically applied or user specified.

2.4 IceFloe subroutine description

The ice force models listed in Table 2-1 and described in the theory manual are implemented in a suite of subroutines collectively named IceFloe. Each of the ice loading models has unique initialization and update routines, although there are shared base routines for calculations that are common to groups or all of the loading models. The ice force models do not contain states that evolve over time; all variables saved during initialization are parameters that do not change with time.

For all of the models, with the exception of the coupled crushing, the load time series is pre-computed in the initialization routine. The Update Routine then interpolates this time series for the requested simulation time. The coupled crushing model uses the local velocity of the structure in the horizontal plane projected onto the vector direction of the ice motion. This is used to obtain the relative velocity with the ice as a function of the velocity (a fixed parameter) of the ice. The magnitude of the velocity informs whether the ice fails by ductile crushing or brittle failure as described in Appendix A.

The user can specify the direction of ice motion relative to the inertial frame of reference (ground coordinates) of the simulation, although the positive x direction is assumed to be the nominal downwind direction. The forces will be returned as a horizontal, orthogonal pair in the ground frame of reference for each time step of the calling program.

For multi-leg structures modeled as a monolithic element in a simulation, the individual leg loads are calculated internally to IceFloe but an equivalent force vector and torsional moment are calculated and returned to the calling program. The torsional moment is calculated using user supplied coordinates for the legs relative to the structure's elastic axis and applied at that point.

3 VERIFICATION

Since the data on ice loading was not available to DNV GL (it is primarily held by commercial and academic entities and not available), verification of the IceFloe routines is limited to insuring that the algorithms are implemented properly and yield reasonable results within a broad range of possible input conditions. It is noted that the algorithms implemented in IceFloe have been compared by the ice research community against available test data from bridges and other structures.

The verification was conducted in two phases. The initial phase was to compare the output of IceFloe to calculations performed by other means, e.g. manually, spreadsheet, or MATLAB. For some of the models, a spectrum or histogram of the IceFloe output loads was compared to input specifications. The second phase consisted of running the models over a wide range of inputs; these results were reviewed for unexpected behavior.

Table 3-1 and Table 3-2 list the ice and tower parameters used for the first phase of testing. A console version of IceFloe, which can be run from the DOS prompt, was run for each of these combinations and the limit forces (see the theory manual for a detailed discussion of limit forces) for either crushing or flexural loading were recorded. These results are shown in comparison to a verification calculation in Table 3-3 to Table 3-6. Most of the comparisons match exactly. The calculations in Table 3-6 are based on an approximation of elliptical integrals which are not implemented in quite the same way in MATLAB and IceFloe, thus leading to some slight differences.

Table 3-1 Ice properties used for initial phase of verification

Name	Unit	Great Lakes A	Great Lakes B	North Sea
Ice thickness	m	1.0	0.5	1.0
Ice velocity	m/s	0.2	0.2	0.2
Reference strength	Pa	2.2E6	1.5E6	1.8E6
flexural strength	Pa	0.7e6	0.5e6	0.5e6
Ice modulus elasticity	Pa	8.0e9	5.5e9	7.0e9
Poisson ratio	-	0.3	0.3	0.3
Ice-to-ice coefficient of friction	-	0.05	0.05	0.05
Water density	kg/m ³	999.8	999.8	1044.2
Ice density	kg/m ³	916.2	916.2	907.5
Rubble angle	deg	40	40	40
Rubble porosity	-	0.3	0.3	0.3
Rubble cohesion	Pa	0	0	0
Friction angle of the ice rubble	deg	45	45	45
Ride-up thickness (2.5*thickness)	m	2.5	1.25	2.5
Korzhaven contact factor	-	0.5	0.5	0.5

Table 3-2 Tower configurations for initial phase of verification

Name	Unit	Prototype	Test
Diameter (width)	m	5.0	14.2
Cone angle	Deg	60	52.0
Ride-up (rubble) height	m	3.0	4.0
Tower cone top diameter	m	1.5	8.0
Fundamental frequency	Hz	0.33	0.25
Ice-to-structure coefficient of friction	-	0.15	0.15
Korzavin shape factor	-	0.9	0.9

Table 3-3 Limit crushing loads with the ISO algorithm

Ice Source	Tower	Load (Newtons)	
		Calculation Check	From IceFloe
Great Lakes A	Test	20.4336e+06	20.4336e+06
Great Lakes A	Prototype	8.50271e+06	8.50271e+06
Great Lakes B	Test	8.22679e+06	8.22680E+06
Great Lakes B	Prototype	3.42329e+06	3.42329E+06
North Sea	Test	16.7184e+06	16.7184E+06
North Sea	Prototype	6.95676e+06	6.95676E+06

Table 3-4 Limit crushing loads with the IEC algorithm

Ice Source	Tower	Load (Newtons)	
		Calculation Check	From IceFloe
Great Lakes A	Test	16.3467E+06	16.3467E+06
Great Lakes A	Prototype	7.0004E+06	7.0004E+06
Great Lakes B	Test	5.1973E+06	5.1973E+06
Great Lakes B	Prototype	2.0668E+06	2.0668E+06
North Sea	Test	13.3756E+06	13.3746E+06
North Sea	Prototype	5.7276E+06	5.7276E+06

Table 3-5 Limit flexural loads with the ISO algorithm

Ice Source	Tower	Load (Newtons)	
		Calculation Check	From IceFloe
Great Lakes A	Test	3.37565E+06	3.37565E+06
Great Lakes A	Prototype	2.65997E+06	2.65997E+06
Great Lakes B	Test	1.38542E+06	1.38542E+06
Great Lakes B	Prototype	0.83717E+06	0.83717E+06
North Sea	Test	2.91898E+06	2.91898E+06
North Sea	Prototype	2.10695E+06	2.10695E+06

Table 3-6 Limit flexural loads with the IEC algorithm

Ice Source	Tower	Load (Newtons)	
		Calculation Check	From IceFloe
Great Lakes A	Test	5.0101E+06	5.04547E+06
Great Lakes A	Prototype	3.7443E+06	3.74475E+06
Great Lakes B	Test	1.7564E+06	1.77403E+06
Great Lakes B	Prototype	9.2864E+05	9.28864E+05
North Sea	Test	4.3404E+06	4.37543E+06
North Sea	Prototype	2.9012E+06	2.90165E+06

To check the random crushing model which is driven by an analytical spectral distribution, a power spectrum was calculated from the IceFloe output time series and compared to the analytical power spectral density (PSD) curve as shown in Figure 3-1. To check the coupled crushing implementation, the analytical curve of ice strength as a function of relative velocity between the tower and ice is compared to the results from FAST in Figure 3-2.

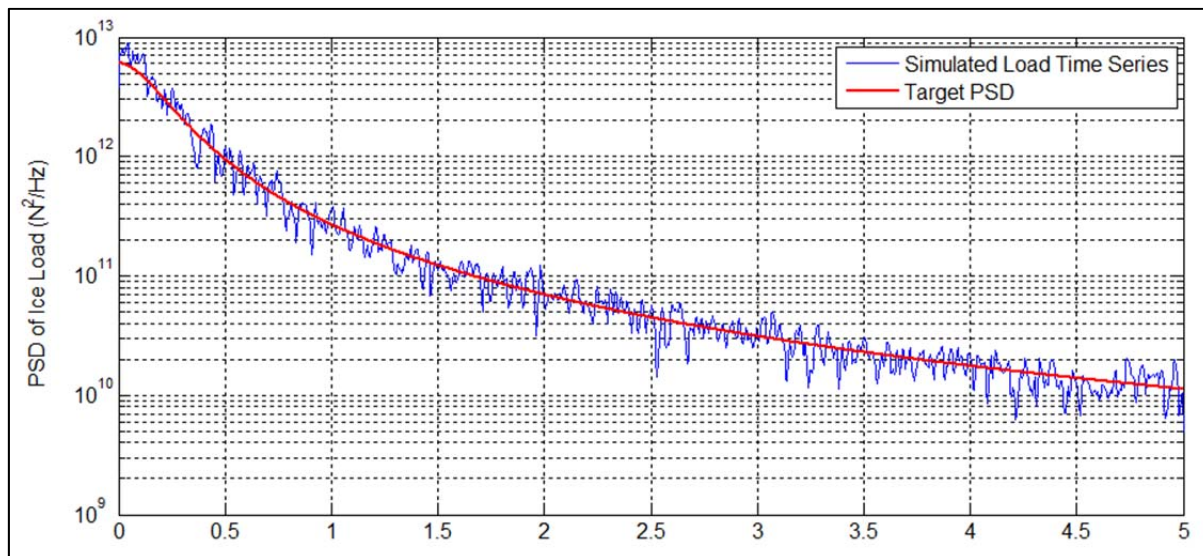


Figure 3-1 Spectrum of ice forces compared to analytical basis

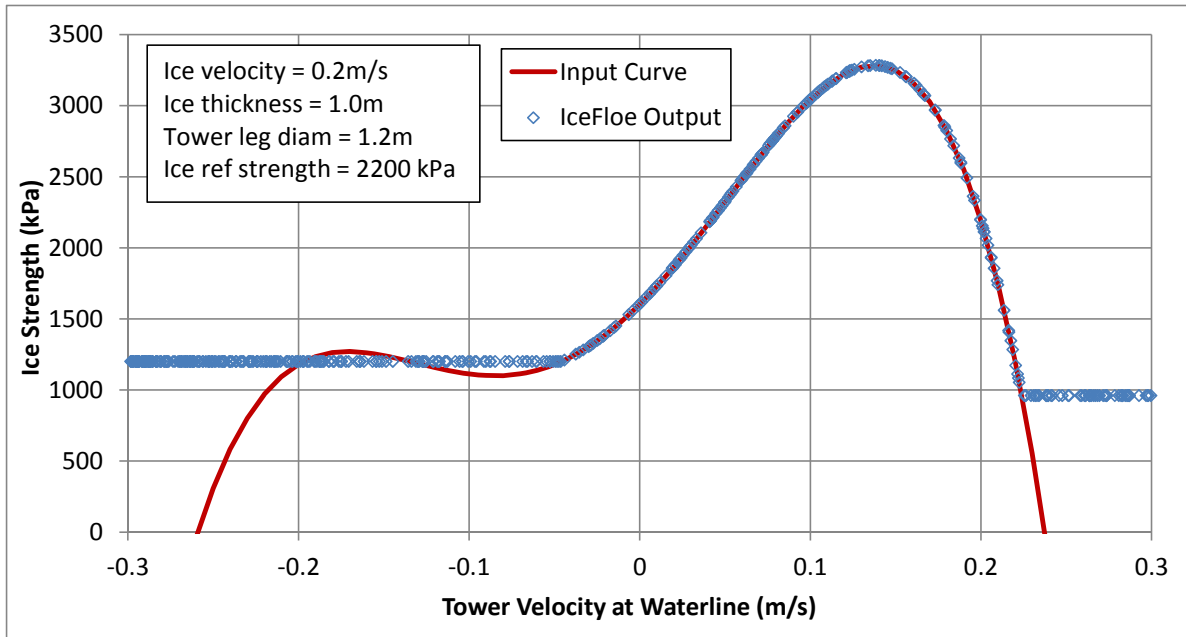


Figure 3-2 Check of coupled crushing strength curve

The second phase of the verification was to run the various models across a wide range of input values. To this end, the test cases shown in Table 3-5 to Table 3-9 were developed. The ice properties were selected to represent a wide but realistic range of possible conditions in which wind turbines might be installed. These cases were run, plotted, and reviewed to check for unexpected behavior. An example set of plots is shown in Figure 3-3. Note that the term “fast ice” implies a large expanse of ice which is essentially one sheet, as opposed to “open ice” where there may be breaks or gaps in the sheet. The plots of these results were reviewed for unexpected behavior and in some cases, recommended parameter ranges were adjusted accordingly. For example, the random crushing model had a tendency to produce negative loads when the coefficient of variance was set too high. The recommended maximum for this parameter was lowered, and the case was re-run.

Table 3-7 Ice properties used for verification of parameter range – Baltic Sea

Name	Unit	Slow Moving Fast Ice	Mobile Fast Ice	Open Ice
Ice thickness	m	1.2	0.5	0.9
Ice velocity	m/s	0.001	0.1	0.05 to 0.30
Reference strength	MPa	2.2	1.8	0.5
Flexural strength	MPa	0.6	0.6	2.2
Ice modulus elasticity	MPa	5,000	5,000	5,000
Poisson ratio	-	0.3	0.3	0.3
Ice-to-ice coefficient of friction	-	0.05	0.05	0.05
Water density	kg/m ³	1043.8	1043.8	1043.8
Ice density	kg/m ³	927.6	927.6	927.6
Rubble angle	deg	40.0	40.0	40.0
Rubble porosity	-	0.3	0.3	0.3
Rubble cohesion	Pa	0.0	0.0	0.0
Friction angle of the ice rubble	deg	45.0	45.0	45.0
Ride-up thickness (2.5*thickness)	m	3.0	1.5	2.25
Korzhasin contact factor	-	0.5	0.5	0.5

Table 3-8 Ice properties used for verification of parameter range – Great Lakes

Name	Unit	Lake Erie (Cleveland)	Lake Erie (West Basin)	Lake Michigan (Milwaukee)	Lake Huron (West/Sarnia)	Lake Superior (Duluth)
Ice thickness	m	0.7	1.0	0.3	0.7	1.0
Ice velocity	m/s	0.02 to 0.3	0.02 to 0.08	0.02 to 0.2	0.02 to 0.2	0.02 to 0.15
Reference strength	MPa	1.8	1.8	1.8	2.0	2.5
Flexural strength	MPa	0.8	0.8	0.8	1.0	1.2
Ice modulus elasticity	MPa	5,500	5,500	5,500	5,500	5,500
Poisson ratio	-	0.3	0.3	0.3	0.3	0.3
Ice-to-ice coefficient of friction	-	0.05	0.05	0.05	0.05	0.05
Water density	kg/m ³	999.0	999.0	999.0	999.0	999.0
Ice density	kg/m ³	927.6	927.6	927.6	927.6	927.6
Rubble angle	deg	40.0	40.0	40.0	40.0	40.0
Rubble porosity	-	0.3	0.3	0.3	0.3	0.3
Rubble cohesion	Pa	0.0	0.0	0.0	0.0	0.0
Friction angle of the ice rubble	deg	45.0	45.0	45.0	45.0	45.0
Ride-up thickness	m	1.75	2.5	0.75	1.75	3.0
Korzhasin contact factor	-	0.5	0.5	0.5	0.5	0.5

Table 3-9 Structure properties used for verification of parameter range

Name	Unit	Cylindrical	Conical
Diameter (width)	m	6	7.55
Cone angle	deg	0	55
Ride-up (rubble) height	m	NA	1.75
Tower cone top diameter	m	NA	6.0
Fundamental frequency	Hz	0.25	0.25
Ice-to-structure coefficient of friction	-	0.15	0.15
Korzhasvin shape factor	-	0.9	NA

Lake Erie - Western Basin, Ice Vel = 0.08m/s

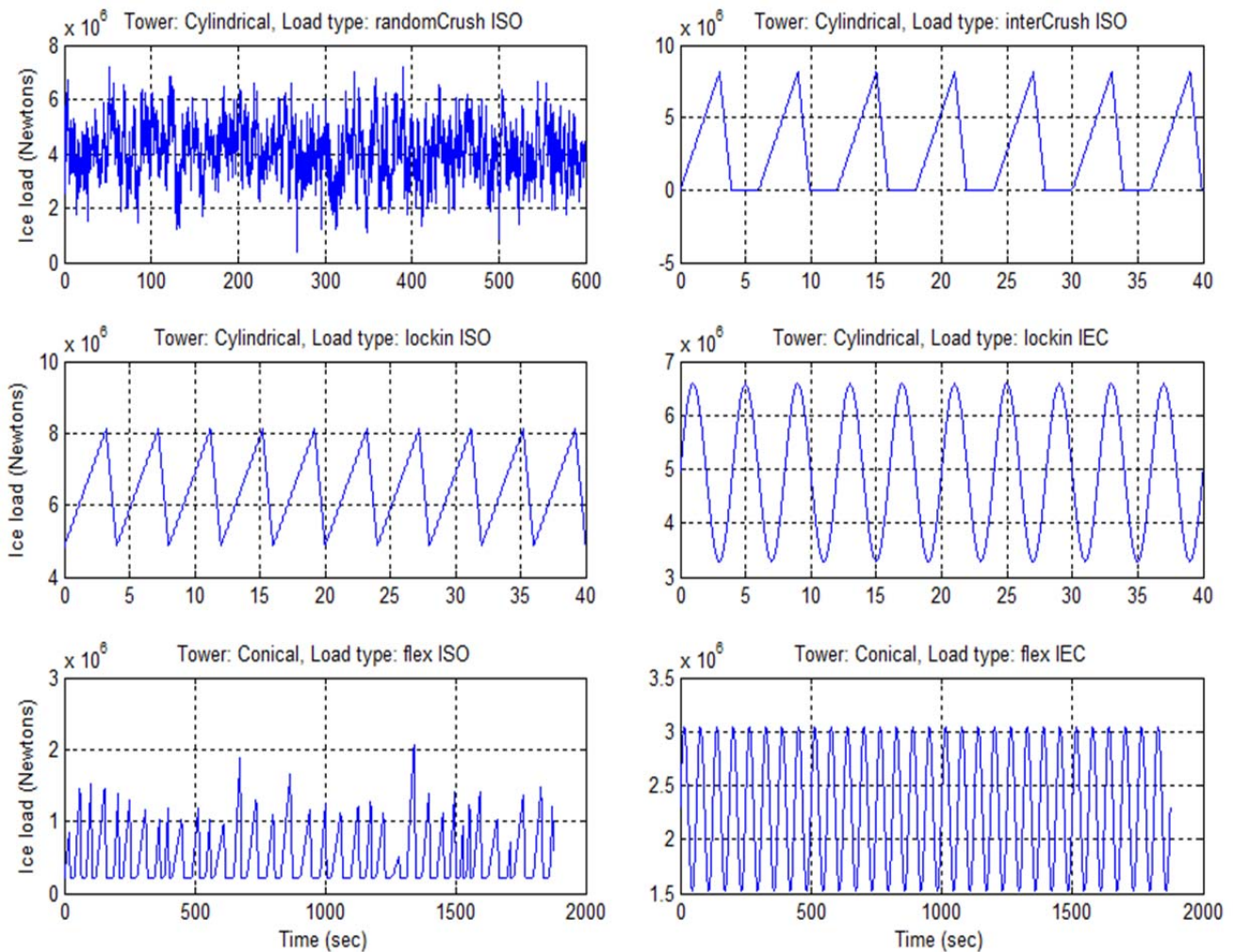


Figure 3-3 Example verification set

4 ICEFLOE WITH FAST

The primary target for the IceFloe subroutines is the FAST framework under development at NREL. DNV GL provided the programmers at NREL with the IceFloe subroutines for integration and the resulting package was returned to DNV GL for testing. This was iterated several times to resolve specific integration details and a version of the FAST framework was then exercised thoroughly by DNV GL with acceptable results.

4.1 Initial verification

Initial testing was intended to verify that the integration of FAST and IceFloe was performing as expected, followed by additional testing to understand the impact of ice loads on turbine structural loads. To accomplish the first task, the NREL 5 MW offshore baseline turbine model [12] was run in FAST with all external sources of load turned off except for the ice loading. The aerodynamic, hydrodynamic, and gravity terms were all disabled. The results were checked by comparing the shear and moment forces at the turbine foundation against the applied ice forces.

4.1.1 Monopile

A monopile structure was tested using a version of the NREL 5 MW model paired with all ice models. All other external load sources were turned off. The ice load is applied at the waterline, 20 m above the base of the support structure on the sea bed. The ice loads and reaction loads at the base of the structure for IEC crushing, ISO flexural failure, and random crushing are shown in Figure 4-1, Figure 4-2, and Figure 4-3, respectively. As expected, the shear force is approximately equal and opposite to the total applied ice force. Small variations between the applied and reaction loads are due to the dynamics of the structure.

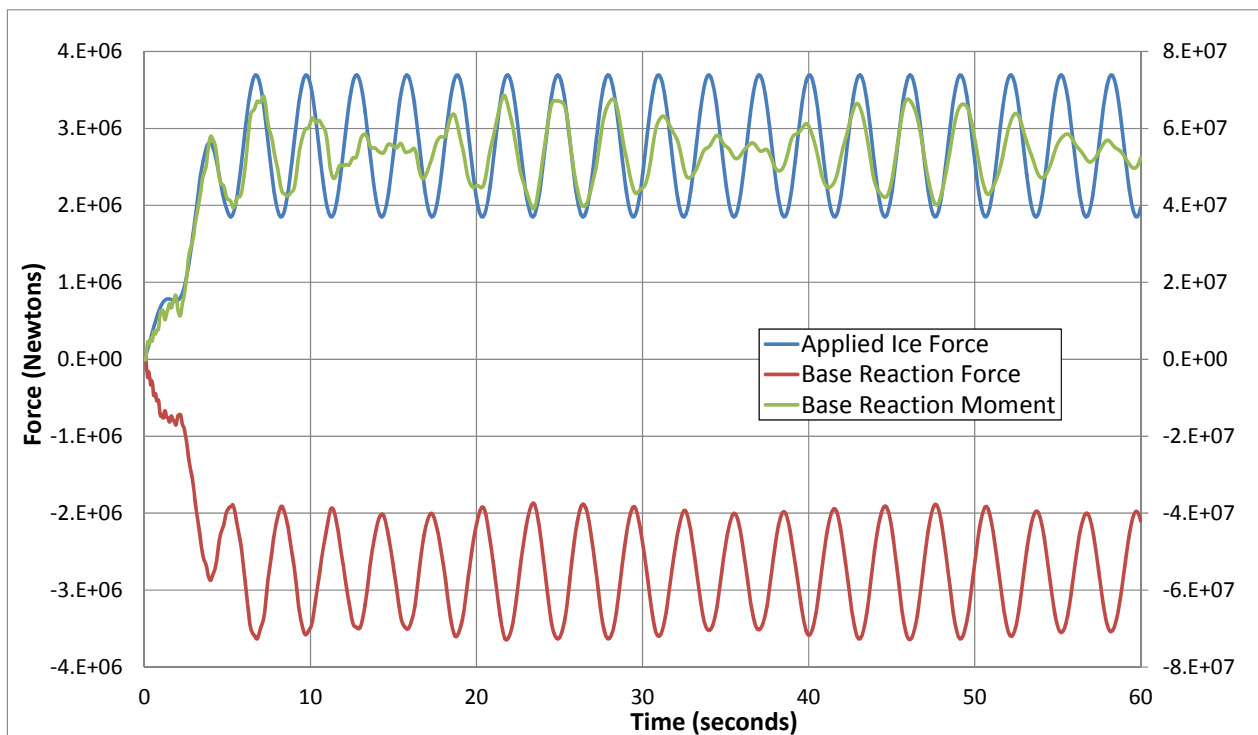


Figure 4-1 Ice load and base reaction force in FAST for IEC crushing

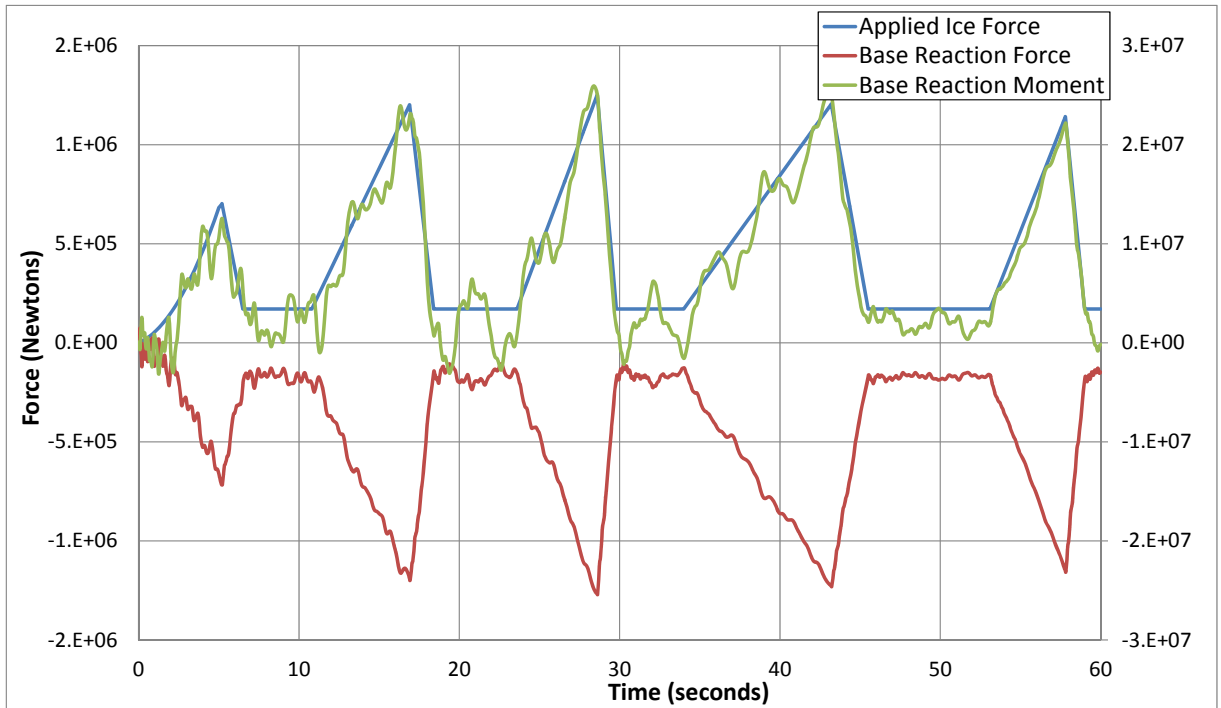


Figure 4-2 Ice load and base reaction force in FAST for ISO flexural failure

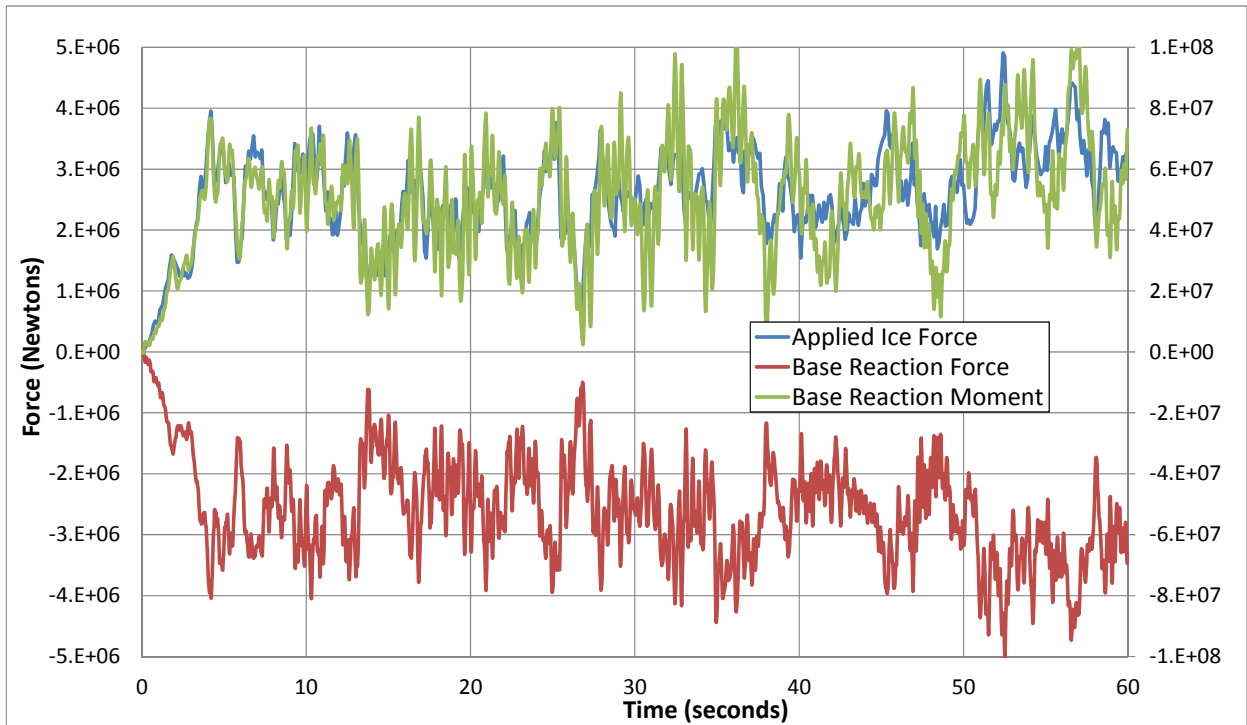


Figure 4-3 Applied ice load and base reaction force in FAST for random crushing

4.1.2 Multiple leg structure (Jacket)

The multi-leg features of IceFloe were tested using the version of the NREL 5 MW model with a 4-leg jacket support structure [13]. As this type of support structure is intended for use in deeper waters, depths of 50 and 60 m were tested. Again, all other external load sources were turned off. The IEC crushing model was applied with a unique phasing for each of the four legs. The individual leg loads and total applied load are shown in Figure 4-4. The reaction loads at the base of the structure are shown in Figure 4-5. As expected, the shear force is approximately equal and opposite to the total applied ice force and the moment is equal to the applied force times the water depth. Small variations between the applied and reaction loads are due to the dynamics of the structure and resulting inertial forces.

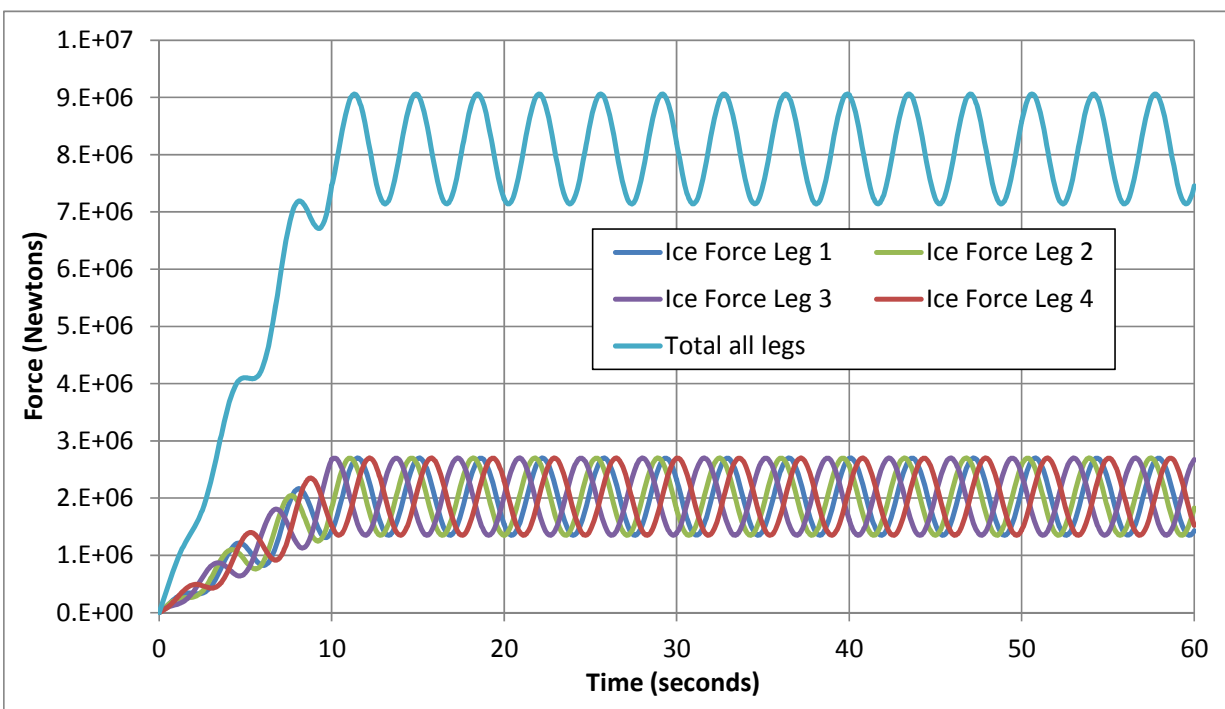


Figure 4-4 Check of applied ice loads on a multi-leg structure

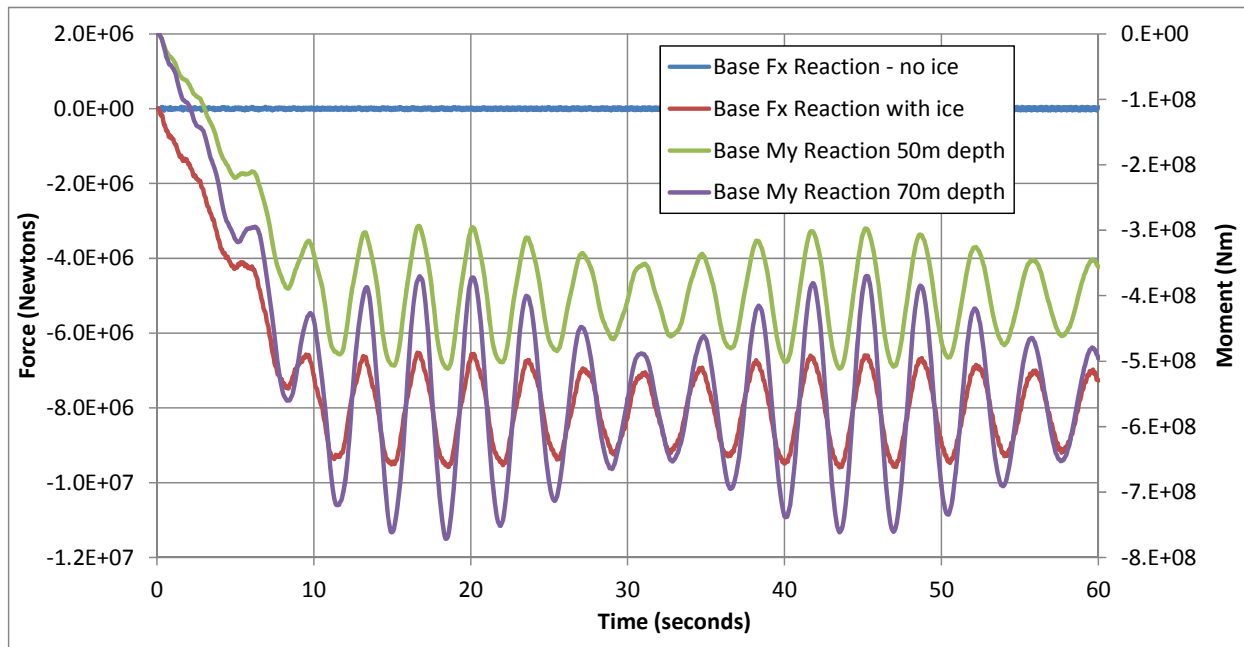


Figure 4-5 Check of base reaction loads in FAST on a multi-leg structure

4.2 Simulations with turbine operation in turbulence

Simulations of operation of the NREL 5 MW turbine on a monopile foundation were conducted to gain an understanding of the influence of ice forces on support structure loads. For these simulations the aerodynamic and gravity forces were turned on but the hydrodynamics remained off. Since this project focuses on loads caused by fully frozen ice sheets, wave and ice loading are mutually exclusive, although exceptions may exist. Figure 4-6 shows a comparison time series of tower base reaction moments with and without ice loading using three ice load models: coupled crushing, random crushing, and flexural ice failure based on the ISO model. The ice properties in this figure represent an ultimate loading condition.

Two sets of turbulent runs were made across the operating wind speed range of the turbine. One set used ultimate ice loading properties, the other used lower ice load properties for fatigue loading. The wind conditions modeled were per IEC IIB (average wind speed of 8.5 m/s and characteristic turbulence intensity of 16% at 15 m/s). The ice loading is based on the Lake Erie properties from Table 3-8 with ice velocities consistent with the type of ice model used. The ice strength and thickness properties are consistent with 50-year return values used for evaluation of peak loads. For fatigue the thickness was reduce to 0.2m. Figure 4-7 shows how the mean level of the support structure base reaction moment is affected by three types of ice loading, while Figure 4-8 shows the maximums at each wind speed. The difference between the load levels is largely due to the ice velocity. Random continuous crushing is a phenomenon that occurs when the ice velocity is high (0.2 m/s was used) and the ice is failing in a brittle manner. Coupled crushing imparts higher loads when the ice velocity is low (0.05 m/s was used) and the ice is failing in a ductile manner. Flexural failure of the ice results in the smallest increase above the no-ice case since failure of ice in bending requires much less reaction force from the support structure.

Figure 4-9 depicts the fatigue damage equivalent loads. As with the peak loads, flexural failure results in the lowest increase above the no-ice case, but the random and coupled crushing results are reversed. This appears to be due to the more dynamic nature of the random ice crushing forces.

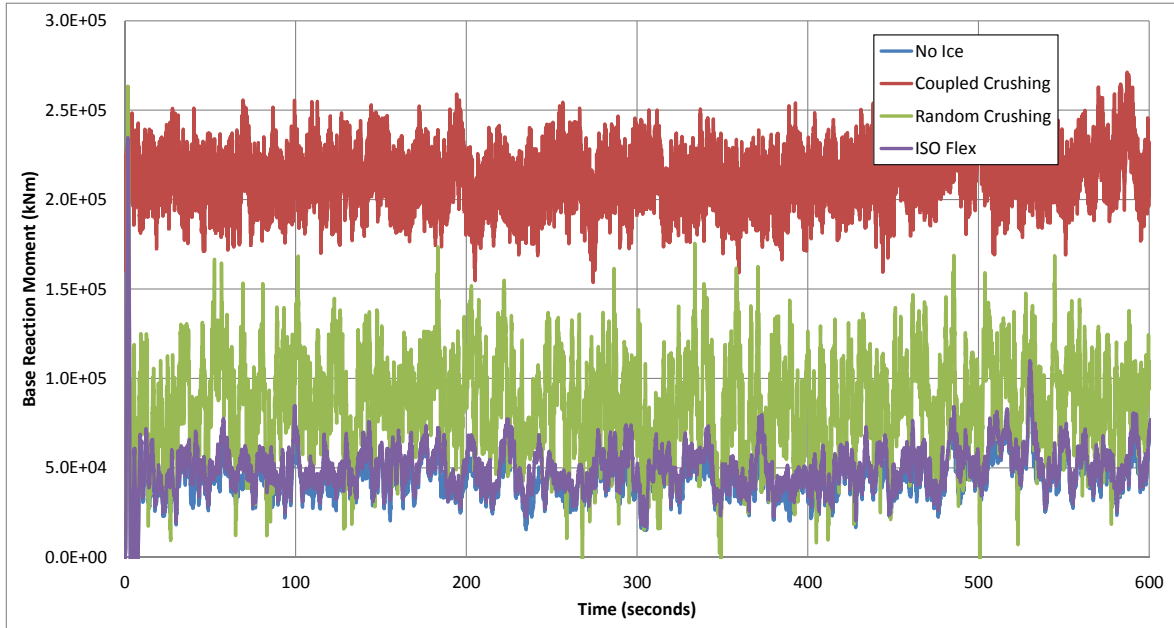


Figure 4-6 Time series of base reaction moments in 16 m/s turbulent wind in FAST

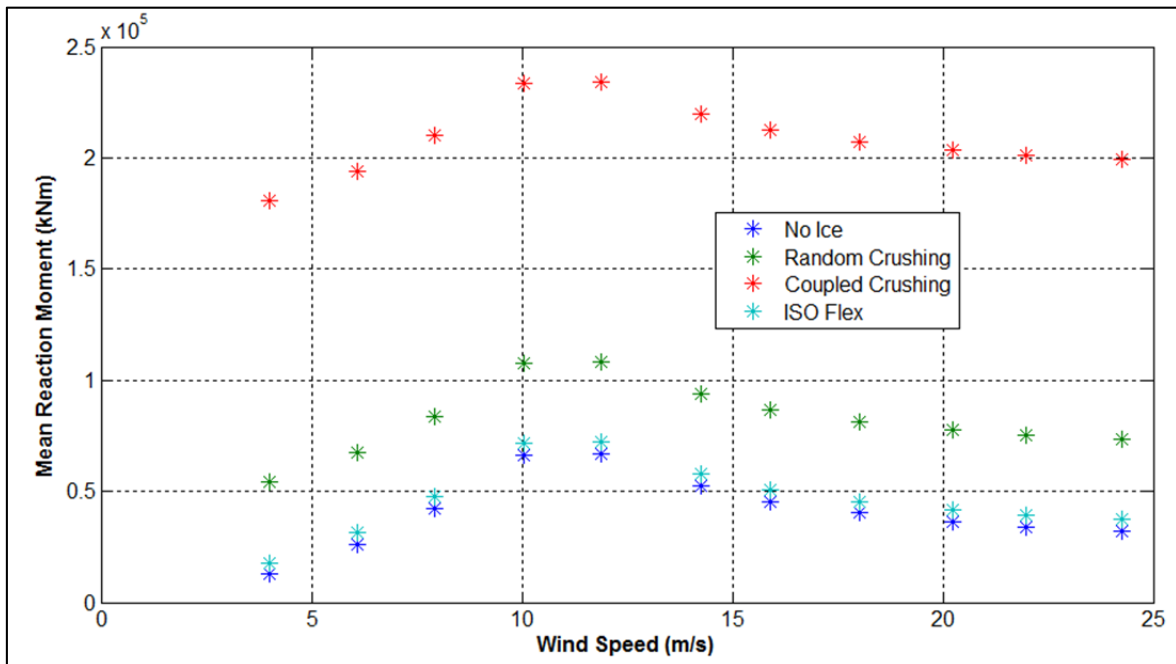


Figure 4-7 Mean base reaction moments vs. wind speed

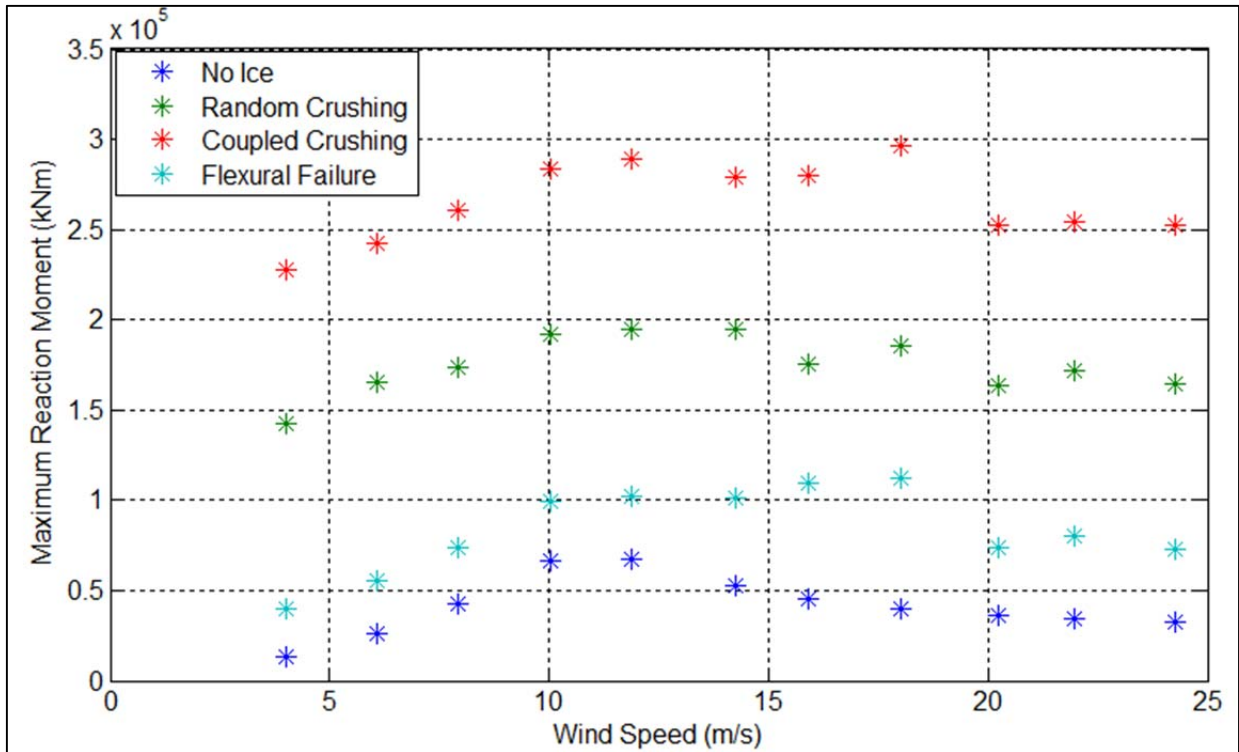


Figure 4-8 Peak base reaction moment vs. wind speed

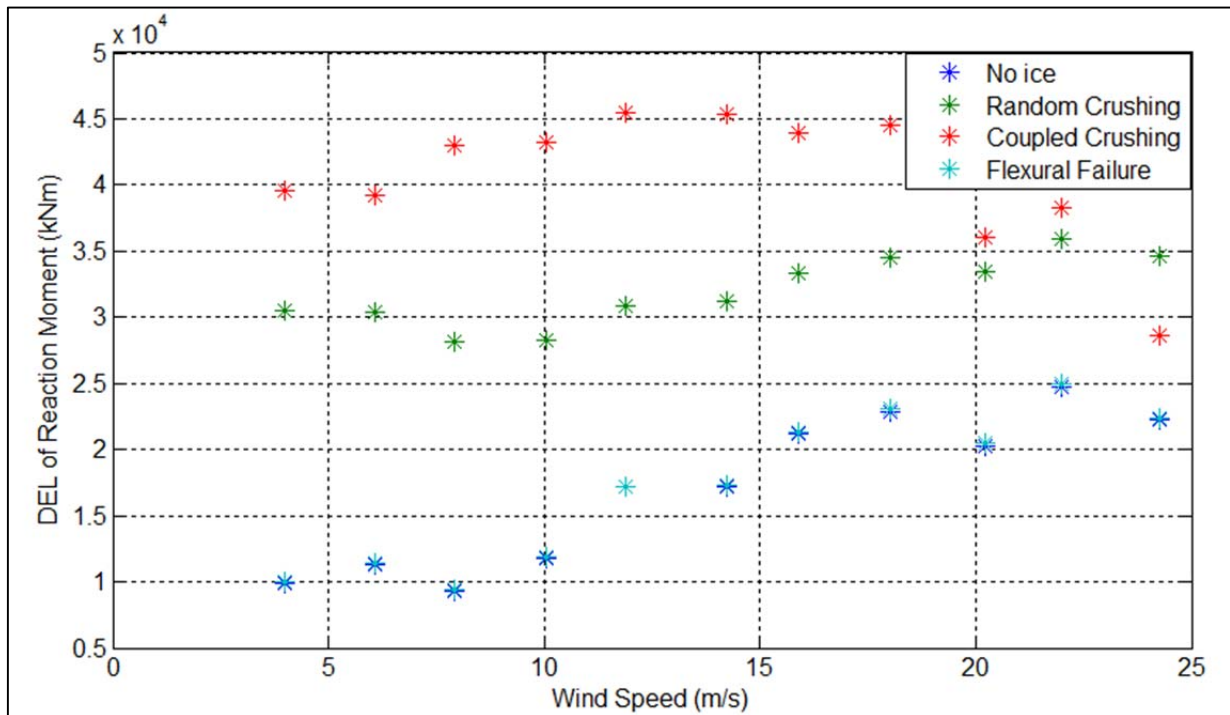


Figure 4-9 Base reaction moment DEL (N=600, m=3.5) vs. wind speed

5 ICEFLOE WITH OTHER CODES

The IceFloe subroutines can be used with any simulation code that allows either direct subroutine integration, or integration via dynamic link library (dll). A simulation code that accepts force time series files as input can also be used for all ice models except the coupled model. Examples of each of these approaches are given herein using three popular wind turbine aeroelastic simulation codes.

5.1 HAWC2

The HAWC2 simulator, available from DTU, has a feature that allows the input of forces on any part of the wind turbine structure via dll. The 5 MW offshore model is available as an example model for HAWC2 and was run with similar conditions as the FAST testing. The results of a test run in HAWC2 with all external forces turned off (gravity, aerodynamics, and hydrodynamics) except for ice loading is shown in Figure 5-1. The applied ice forces match the base reaction force as expected. The base reaction moment rings as the tower oscillation increases but otherwise matches the ice force times height in the mean.

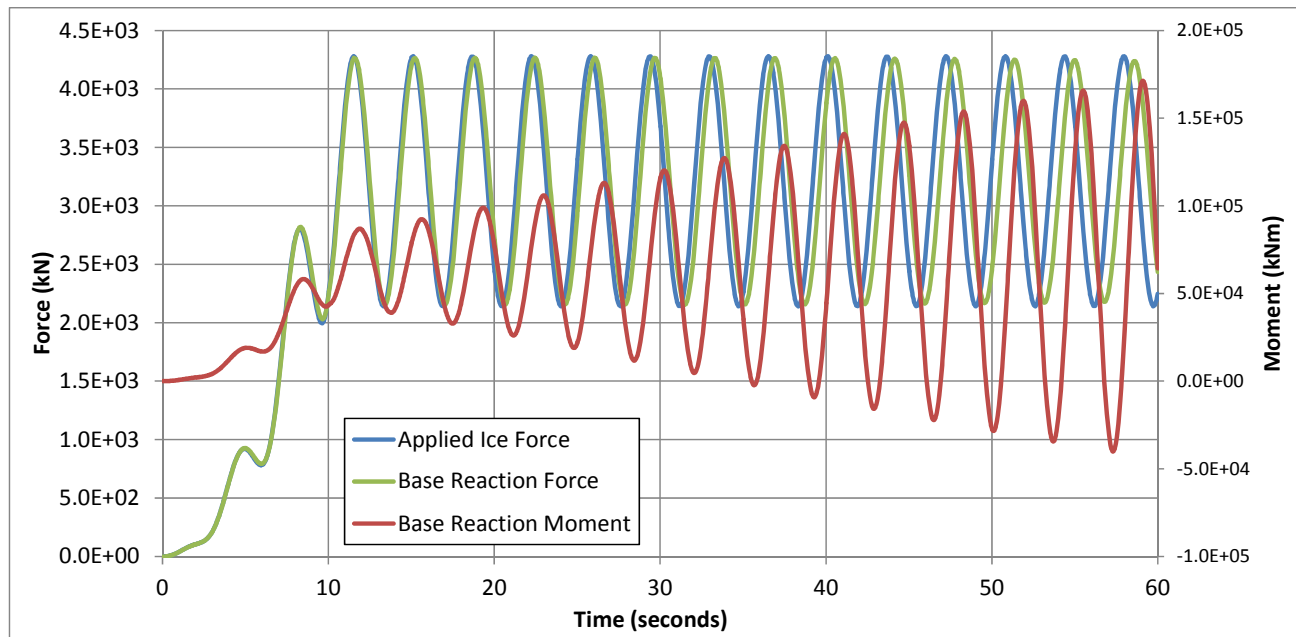


Figure 5-1 Check of ice force and base reaction loads in HAWC2

Figure 5-2 shows a comparison of time series of tower base reaction moments with and without ice loading using three ice load models: coupled crushing, random crushing, and flexural ice failure. While similar, the HAWC2 and FAST results are not directly comparable because they use different turbulence models (HAWC2 uses a Mann turbulence model while FAST uses a Kaimal spectrum turbulence model). An example of the HAWC2 interface code for the ice load dll is available in the distribution of IceFloe on the NREL/NWTC website.

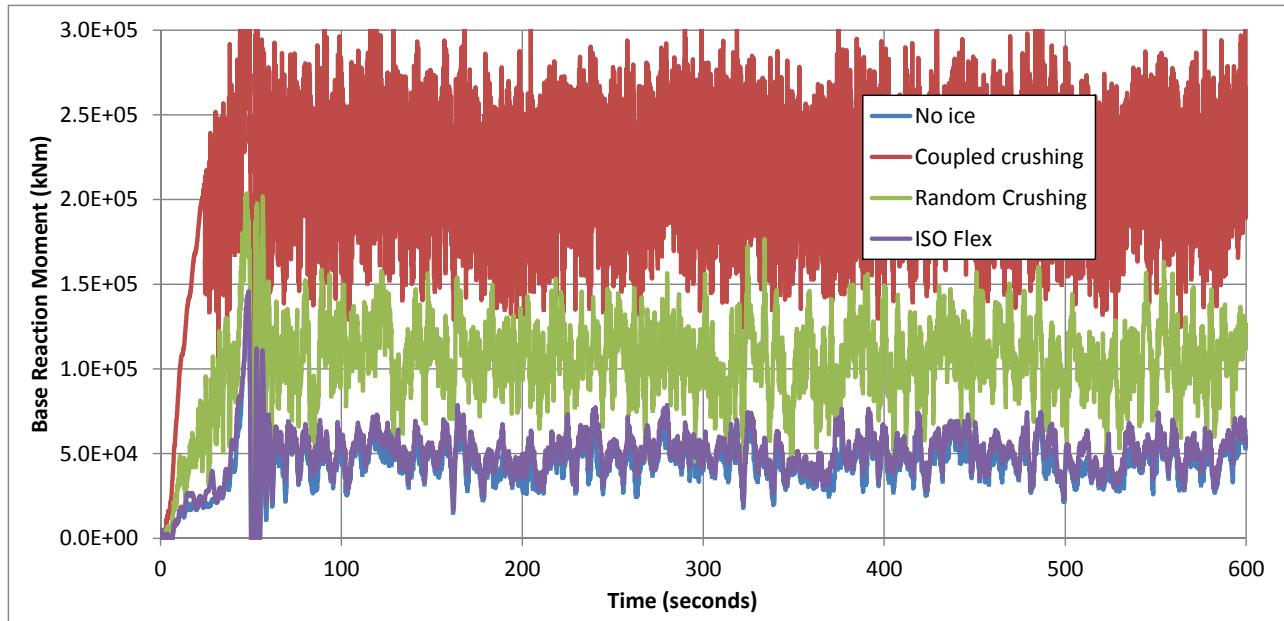


Figure 5-2 Time series of base reaction moments in 16 m/s turbulent wind in HAWC2

5.2 Bladed

The Bladed simulator, available from DNV GL, has a feature that allows the input of forces on any part of the wind turbine structure via data file. A model similar to the NREL 5 MW offshore model is available as an example model for Bladed and was run with similar conditions as the FAST testing. The check without gravity or aerodynamic forces is shown in Figure 5-3. Time series of base reaction moments for different ice models are shown in Figure 5-4. It is noted that since ice loads in Bladed are read from a pre-existing file, the coupled model cannot be run.

The stand-alone code that generates ice loads in Bladed format is available in the distribution of IceFloe on the NREL/NWTC website.

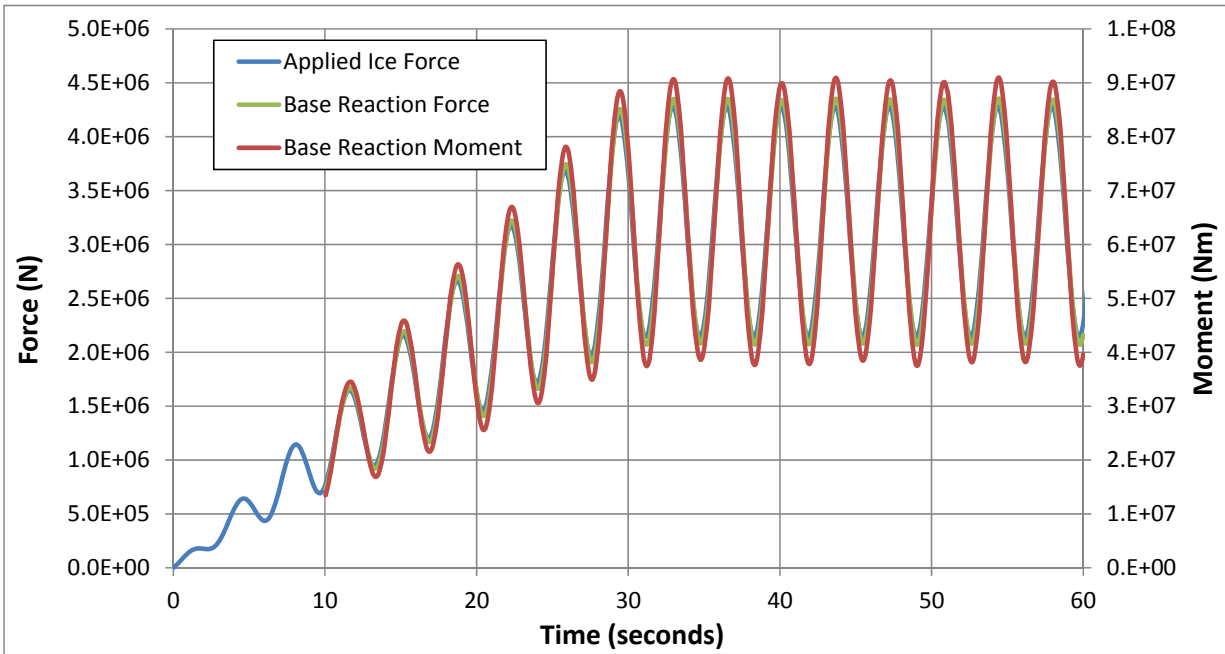


Figure 5-3 Check of ice force and base reaction loads in Bladed

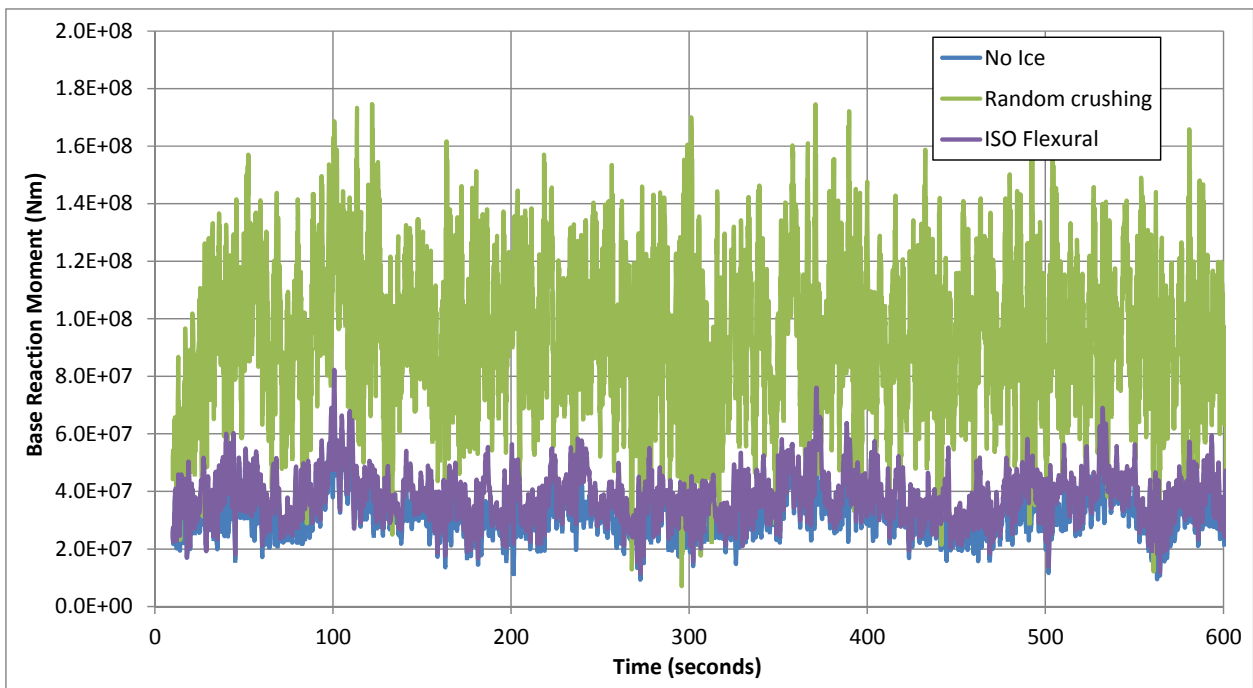


Figure 5-4 Time series of base reaction moments in 16 m/s turbulence in Bladed

5.3 ADAMS

The ADAMS simulator, available from MSC Software, in combination with Aerodyn (an aerodynamics software module developed by NREL), allows for the use of custom subroutines that provide forces to the simulation. The 5 MW offshore model in ADAMS format is available from NREL and was used to perform a check with gravity and aerodynamics turned off. The results are seen in Figure 5-5. The model was also run with similar conditions as the FAST testing, as shown in Figure 5-6 for multiple ice load models. It is noted that the coupled model results are somewhat different with ADAMS compared to FAST and HAWC2. This is likely due to the use of finite element formulations for the support structure in those codes as opposed to the multi-body formulation used in ADAMS. The former presumably allows for larger local deflections at the ice loading point. An example of the ADAMS interface code for the ice load dll is available in the distribution of IceFloe on the NREL/NWTC website.

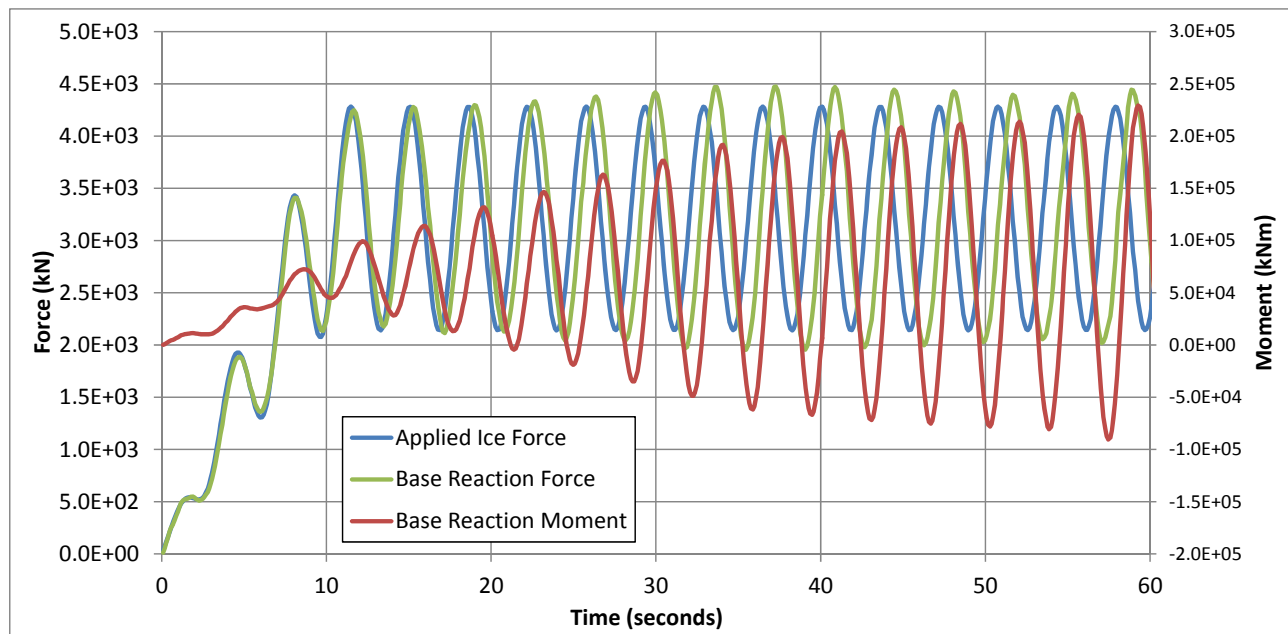


Figure 5-5 Check of ice force and base reaction loads in ADAMS

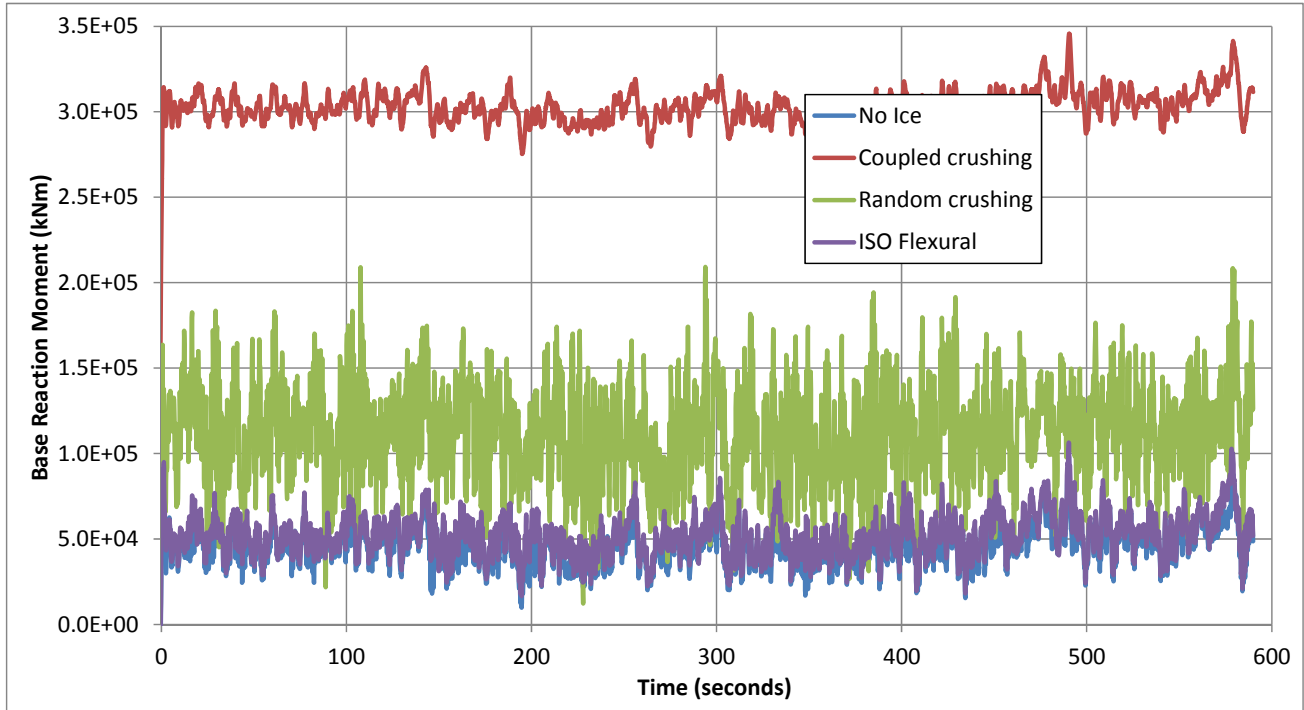


Figure 5-6 Time series of base reaction moments in 16 m/s turbulence in ADAMS

6 CONCLUSIONS

This project has resulted in the development and testing of subroutines that can be used to include the effect of ice loads on fixed bottom offshore wind turbines, particularly the support structures but also including other structural components. These routines include models that are consistent with the requirements of applicable standards and can be used with a variety of wind turbine aeroelastic simulation codes for extreme and fatigue loading.

Commercialization of this technology is achieved through distribution of the open source code on the NREL/NWTC website: <http://wind.nrel.gov/designcodes/simulators/IceFloe/>.

The primary lesson learned by the authors of this report is that ice loading will likely play a significant role in the design of offshore support structures for wind turbines located where surface ice can develop. In particular the assessment of historical icing conditions is of critical importance when making design calculations. These assessments must include probability distributions of ice thickness, speed of the ice sheets, and ice properties such as crushing or flexural strength.

Further, industry experience required to make these design choices with confidence is lacking. The effects of dynamic ice loading on a structure as flexible and dynamic as a wind turbine are still largely unknown. Frequency lock-in in particular is an area of concern and large uncertainty. In order to take advantage of the wind resources in ice prone offshore environments such as the Great Lakes, research, standardization, and testing and demonstration projects are all needed.

Mitigation approaches available to designers include the use of conical structures that allow ice to fail in bending rather than crushing. It is also clear that the coupled model should be used with care as the results are sensitive to model structure (i.e., multi-body vs. modal vs. finite element).



7 RECOMMENDATIONS

Based on the experience gained in the context of this project, it is clear that there are many challenges facing the designers of offshore structures with regard to surface ice loading. The uncertainties surrounding ice properties, motions, and failure modes lead to the need for conservative models. These issues will be highly variable from site to site and from year to year. It is imperative that a careful study be conducted of the local history of ice characteristics at a given location to inform the design of a support structure. These studies should include development of probability distributions of the parameters needed for load calculations.

To that end, an investment in ice monitoring at likely offshore wind sites is recommended. The measurements should include ice thickness, strength, and velocity with both spatial and temporal resolution. Demonstration projects to test various means of ice load mitigation would be of considerable benefit. Test programs to make measurements of the applied ice forces and understand the resulting wind turbine behavior are highly recommended. In particular the interaction between ice forces, turbine motions, and controls should be examined.

Lastly, the subject of ice loading should be addressed more comprehensively in the standards process. Issues such as combinations of wind, operation, and ice loading, fatigue versus ultimate loading, and others must be included to give guidance to support structure designers. Design of wind turbine support structures is based largely on reliability analysis wherein probabilities of both typical and extreme loading conditions are used in combination with strength distributions to achieve a target nominal reliability. To include ice loading in this framework will require providing careful guidance as to load combinations and how to treat the inter and intra annual variability of ice loading events. As with other standards, a review and update cycle on best practice for treating ice loads is recommended.

8 REFERENCES

- [1] Jonkman, Jason, *The New Modularization Framework for the FAST Wind Turbine CAE Tool*, 51st AIAA Aerospace Sciences Meeting, January 2013.
- [2] International Electrotechnical Commission, *Wind Turbines – Part 3: Design requirements for offshore wind turbines*, IEC 61400-3, Ed. 1, 11 February 2009.
- [3] International Standards Organization, *Petroleum and natural gas industries – Arctic offshore structures*, ISO 19906, first Edition, 15 December 2010.
- [4] <http://www.gl-garradhassan.com/en/software/GHBladed.php>
- [5] <http://www.mscsoftware.com/product/adams>
- [6] <http://www.hawc2.dk/>
- [7] Karna, T. et al., *A Spectral Model for Forces due to Ice Crushing*, Journal of Offshore Mechanics and Arctic Engineering, May 2006.
- [8] Korzhavin, K.N., *Action of Ice on Engineering Structures*, US Army CRREL Translation TL260, Hanover, N.H., USA, 1971.
- [9] Croasdale, K.R. and Cammaert, A.B., *An Improved Method for the Calculation of Ice Loads on Sloping Structures*, Hydrotechnical Construction, Vol. 28 No. 3, March 1994.
- [10] Ralston, T., *Ice Force Design Considerations for Conical Offshore Structures*, POAC Conference, 1977.
- [11] Määttänen, M., *Numerical Model for Ice Induced vibration load lock-in and Synchronization*, Proceedings of the 14th International Symposium on Ice, Potsdam, NY, USA, 1998, Vol. 2, pp 923-930.
- [12] Jonkman, J., et al., *Definition of a 5-MW Reference Wind Turbine for Offshore System Development*, NREL/TP-500-38060, February 2009.
- [13] Jonkman, J. et al., *Offshore Code Comparison Collaboration Continuations (OC4), Phase 1 – Results of Coupled Simulations of an Offshore Wind Turbine with Jacket Support Structure*, NREL/CP-5000-54124, March 2012.

APPENDIX A – THEORY OF ICE FORCES ON OFFSHORE WIND TURBINE PIERS

1. Introduction

Ice forces on bottom-fixed offshore structures are caused by the interaction between the moving ice feature and the fixed structure. The ice motion can be caused by the effects of wind and/or current, depending on the location. The interactive force between the ice feature and the structure is limited by a number of factors: the available kinetic energy of the ice feature, the limited force within the adjacent ice field, and the failure force of the ice feature at the interface with the structure. These are respectively referred to as: limit energy, limit force, and limit stress.

While the limit energy and limit force can be important and must be considered in a comprehensive probabilistic analysis of ice forces, it is usually assumed that there is sufficient energy and/or driving force to cause the ice to fail at the interface and hence the limit stress force is assumed to govern ice loads on structures.

Ice interaction behavior with fixed structures can take several forms, depending on the structure shape and ice feature characteristics. These behaviors include ice crushing and flexural failure of the ice against the structure, out-of-plane buckling of the ice feature, and far-field ice deformation, primarily ridging (see later discussion). However, the scale of wind turbine support structures generally precludes several of these forms of behavior that one might otherwise expect with larger structures, namely buckling and far-field deformation. These latter forms of behavior are more common when there is a limit force condition in which the force transferred to the fixed structure is limited by the available driving force, and this is a more likely occurrence when the structure is larger than a typical wind turbine support. The primary determinant of the limit stress ice behavior, where the ice actually fails when it comes into contact with the structure, is the structure's waterline shape. Shapes that are vertical, or near-vertical, will cause the ice to fail by crushing, whereas conical or sloping shapes will cause the ice to fail in flexure, either upward or downward, depending on the orientation of the sloped surface relative to the moving ice.

The loads caused by ice crushing depend on a number of parameters, including grain structure, temperature, brine content in sea ice, strain rate, ice thickness, and structure shape and size (scale). The effect of strain rate can cause the ice behavior to vary from creep to plastic deformation to brittle behavior. As the strain rate primarily depends on the ice speed, all forms of behavior are possible, and the resulting ice load across behaviors vary by several orders of magnitude (Sanderson, 1988). Ice crushing can also contribute a significant dynamic component to the interaction.

Flexural loads depend on some of the same parameters as crushing loads, but are less dependent on grain structure or ice temperature, and are largely independent of strain rate. However, they do depend on the friction between ice and the conical surface. Loads caused by ice failing in flexure are generally lower than those caused by ice crushing, but can be affected by the accumulation of ice rubble at the ice/structure interface that is the residue from the fracturing ice over time.

Regardless of the form of the ice failure, induced dynamics may occur. This is a result of the inherent randomness of the ice force with respect to time, or it may be caused by some coupling effect between the ice failure process and the structure. Ice failure dynamics can exhibit both random and cyclic characteristics,

with the latter form of behavior being of importance in wind turbine dynamics. Severe dynamic effects can occur when there is coupling between the ice failure dynamics and the structure dynamics.

Thus, to understand ice forces on structures, it is important to understand the behavior of ice at the temperatures normally encountered in ice-prone areas and to understand the nature of the possible interactions between the ice feature and the structure.

2. Ice properties and behavior

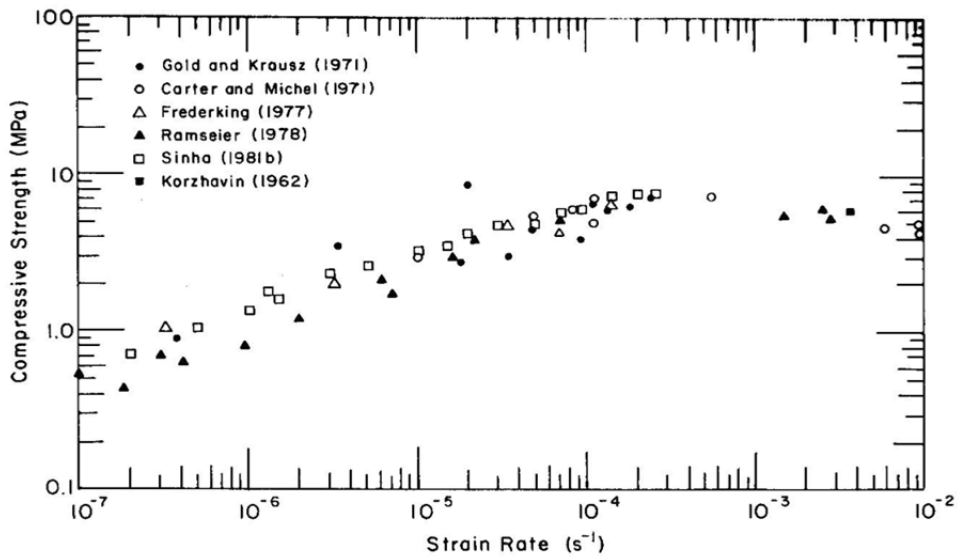
Lake and sea ice exist at temperatures close to their melting temperature, and thus their mechanical properties can be affected by temperature. This relationship is stronger with sea ice because of the presence of brine and the effect of temperature on brine volume. The mechanical properties are also affected by the crystal structure. While the characteristic ice crystal structure consists of tetrahedra of oxygen atoms, the structure looks like a honeycomb of parallel layers of slightly crumpled hexagons (Wadhams, 2000). However, these crystal structures can exist in a variety of different grain structures depending on how the ice has grown and the initiating process. Thus there exists columnar ice, and granular ice. One effect of this is that ice is neither homogeneous nor isotropic, though granular ice (as found for example in ice of glacier origin, e.g. ice islands, icebergs) is isotropic. These differences in grain structure can affect the ice mechanical properties at scales that are close to the scale of the grains – typically laboratory scale. However, at larger scales, i.e. those associated with ice interactions with offshore structures, these effects are not as significant.

The rate at which ice deforms can also affect its behavior. At very low strain rates, typically those associated with glacial processes, ice behavior is creep-like. At higher rates of deformation, typical of interactions between ice and fixed offshore structures, ice behaves in a ductile or brittle manner and the failure behavior is dominated by fracture processes. Ice is a very brittle material, with a fracture toughness (the mechanical property that defines brittle behavior) that is $1/10^{\text{th}}$ that of glass, and $1/1000^{\text{th}}$ that of steel. Thus, regardless of the mechanics of the ice failure process, fracture defines the behavior.

Because ice is a brittle material, its mechanical properties are scale dependent, similar to other brittle materials such as rock. Thus, the larger the loaded specimen, the lower the strength at failure, regardless of how the strength is defined. The relationship between strength and loaded area is not simple and is further complicated because non-deformed sea or lake ice in nature is thin in relation to its areal extent, and so may be in a state of plane stress, if loaded edge-on. Thus the aspect ratio of the loaded area (width/thickness) can also play a role in defining the effective failure strength.

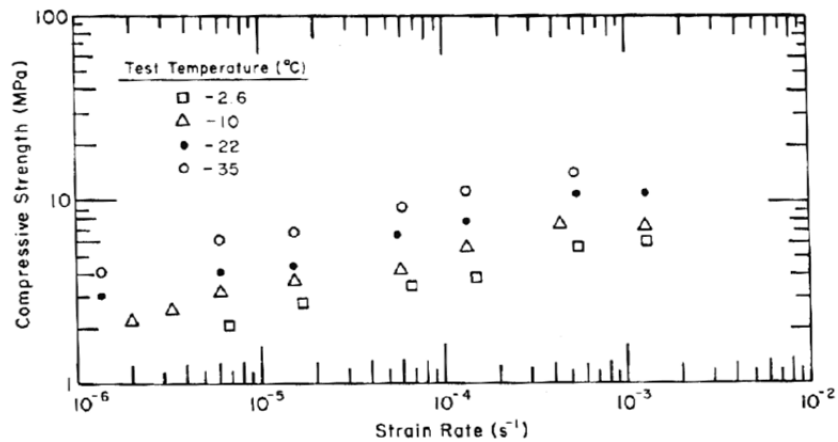
The mechanical properties of sea ice have received relatively more attention (see Timco and Weeks, 2011) than lake ice (see Ashton, 1986); nevertheless, most of the mechanical properties, and the effects of temperature, strain rate, and scale, are relatively well-defined.

Figure A-1 illustrates a typical plot of lake ice compressive strength for columnar grained (Ice Type S2) as a function of strain rate, showing an order of magnitude increase in strength for a strain rate increase from 10^{-7} to about 5×10^{-4} , where the transition between ductile behavior and brittle behavior takes place. Figure A-2 presents much of the same data, but also defines the temperature at which the tests were conducted, thus illustrating the importance of temperature. It is noted that the results presented in Figure A-2 are for pure polycrystalline ice (Ice Type T1), relevant to lake ice conditions.



Source: Ashton, 1986, with permission

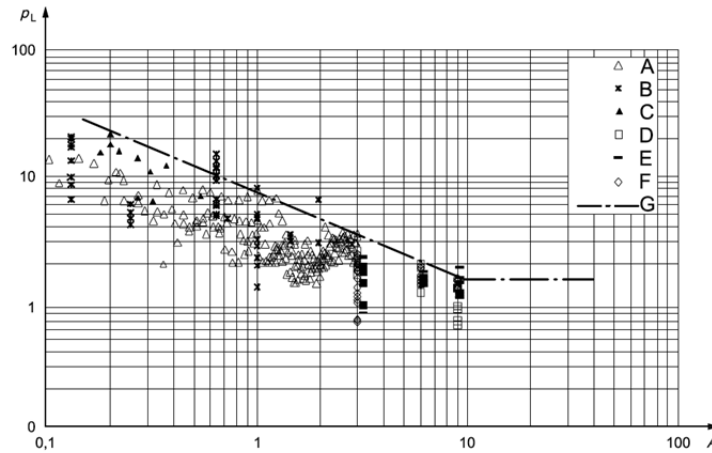
Figure A-1 Freshwater ice compressive strength as a function of strain rate at -10°C



Source: Ashton, 1986, with permission

Figure A-2 Effect of temperature on freshwater ice compressive strength

Figure A-3, originally developed by Sanderson (1988) but here taken from ISO 19906:2010 (ISO, 2010) illustrates the effect of scale on compressive strength for loaded areas up to 10 m². Although this plot suggests a leveling off for areas greater than 10 m², there is other evidence to suggest that the effective strength continues to decrease.



Source: ISO, 2010, with permission

Figure A-3 Strength of sea ice as function of loaded area

The strength of ice as used in expressions for the ice crushing force on fixed offshore structures is specified as the “reference strength” with values defined for typical specified ice conditions. For ice conditions that are not specified, it is beneficial to relate the reference strength to the compressive strength of ice for those conditions, using the same loading conditions as those used for the specified reference strengths.

Various expressions have been developed for the strength of ice. These have generally been developed either for ice behaving in a ductile manner, or ice behaving in a brittle manner. For the ductile behavior of sea ice, Timco and Frederking (1990) have provided expressions for the compressive strength of sea ice as functions of the strain rate and the total porosity of the ice. For horizontally-loaded columnar ice, they give the following expression:

$$\sigma_c = 37(\dot{\epsilon})^{0.22} \left[1 - \sqrt{\frac{v_T}{270}} \right] \quad (1)$$

As the porosity, v_T , is a function of temperature, the ice temperature is implicitly included as a variable in the strength equation. For freshwater ice, Timco and Frederking (1982) provide a similar expression but omit the bracket accounting for the porosity:

$$\sigma_c = 91(\dot{\epsilon})^{0.29} \quad (2)$$

This latter equation does not include v_T as a variable and thus leads to the compressive strength being independent of temperature, seemingly in contradiction to the results presented in Figure A-2. However, there are other influences, not captured by the expressions provided in Equations (1) and (2). These relate to the effects of grain size and type, and to stiffening of the ice matrix as the temperature decreases.

The total porosity used in Equation (1) is a combination of the porosity associated with brine accumulations and air porosity. The former is a strong function of temperature, while the latter is not (Cox and Weeks, 1983). Table A-1 presents some results on porosity for different levels of salinity and temperature for a bulk ice density of 0.90, using the expressions from Cox and Weeks (1983). The results presented in Table A-1

illustrate two offsetting trends: as the ice temperature decreases, the air volume (porosity) increases while the brine volume (porosity) decreases.

Table A-1 Total porosities

Temperature [°C]	Salinity (parts per thousand)			
	0	2	6	10
-2	18.83	24.55	35.98	47.41
-6	19.43	22.39	28.28	34.18
-10	20.04	22.45	27.27	32.10
-20	21.53	23.51	27.47	31.44

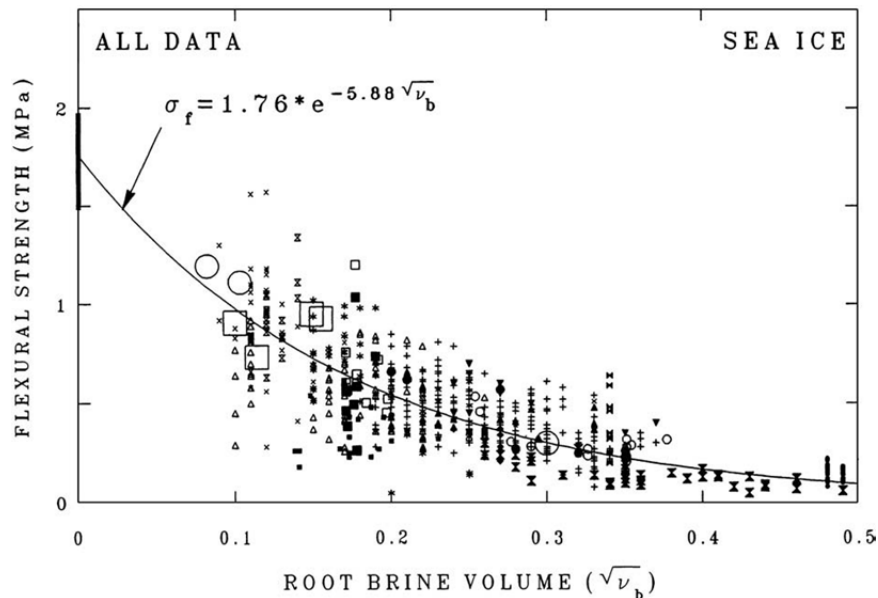
The reference strengths of ice of various types/conditions, for the same loading conditions (i.e. strain rate) are summarized in Table A-2. In addition, Table A-2 also provides the recommended reference strengths for the same ice. A strain rate of 5×10^{-4} has been used for the values in Table A-2; this represents the transition between ductile behavior and brittle behavior of the ice.

Table A-2 Ice strengths

Description	Compressive Strength [MPa]	Reference Strength [MPa]
Arctic ice, low salinity, cold	4.90	2.8 (ISO)
Baltic Sea ice, brackish, moderate salinity, warm	4.41	1.8 (ISO)
Freshwater ice, T1, no salinity, warm	6.0	0.5 – 3.0 (IEC) Depending on ice state and temperature.

These results do not provide a rational basis for the derivation of the reference strength from the compressive strength, and would suggest that the reference strength for Type T1 freshwater ice should be higher than that used for the Beaufort Sea. The peak value suggested by IEC (3.0 MPa) would seem to be an appropriate value, given the results provided in Table A-2.

The flexural strength of ice, important when ice is failing against sloping or conical structures, is subject to fewer functional relationships than compressive strength. The loading rate appears to have little or no effect, nor is there a strong relationship between flexural strength and scale (Timco and Weeks, 2010). For sea ice, however, there is a strong effect of brine volume (see Figure A-4), although it has been argued that the relationship should instead be with total porosity.

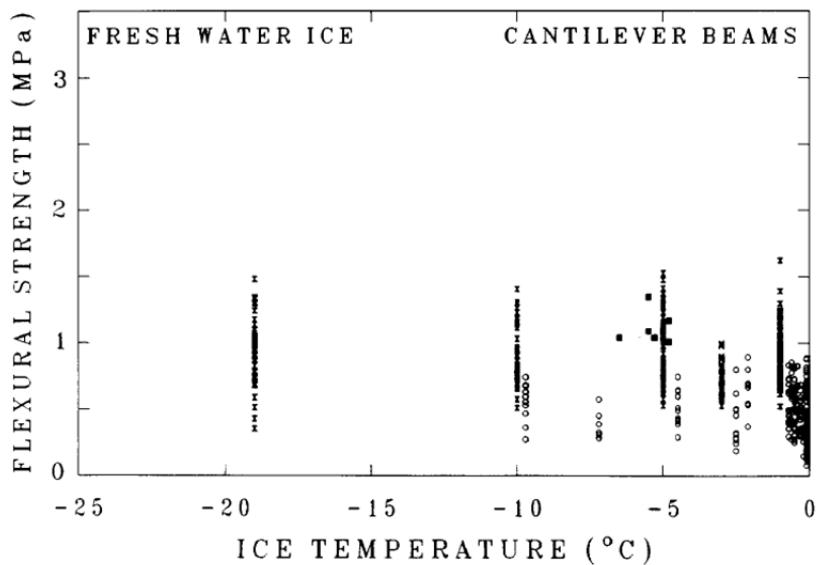


Source: Timco and O'Brien, 1994, Reprinted with permission from Elsevier

Figure A-4 Flexural strength of sea ice as function of brine volume

For freshwater ice, Timco and Obrien (1994) provide plots of strength as a function of temperature for two types of tests: simple beam tests and cantilever beam tests. They argue that the flexural strength should be based on the simple beam tests on the grounds that the cantilever beams results are affected by the stress concentration at the root of the in-situ beams when they are carved from an intact ice sheet. However, the failure process in flexural failure is dominated by cantilever action; therefore, it is the cantilever beam strength that is reported here. Figure A-5 (from Timco and Obrien, 1994) presents the results for cantilever beam tests for freshwater ice. Two aspects of this plot are important: the considerable scatter of the results, even when conducted at one temperature, and by one researcher (this is a result of the very brittle behavior of freshwater ice), and the relative independence of the strengths with respect to ice temperature. Figure A-5 does suggest a drop in strength as the temperature approaches the melting point due to the initiation of the melting process, though there is considerable uncertainty regarding the behavior at these temperatures.

Timco and Obrien (1994) recommend a value for the flexural strength of freshwater ice of 1.73 ± 0.25 MPa, based on simple beam tests. Figure A-5 suggests that this value is high for cantilever beams, and a value closer to 1.0 MPa is more appropriate.



Timco and O'Brien, 1994, Reprinted with permission from Elsevier

Figure A-5 Flexural strength of freshwater ice as a function of temperature

While there are many other mechanical properties for ice that have been studied and can be important under certain circumstances, the only other ice properties that are useful in the assessment of forces on wind turbine bases are the elastic modulus, E , and Poisson's ratio, ν . Values of the elastic modulus have been determined for single crystals and for ice sheets. Values range from a high of more than 9.0 GPa down to 1.0 GPa. Generally, a value of 4.0 GPa is used when required for ice force determination. A value of 0.3 for Poisson's ratio is appropriate.

When ice fails in flexure, broken ice pieces are formed that can ride up onto the conical structure and possibly form rubble piles. If a rubble pile forms, the bulk mechanical properties of the rubble pile are required in order to quantify the load necessary to move the rubble pile as the interacting ice sheet continues to move against the structure. Rubble piles are often assumed to behave as a Mohr-Coulomb material where the failure is assumed to occur along shear planes, and the shear strength is determined from the cohesive and frictional properties of the ice rubble.

Many field and model tests have been conducted in attempts to quantify these properties (see for example Palmer and Croasdale, 2013). However, there remains considerable uncertainty as to the appropriateness of the Mohr-Coulomb model and the appropriateness of the tests used to determine the cohesion and frictional properties. One issue that is generally agreed upon is that the two phenomena seldom occur simultaneously, as the amount of deformation necessary to cause the friction to be mobilized ensures that any cohesive bonds have already been broken.

Based on full-scale, in-situ tests, Palmer and Croasdale (2013) suggest that the shear strength of ice rubble is in the order of 10 kPa and that it has a weak dependence on the scale of the interaction.

3. Ice feature interactions

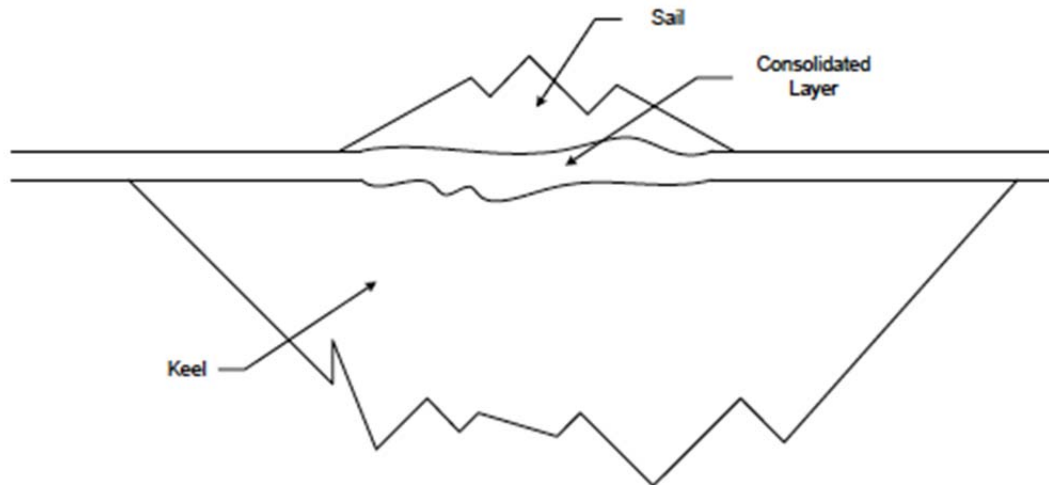
The characteristics of any interaction between floating ice and a fixed offshore structure depend on the nature of the ice feature, the shape and stiffness of the structure, the motion of the ice feature and the prevailing atmospheric conditions.

Floating ice in regions when only annual ice exists as opposed to multi-year ice and ice of glacial origin (icebergs and ice islands) consists predominantly of level ice that may also include rafted ice (two or more layers of ice superimposed on each other), and deformed ice, typically ice ridges and rubble fields. Ridges are formed when two discrete ice floes are pressed together (pressure ridges) or when one floe slides against a second floe (shear ridges). At the scales associated with ice-structure interactions, level ice is generally homogeneous with uniform thickness and mechanical properties. In practice, there are small variations in thickness and mechanical properties. Deformed ice consists of ice rubble, an agglomeration of discrete ice blocks that can be adfrozen together, or may be loose under the effects of gravity (above waterline) or buoyancy (below waterline). Figure A-6 illustrates the sail (above water) portion of a shear ridge.



Figure A-6 Rubble ice accumulation

Ridges generally consist of an above-water sail, a below-water keel and, at the waterline, a consolidated layer (Figure A-7).



Source: Obert, 2010, with permission

Figure A-7 Typical pressure ridge arrangement

The sail and keel both consist of loosely associated blocks of ice that, depending on the thermal regime since the formation of the ridge, may be adfrozen together, or may simply be in contact. The consolidated layer, existing at the water surface, will have re-consolidated; again, the extent to which this re-consolidation has taken place depends on the thermal regime. This layer, however, is often modeled as a uniform ice sheet.

Rafted ice is also modeled as a uniform ice sheet, but, because the layers are often not fully consolidated, the strength is generally lower than the strength of the original ice sheets.

As has been previously noted, the nature of the ice failure depends on the structure shape: vertical-sided structures cause level ice to fail by crushing, while sloped structures cause level ice to fail in flexure. As suggested above, rafted ice will fail in the same way. The consolidated layers of ridges are also assumed to behave in this manner when they interact with similarly-shaped structures. The unconsolidated rubble in the sails and keels of ridges is assumed to behave as a Mohr-Coulomb material, although the sail is often ignored. Failure is assumed to occur along planes defined by the maximum shear stress.

This is illustrated in Figure A-8 which shows a plan view of a typical plug failure of rubble by two essentially parallel failure planes. However, there are numerous different failure arrangements for the keels of first-year ridges that have been proposed (see for example, Dolgoplov et al., 1975; Croasdale, 1980; Cammaert et al., 1993).

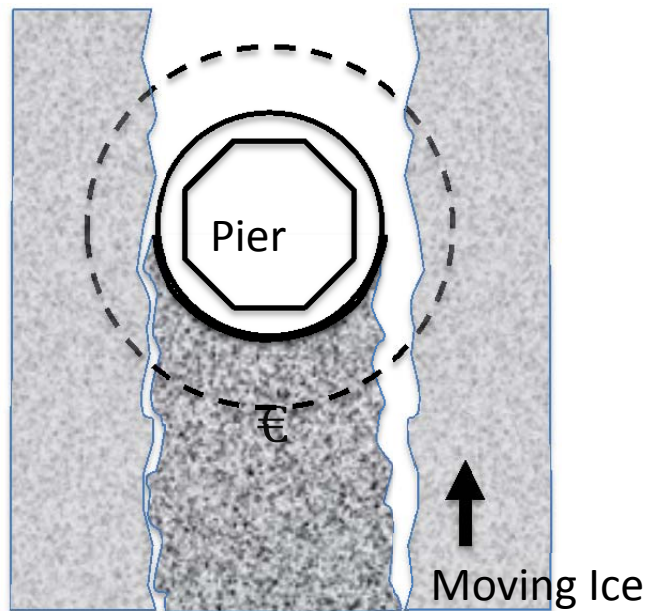


Figure A-8 Plug failure of rubble ice – plan view

The final form of interaction that needs to be considered is that associated with thermal expansion or contraction of an ice sheet. This can be important for structures close to shore or when structures are adjacent to each other and an ice sheet forms between them. Clearly, such forces are static, as the time scale for the development of these forces is large.

From the above, a number of ice parameters are required as input data for the determination of ice forces. While all of the following parameters can play a role in the resulting determination of forces, some are of greater importance than others. Thus, for each parameter, a narrative is provided as to its role in the force determination.

3.1. Ice thickness (h)

Thickness is a critical parameter, regardless of the failure mode of the ice. Although one might expect this parameter to be more critical in flexural failure, this is not necessarily the case, due to the contribution of other characteristics of the failure mechanics, including ride-up and pile-up of the broken ice pieces on the conical surface. Ice thickness is not necessarily uniform, despite surface appearances, because of differences in thermal effects due to the presence or absence of snow, and lake currents. Rafted ice consists of ice cover that has resulted from two or more uniform, relatively thin ice sheets colliding and rafting over each other. Rafting is common in ice thicknesses up to 10 cm (4 inches) and uncommon in thicknesses exceeding 30 cm (12 inches). Such ice can be thicker-than-normal, thermally-grown ice, but the interface is often not fully consolidated and so the ice is generally weaker than a single ice sheet.

3.2. Ice concentration and floe size

Ice concentration (usually reported in 10ths of the surface coverage): In low concentrations (less than 5/10ths), the necessary driving force conditions required to cause the ice to fail against the structure are generally absent.

Ice floe sizes: large floe sizes (or 10/10ths concentration) are required for the necessary confinement necessary for the maximum forces to occur. Small floes, unless present in very pressured ice, tend to split before the limit load is achieved.

3.3. Rubble piles / ride-up

During flexural failure of ice against sloping and conical structures, rubble piles or ride-up can occur. The morphological and mechanical properties of these formations are required for the determination of the resulting limit load.

Height of formation, h_r : Typically, this height is limited by the freeboard between the waterline and the transition between the cone and the cylinder above. This is assumed in the Ralston model (see Section 4.2.2 in this Appendix), but is specified in the Croasdale model (Section 4.2.1 in this Appendix). With small cones, the rubble pile may reach higher than the transition but not more than one quarter the diameter of the cylinder ($w_T/4$).

Angle of rubble pile, θ : This angle cannot be greater than the angle of the cone itself, α . ISO 19906 suggests that an angle equal to the cone angle implies only ride-up, but observations from both the Confederation Bridge (southern Gulf of St. Lawrence, Canada) and from Baltic Sea studies have shown that bilinear rubble pile profiles are possible, and the lower angle of the rubble pile could be the same as the cone angle (see Figure A-9). Obviously, this form of rubble pile requires additional input parameters; however, the important thing is that the volume of the rubble pile is properly accounted for.

Porosity of rubble, e : Observations from Confederation Bridge (Tibbo, 2010) have indicated that values between 0.1 and 0.3 are possible. For the thicker ice normally associated with upper bound loads, the larger value is appropriate.

3.4. Ice strength

Of similar importance as ice thickness, the ice strength, or more generally, the ice mechanical properties are important in determining ice forces on fixed offshore structures. For the two common ice failure processes, the compressive strength (crushing, C_R) or the flexural strength (bending, σ_f) is required. Because C_R is a reference value, data on the compressive strength (σ_c) of ice local to the region of interest can be used to determine an appropriate C_R value. Similarly, the bending strength used should be based on the local ice conditions at the location under consideration, accounting for both the climate and ice type.

3.5. Other ice mechanical properties

Other mechanical properties required in the determination of the forces associated with flexural failure include:

- **Modulus of elasticity, E (MPa):** A default value of 4 GPa is often used.

- **Poisson's ratio, ν :** A value of 0.3 is appropriate.
- **Rubble properties:**
 - **Cohesion, c (kPa):** 0 to 5 kPa
 - **Friction angle, ϕ :** 35° to 50°

These latter properties can vary significantly depending on how long the rubble is present and stationary. If the rubble pile is in continuous motion, the cohesion, c , will have a low value, possibly zero. However, if the rubble pile is stationary, the cohesion will increase as consolidation occurs.

3.6. Other parameters required

Ice to ice friction, μ_i : Typically a value of 0.05 is used.

Ice to structure friction, μ_s : Depends on structure surface type and roughness. For concrete, a value of 0.2 is often used; for steel, a somewhat lower value (0.15) is used, but both are highly dependent on the condition of the surface.

Ice density, ρ_i : Ice density varies within a narrow range, depending on temperature. A value of 917 kg/m³ is median to this range.

Water density, ρ_w : Depends on temperature, reaching a maximum at 4°C. However, its role in the determination of ice forces is minor, and a value of 1000 kg/m³ is appropriate.

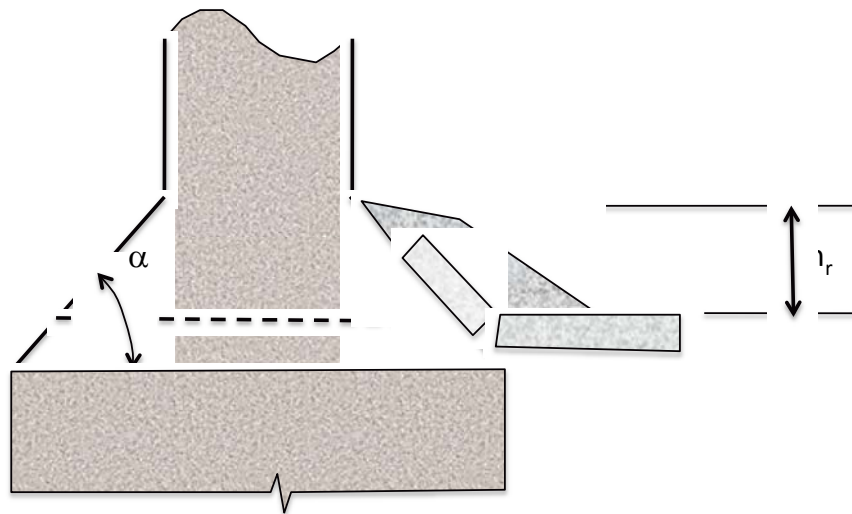


Figure A-9 Bi-linear rubble pile profile

4. Ice limit forces

The particular type of interaction that will occur depends on the nature of the ice feature and the geometry of the structure. As the types of ice feature present in first-year ice regions are limited, the interaction type

is more influenced by the structure geometry. Two principal forms of ice failure are then possible, depending on the geometry of the turbine tower at the waterline. A vertical (cylindrical) structure will cause the ice to fail by crushing; a sloped structure (conical) will cause the ice to fail in flexure. These two forms of behavior are illustrated in Figure A-10.

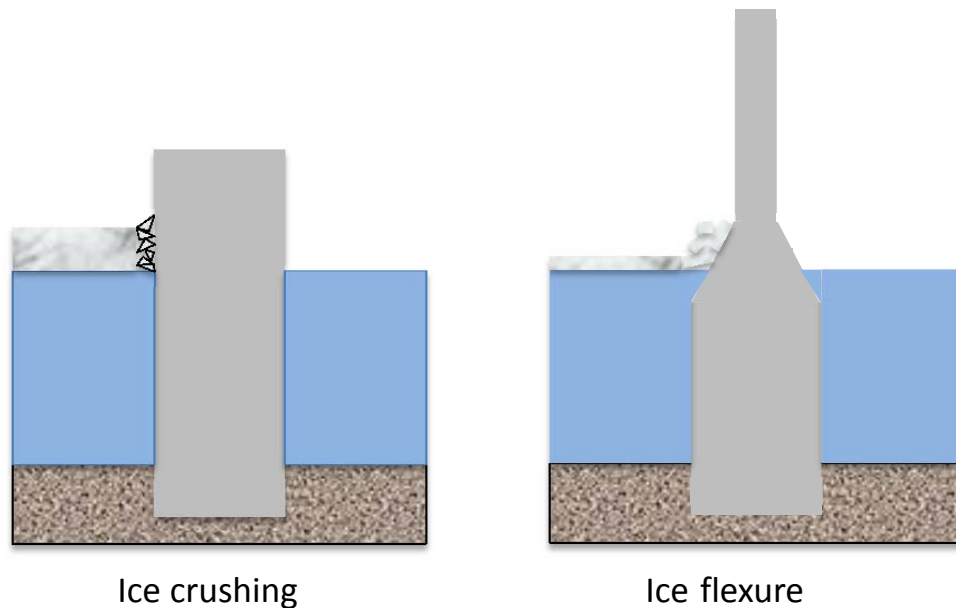


Figure A-10 Typical ice failure modes

The slope at which the transition between flexural failure and crushing failure occurs is not fixed and depends on the coefficient of friction between the ice and the structure surface. It is generally acknowledged that structures with slopes greater than 70° to the horizontal will experience ice crushing, while structures with lower slopes will experience ice flexural failure.

Both forms of behavior may be accompanied by dynamics, which is addressed in a later section. However, the peak loads used for the dynamic analyses are often taken as the limit load, hence the derivations presented in this section.

4.1. Ice crushing

The determination of the forces associated with ice crushing should be straightforward: an effective crushing pressure multiplied by the contact area between the ice and the structure. However, although this is the general form of the expressions, the determination of the effective crushing pressure is not simple, and there are numerous different approaches. These approaches attempt to capture the effects of: scale, aspect ratio, the degree of contact between the ice and the structure, and the confinement within the ice sheet. Some of these require attributes of the structure in order to be properly defined, specifically structure width and shape.

One of the initial approaches to ice crushing loads is ascribed to Korzhavin (1971), and his approach, sometimes with modifications, is still in use today. In recent years, empirical data have been used to determine crushing loads with the acknowledgement that the Korzhavin equation was overestimating crushing ice forces, and that some of the parameters were difficult to properly define. Both approaches require the selection of an ice strength, often referred to as the reference ice strength.

Currently, ISO 19906 proposes an approach for the determination of ice forces due to crushing that relies on empirically-derived corrections to a reference strength, while IEC (IEC 61400-3) proposes the Korzhavin equation. Both approaches are described herein.

4.1.1. Ice crushing limit per ISO 19906

For ice crushing, the global limit load is given by ISO 19906 as:

$$P = p_G h w \quad (3)$$

$$p_G = C_R \left(\frac{h}{h_1} \right)^n \left(\frac{w}{h} \right)^m$$

where:

p_G is the global average ice pressure [MPa]

C_R is the ice reference strength [MPa]

w is the projected width of the structure [m]

h is the ice thickness [m]

h_1 is the reference ice thickness (1.0 m)

m is an empirical constant (-0.16)

n is an empirical constant dependent on ice thickness:

$$n = (-0.5 + h/5, h < 1.0 \text{ m}; -0.3, h > 1.0 \text{ m})$$

C_R depends on the ice regime and the severity of the winter, ISO 19906 provides two values, both based on annual probabilities of exceedance of 10^{-2} . These are for the Beaufort Sea (2.8 MPa) and the Baltic Sea (1.8 MPa). The ice reference strength can be influenced by structure stiffness – thus the value for the Baltic Sea was derived for structure displacements that were less than 0.4% of the ice thickness. For fresh water ice, an appropriate ice reference strength should be used. No guidance is provided but a value much in excess of the value recommended for the Beaufort Sea would be excessive, even allowing for the higher strength of fresh water ice. Accordingly, values between 1.0 MPa and 3.0 MPa may be expected, depending on the location and the ice regime (Schwarz, 1970; Timco and Frederking, 1982).

The ISO approach to ice crushing forces includes two terms that account for the effects of scale and aspect ratio. As indicated previously, these are empirical and are derived from measurements from both the Beaufort Sea and the Baltic Sea (see Kärnä and Masterson, 2011).

4.1.2. Ice crushing limit per IEC

The IEC standard recommends using the Korzhavin equation for the limit force due to ice crushing against a vertical structure which is given as:

$$P = k_1 k_2 k_3 h w \sigma_c \quad (4)$$

where:

w is the projected width of the structure [m]

h is the ice thickness [m]

k_1 is a shape factor

k_2 is a contact factor

k_3 is a factor based on the aspect ratio

σ_c is the ice crushing strength [MPa]

The shape factor, k_1 , can take two values:

$k_1 = 1.0$ for rectangular shapes

$k_1 = 0.9$ for circular shapes

The contact factor, k_2 , accounts for the level of contact between the moving ice sheet and the structure. It typically can take two values, but IEC introduces a third value to account for locally thickened ice around the structure. Local thickening occurs only when the ice is stationary around the structure for extended periods. IEC does state that this third case can be accounted for by using a greater ice thickness instead.

$k_2 = 0.5$ for moving ice

$k_2 = 1.0$ for frozen in ice

$k_2 = 1.5$ for locally thickened ice

The factor for aspect ratio, k_3 , can be likened to the $(w/h)^m$ term of the ISO expression for crushing loads. In the Korzhavin equation, the factor takes the form:

$$k_3 = \sqrt{1 + 5h/w} \quad (5)$$

The values for the crushing strength should be determined from statistical data of crushing strength or of the product $\sigma_c h$. The available data should be corrected for the actual temperature and brine content in order to carry out a statistical analysis of the reference crushing strength.

In the event no local ice data are available for the crushing strength, σ_c , IEC suggests the following values which are typical for the Northern Baltic Sea and Arctic Canada:

- 3.0 MPa for ice in motion from wind and current at the coldest time of the year;

- 2.5 MPa for moving ice at a very low velocities caused by thermal expansion or shrinking;
- 1.5 MPa for ice during spring at temperatures near the melting point;
- 1.0 MPa for partly deteriorated ice at temperatures near the melting point; and
- 0.5 MPa for saline first-year ice in the open sea, e.g. in the North Sea.

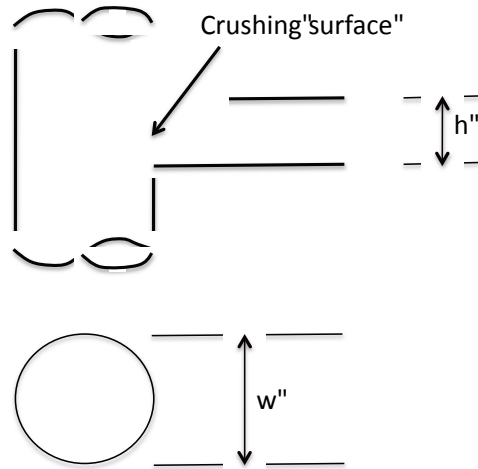


Figure A-11 Ice crushing – vertical structure

Ice crushing can also result in very high local pressures, depending on the degree of confinement and the rate of the interaction. Whether or not this is important depends on the detailed nature of the structure at the waterline: steel-framed structures will require assessment for these pressures; thick-walled concrete structures are unlikely to require assessment.

Ice crushing can also result in a significant dynamic component to the interaction, which has led to difficulties with some offshore structures in the Baltic Sea and Bohai Bay, China (Määttä, 1998, Yue et al., 2009). Although there are several theories to explain this behavior, the actual cause is not yet fully understood, although it is clear that some form of self-excitation takes place and that the resulting condition can result in resonance. This behavior could result in significant dynamic effects being transferred to the above-water structure and may influence the behavior of the wind turbine.

It is useful to compare the limit loads associated with the two approaches to crushing failure, that of ISO with that of IEC. The following plots compare these loads for two different structure widths, 2 m and 4 m, and for two different sets of reference strengths:

- The ISO value of 2.8 MPa, typically recommended for the Beaufort Sea, and thus an extreme value, with the maximum 3.0 MPa crushing strength recommended by IEC; and
- The value of 1.8 MPa recommended by ISO as representative of the Baltic Sea environment with the value of 1.5 MPa recommended by IEC for spring conditions. Note that the 2.5 MPa value suggested by IEC is for thermally-induced ice strains.

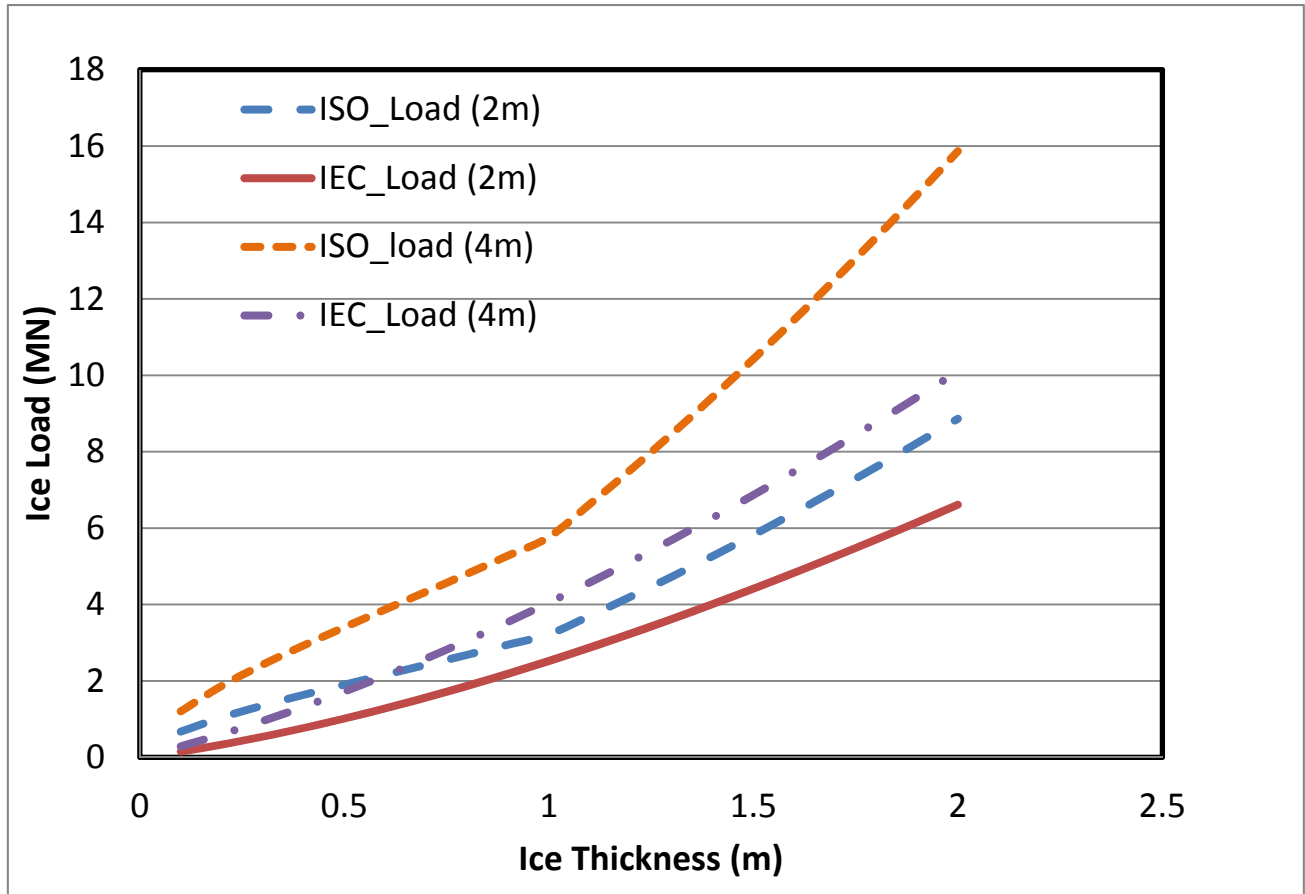


Figure A-12 Comparison of ISO 2.8 MPa with IEC 3.0 MPa

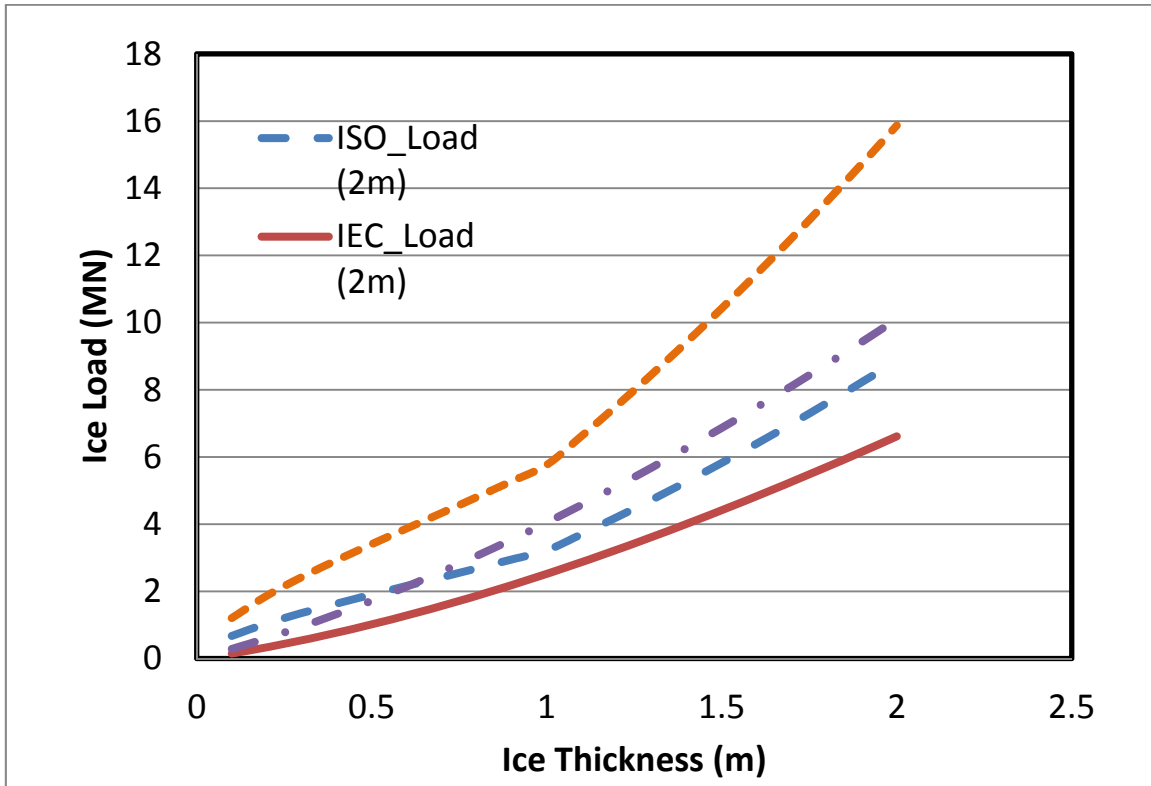


Figure A-13 Comparison of ISO 1.8 MPa with IEC 1.5 MPa

In all cases, the IEC values are lower than the ISO values with the divergence becoming more pronounced at the larger ice thicknesses. There are also significant percentage differences between the two approaches at very low thicknesses (< 0.3 m), but there is some question as to the applicability of the ISO formulation at these thicknesses. In Figure A-12, for the higher ice strengths, the results for the 2 m diameter structure are very similar, except at the low thicknesses.

As the ISO approach is more rigorously based on field indentation measurements, it is the recommended approach, but it is beneficial if both approaches result in similar limit loads. For comparison, the peak load measured in model tests on a 5 m diameter turbine base for a Danish development (Gravesen et al., 2005) was approximately 5 MN for an ice thickness of 0.57 m. Figure A-14 compares ISO results with the 1.8 MPa reference strength and a value of 2.2 MPa used with the IEC formulation. The IEC formulation is still below the ISO formulation, particularly at ice thicknesses in the range of 0.5 m to 1.0 m, which is the most probable range of peak ice thicknesses in waters where wind turbines would be deployed. However, the comparison over the full range of ice thicknesses is reasonable.

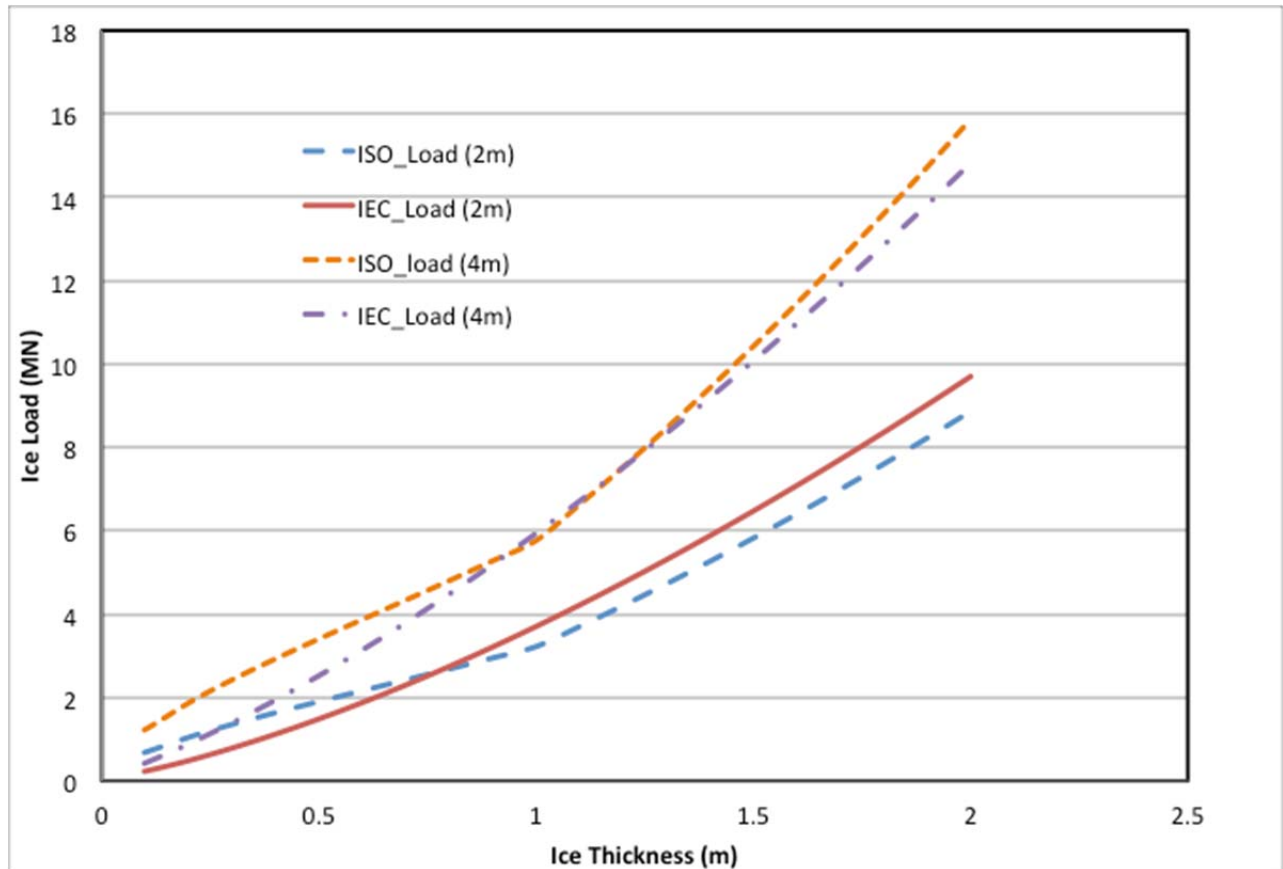


Figure A-14 Comparison of ISO 1.8 MPa with IEC 2.2 MPa

4.2. Ice flexural failure

Loads caused by ice failing in flexure are generally lower than those caused by ice crushing, but can be affected by the presence of ice rubble caused by the ice failure process. This is more of a problem with upward-breaking conical structures than downward-breaking ones, although the issue can be a problem with the latter in the absence of currents that might clear the rubble. They also depend on the friction between ice and the conical surface.

Although dynamic behavior has been seen in association with flexural failure, it is less common, and seems to be associated with very specific conditions, e.g. the absence of snow cover on the ice surface and relatively high temperatures that result in a very low ice-to-ice coefficient of friction (Yue et al., 2007). This results in the absence of a rubble pile and a potentially cyclic flexural failure process. The presence of rubble seems to eliminate dynamic effects in flexural failure (Brown et al., 2010).

For ice flexural failure, the guidance provided in ISO 19906, while based on well-established algorithms, can be improved with recent models that have been shown to better predict full-scale measurements (Mayne, 2007, Tibbo, 2010). These can be used for conically-shaped waterline structures, and can incorporate the effects of rubble piles on upward-breaking cones, and the effects of submerged rubble on downward-

breaking cones. However, as they have not been fully tested and validated, it is premature to propose their use in a publicly available design application.

For ice flexure, there are a number of different approaches that have been used to obtain the upper bound static ice load. ISO 19906 discusses two approaches: a plasticity-based approach (Ralston, 1979) and an elastic-beam-on-elastic-foundation approach (Croasdale, 1994, 2012). Other approaches are available (e.g. Nevel, 1992, and Mayne, 2007). The latter model, while based on observed ice behavior, has not been widely verified at this time. Accordingly, the Croasdale model is recommended. This model has recently been modified to improve the rubble pile modeling.

Flexural failure of ice on sloping and conical structures involves out-of-plane failure of the ice sheet as it interacts with the sloping structure surface. Depending on the structure arrangement, this can be upward breaking or downward breaking. This failure can lead to broken ice blocks being pushed up the surface of the structure (ride-up). Further accumulations of ice blocks can occur both on the surface of the ice sheet and cone, and under the ice sheet. These are ice rubble accumulations and can lead to very substantial accumulations on the conical surface (rubble pile). It has been postulated that both ride-up and rubble piles can occur simultaneously, but observations from Confederation Bridge (Brown et al., 2010) indicate that the presence of a rubble pile can prohibit ride-up, unless very thick ice (relative to the structure size) is being broken. Observations in Bohai Bay (China) (Yue et al., 1998) have shown that ride-up can occur with an absence of rubble piles. This occurs with relatively thin uniform ice and the absence of snow on the surface of the ice. Similar observations have been made at Confederation Bridge but are rare, as snow on the surface of the ice is common.

The rubble pile is often modeled as a Mohr-Coulomb material, with its strength defined by cohesion and an internal friction angle. The cohesion can depend on the history of the rubble pile, with rubble piles that are in continuous motion having very low cohesion, and rubble piles that remaining stationary for some time having high cohesion.

4.2.1. Ice failure limit per the Croasdale model

The flexural ice failure load, including the effects of rubble pile, is obtained from a series of formulae, each term of which represent different effects:

$$F_H = H_B + H_P + H_R + H_L + H_T \quad (6)$$

The breaking load, H_B , is given by:

$$H_B = 0.68 \xi \sigma_f \left(\frac{\rho_w g h^5}{E} \right)^{1/4} \left(w + \frac{\pi^2 L_c}{4} \right) \quad (7)$$

where:

$$\xi = \frac{\sin \alpha + \mu_s \cos \alpha}{\cos \alpha - \mu_s \sin \alpha} \quad (8)$$

$$L_c = \left[\frac{Eh^3}{12\rho_w g(1-\nu^2)} \right]^{1/4} \quad (9)$$

ξ is termed the resolution factor, relating the horizontal load to the vertical load required to break the ice and L_c is the critical length, based on the theory of beams on elastic foundation. Other terms are defined as:

- α , the slope angle of the structure;
- μ_s , the coefficient of friction between ice and structure;
- σ_f , the flexural strength of the ice;
- ρ_w , the density of water;
- E , the elastic modulus of ice; and
- ν , Poisson's ratio for ice.

The other terms for the flexural failure load account for different components of the ride-up and rubble pile effects. Thus, H_p is the load required to push the incoming ice sheet through the rubble:

$$H_p = wh_r^2 \mu_i \rho_i g (1-e) \left(1 - \frac{\tan \theta}{\tan \alpha} \right)^2 \frac{1}{2 \tan \theta} \quad (10)$$

where:

- h_r is the height of the rubble;
- μ_i is the ice-to-ice coefficient of friction;
- e is the porosity of the rubble;
- θ is the angle the rubble pile makes with the horizontal; and
- ρ_i is the density of the ice.

H_R is the load required to push the ice blocks through the rubble and up the slope of the structure:

$$H_R = wP \frac{1}{\cos \alpha - \mu \sin \alpha} \quad (11)$$

$$P = 0.5 \mu_i (\mu_i + \mu) \rho_i g (1-e) h_r^2 \sin \alpha (\cot \theta - \cot \alpha) \left(1 - \frac{\tan \theta}{\tan \alpha} \right) +$$

$$\dots 0.5 (\mu_i + \mu) \rho_i g (1-e) h_r^2 \frac{\cos \alpha}{\tan \alpha} \left(1 - \frac{\tan \theta}{\tan \alpha} \right) + h_r h \rho_i g \frac{\sin \alpha + \mu \cos \alpha}{\sin \alpha}$$

where P is effectively the weight of the rubble pile.

H_L is the force required to lift the rubble pile that is on top of the advancing ice sheet:

$$H_L = 0.5wh_r^2\rho_i g(1-e)\xi(\cot\theta - \cot\alpha)\left(1 - \frac{\tan\theta}{\tan\alpha}\right) + \dots 0.5wh_r^2\rho_i g(1-e)\xi\tan\phi\left(1 - \frac{\tan\theta}{\tan\alpha}\right)^2 + \xi cwh_r\left(1 - \frac{\tan\theta}{\tan\alpha}\right) \quad (12)$$

where:

- c is the cohesive strength of the ice rubble;
- ϕ is the friction angle of the ice rubble.

The final load component, H_T is the force required to rotate the blocks of ice at the transition between the conical surface and the upper cylindrical surface:

$$H_T = 1.5wh^2\rho_i g \frac{\cos\alpha}{\sin\alpha - \mu\cos\alpha} \quad (13)$$

Which of these 4 terms describing the load associated with a rubble pile is used, depends on the particular interaction. Observations from Confederation Bridge have so far failed to indicate any evidence of blocks being turned back on themselves at the transition (H_T). Rather, the blocks tend to slide sideways as they clear from the conical surface. Similarly, although some ride-up may be occurring between the structure surface and the superimposed rubble pile, it certainly does not occur to the full height of the rubble pile, h_r .

ISO 19906 recommends that the flexural strength of the ice sheet be modified to account for the pre-stress effect of the in-plane force in the ice sheet. Thus:

$$F_H = \frac{H_B + H_P + H_R + H_L + H_T}{1 - \frac{H_B}{\sigma_f l_c h}} \quad (14)$$

$$l_c = w + \frac{\pi^2}{4} L_c$$

where l_c is the length of the circumferential crack.

4.2.2. Ice failure limit per the Ralston method

The Ralston model is based on plastic behavior of the ice and is widely cited. The IEC Standard includes only the Ralston model in its Annex on ice forces. While the version provided in the IEC Annex is based on the use of several graphs, the version here is taken from the ISO 19906 Annex, which is based on formulae. The total force is given by:

$$F_H = H_B + H_R \quad (15)$$

where H_B is the breaking term and H_R is the ride-up term. Ralston does not explicitly consider pile-ups, although they can be approximated by selecting higher ride-up thicknesses. The breaking term is given by:

$$H_B = \frac{\sigma_f h^2 \tan \alpha}{3(1 - \mu g_r)} \left[\frac{1 + Yx \ln x}{x - 1} + G(x - 1)(x + 2) \right] \quad (16)$$

where Y is based on the yield criteria selected for the analysis. The value provided for the Tresca criteria is:

$$Y = 2.711$$

And G is a non-dimensional term relating the weight to the strength of the ice:

$$G = \frac{(\rho_i g w^2)}{(4\sigma_f h)} \quad (17)$$

$$x = 1 + \left(3G + \frac{Y}{2} \right)^{-0.5}$$

$$g_r = \frac{\sin \alpha + \frac{\alpha}{\cos \alpha}}{\frac{\pi}{2} \sin^2 \alpha + 2\mu \alpha \cos \alpha}$$

where the latter two terms derive from the application of the plasticity theory to the failure of the ice sheet and the associated velocity field.

The ride-up term, H_R , is then given as:

$$H_R = W \frac{\tan \alpha + \mu E_2 - \mu f g_r \cos \alpha}{1 - \mu g_r} \quad (18)$$

where W , the weight of the ice ride-up on the cone, is given as:

$$W = \rho_i g h_d \frac{w^2 - w_T^2}{4 \cos \alpha} \quad (19)$$

$$f = \sin \alpha + \mu E_1 \cos \alpha$$

E_1 and E_2 are the complete elliptic integrals of the first and second kind:

$$E_1 = \int_0^{\pi/2} (1 - \sin^2 \alpha \sin^2 \eta)^{-0.5} d\eta \quad (20)$$

$$E_2 = \int_0^{\pi/2} (1 - \sin^2 \alpha \sin^2 \eta)^{0.5} d\eta$$

all of the variables are as previously defined, with the addition of the following:

h_d is the ride-up thickness. To properly model pile-ups, this should be taken as 2 to 3 times the ice thickness, h ; and

w_T is the top diameter of the cone.

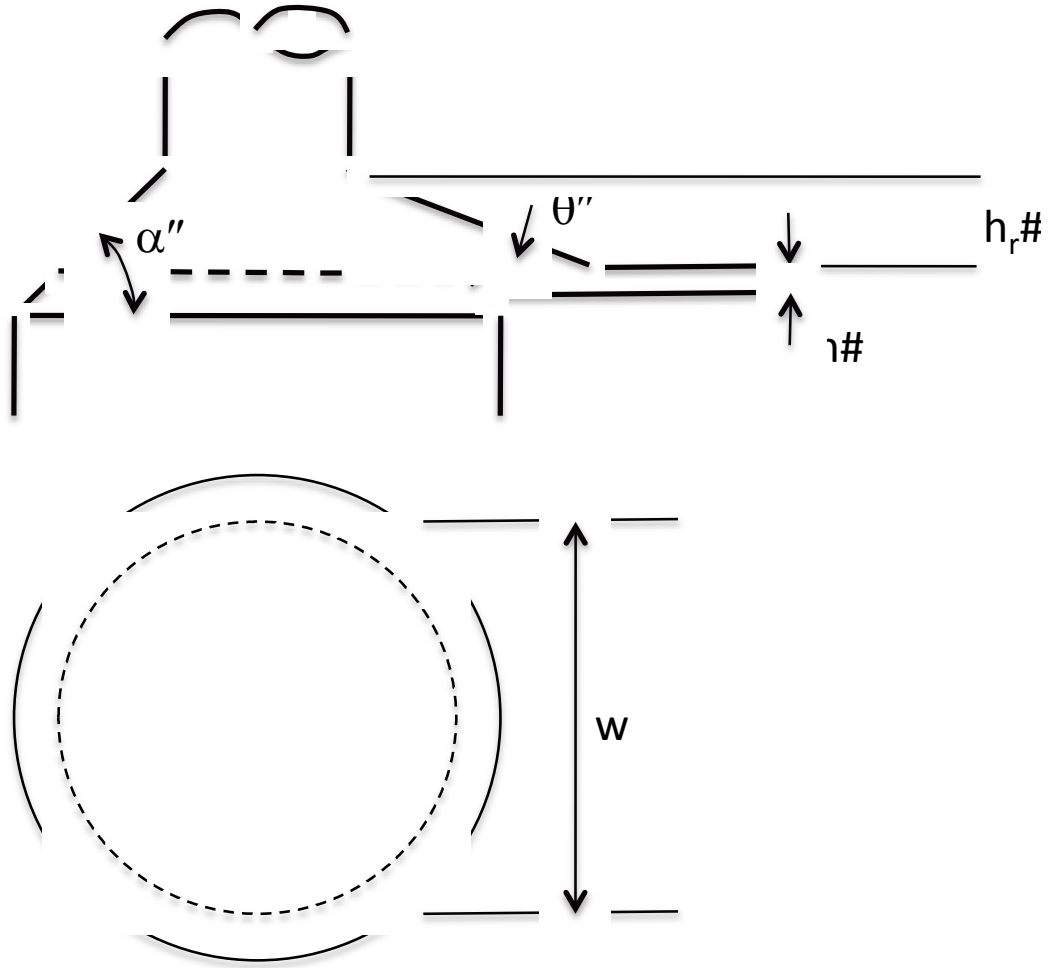


Figure A-15 Flexural failure

5. Dynamic ice forces

5.1. Crushing (vertical or near-vertical structures)

It is generally acknowledged that there are four characteristic forms of dynamic behavior when ice crushes against a vertical structure, and the dynamics in each case are quite different. Which specific form of behavior actually occurs primarily depends on the velocity of the interaction, or more accurately the strain rate in the interacting ice. As the structure may be flexible, the velocity of interaction is often described as the relative velocity between ice sheet and structure. Thus, one often sees reference to behavior with “rigid” structures, and behavior with “compliant” structures. These forms of behavior and the associated dynamics are:

Creep or plastic deformation: low relative velocities, resulting in sustained forces without any significant dynamic component, thus considered a static load. In small-scale laboratory tests, the resulting pressures are often very high as the creep deformation is in-plane and the scaled strength is high. In field tests, the

resulting pressures are much lower, because the behavior is out-of-plane, resulting in creep-buckling of the ice sheet.

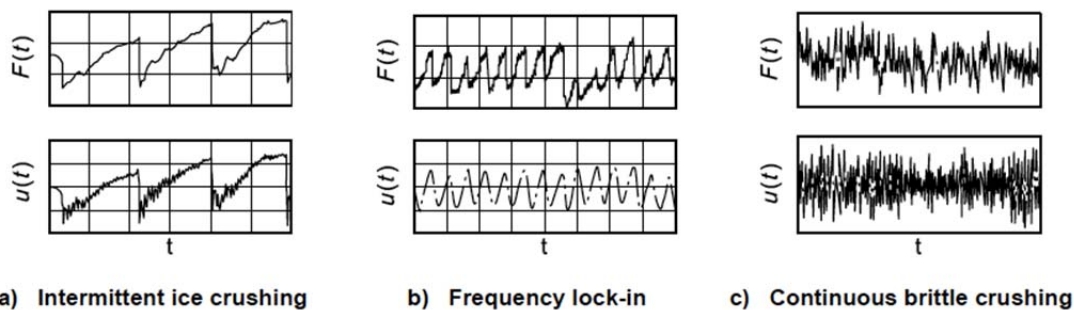
Intermittent crushing: intermediate velocities, resulting in loads that are dynamic, which may or may not have a regular pattern either in peak ice load or in period of interaction. The peak load is governed by brittle crushing of the interacting ice, although the load rise is governed by creep behavior.

Lock-in: This is a special case of intermittent crushing at intermediate velocities where the ice load frequency generally matches that of the structure. This behavior can result in highly amplified response of the structure. This behavior has been experienced both in wide structures such as the Molikpaq drilling platform (Jefferies and Wright, 1988) and in narrow structures (Määttänen, 1978).

Continuous crushing: highest velocities resulting in a sustained crushing load but with low amplitude random vibrations. Here the pressures are lower than at intermediate velocities, though very high local pressures may occur.

Of these behaviors, the third is the one of most concern, and the one that has received considerable attention in the literature. There have been several examples of this behavior in full scale, and these have resulted in damage and operational issues with offshore oil and gas platforms.

More recently, the fourth form of behavior has also received considerable attention, partly from the European studies based on the Norströmsgrund lighthouse in the northern Baltic Sea (Kärnä et al., 2006). This work has attempted to establish a dynamic model for the behavior, and the relation between the peak pressures and ice thickness and aspect ratio.



Key

- t time
- F ice action
- u structure displacement

Source: ISO, 2010, with permission

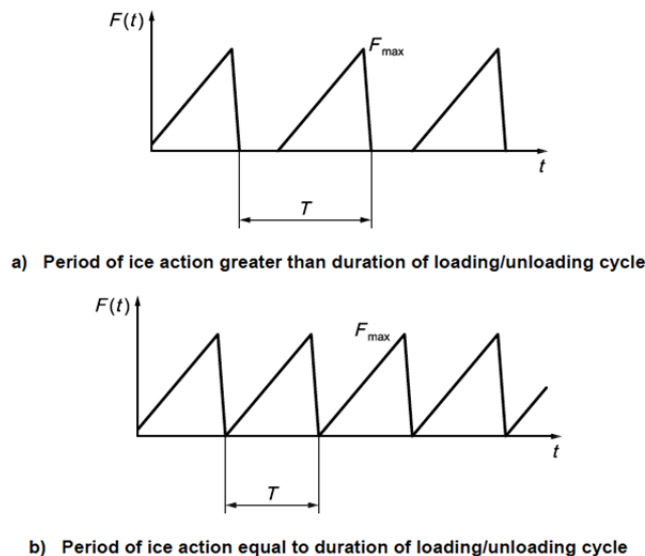
Figure A-16 Modes of time varying action due to ice crushing and corresponding structure dynamic response

Figure A-16, taken from ISO 19906, gives comparative time series of both the ice forces and the structural response corresponding to the three forms of dynamic ice crushing interaction (omitting the low-velocity creep behavior).

ISO 19906 provides excellent guidance on dynamics associated with crushing failure. This guidance is based on many of the studies referenced above which, in turn, are based on observations of the dynamic behavior of structures subject to ice forces.

5.1.1. Intermittent crushing

The load build-up can be governed by creep/plastic processes of the interacting ice, while the peak load is governed by crushing. The load drop is controlled by the amount of damping in the structure. Although Figure A-16(a) above shows a continuous process, this is not necessarily the case, and there could be a period of zero load between the load pulses, especially if the load drop is governed by far-field processes such as floe splitting. The period of the load pulses is greater than the largest natural period of the structure (lowest frequency), so there is no "lock-in" between the load frequency and the structure frequency. Figure A-17 illustrates the time function to be used for the analysis of the effects of intermittent crushing. The peak load is the limit force as described in Section 4 in this Appendix and the period of the load cycle will depend on the ice velocity but will be longer than the lowest natural frequency of the structure.



Source: ISO, 2010, with permission

Figure A-17 Ice load time function for intermittent crushing

5.1.2. Frequency lock-in

Frequency lock-in is in fact a special case of the intermittent crushing described above, and is a difficult phenomenon to fully define. The lock-in condition is certainly the most significant form of ice failure against a vertical structure, and there is enough experience to be confident that it can occur, and can be dangerous to the structure. While there are several examples of this behavior on structures that vary from 110 m in



width to those that are less than 10 m in width, there are many more examples of structures where this behavior has not been observed.

Although the transition from intermittent crushing to lock-in has been investigated, there is no accepted theory as to how it occurs. The view of many is that as the ice fails in one location within the contact zone, the stress on the adjacent ice is suddenly increased, leading to its failure and so on. As this continues, the failures tend to occur closer and closer together in time, until they are synchronized and lock-in occurs. Obviously, there has to be a structural effect here in that the structure must be able to deflect back as the ice fails and starts the next failure sequence. However, there is at least one example where this did not occur and the frequency of the failure reduced throughout the interaction as the ice velocity decreased.

Palmer and Bjerkas (2013) in a very recent paper have postulated a fairly simple approach to explaining the transition from intermittent crushing to frequency lock-in. They present a model that shows how the failure transitions from intermittent or continuous crushing to the lock-in condition, based on transitioning of the phase angles between otherwise independent ice failure mechanisms. Their model is more applicable to large-scale crushing where the contact zone is divided into a number of discrete ice failure zones rather than to independent ice failure zones.

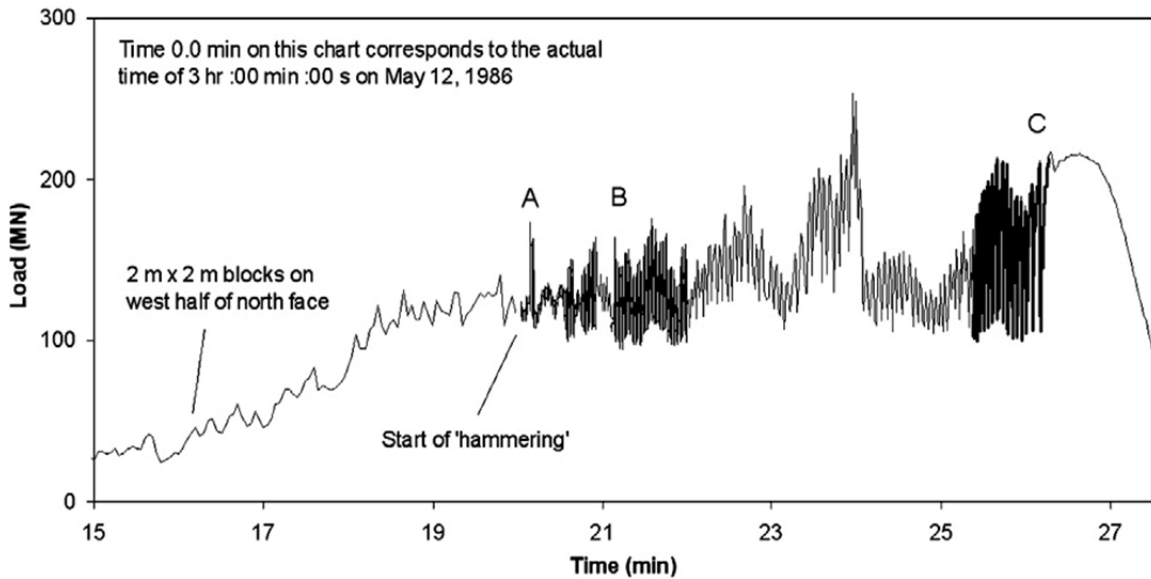
Lock-in or “phase-lock” behavior has been recorded on light piers in the Baltic Sea, the drilling platform Molikpaq in the Beaufort Sea, by Chinese jacket structures in Bohai Bay, and at bridge piers in Alberta. The first observation was probably made by Määttänen (1978) on light piers in the Baltic Sea. Jefferies and Wright (1988) describe the experiences of the Molikpaq, and Lipsett and Gerard (1980) describe the dynamic force fluctuations on the Alberta bridge piers.

5.1.2.1. Molikpaq

Jefferies and Wright (1988) report on the behavior of the Molikpaq during the event of 12 April 1986, when the vibrations were severe enough to initiate liquefaction of the sand core and prompted preparations for the crew to abandon the structure (they were all on the helicopter ready to leave the structure). The load period was about 0.7 seconds, which coincided with one of the natural periods of the structure.

Exactly one month later, the structure again experienced vibrations over an extended time period, during which the ice floe slowed down considerably, ultimately resulting in creep behavior and no vibrations.

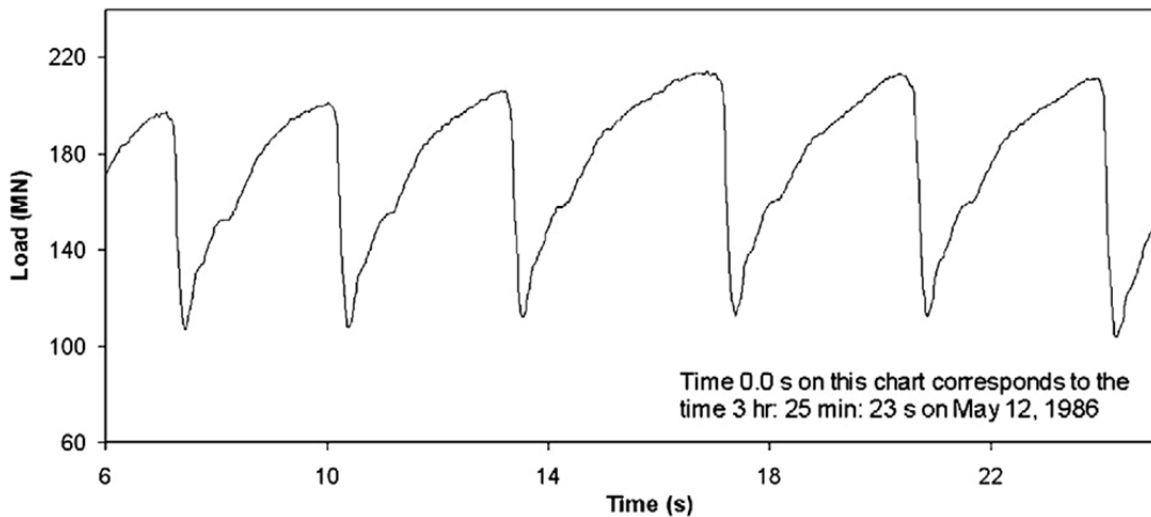
Figure A-18 shows the entire load history for a later event and Figure A-19 shows a snapshot of the load history immediately before the onset of the creep behavior.



Source: Gagnon, 2012. Reprinted with permission from Elsevier

Figure A-18 Molikpaq Load History, 12 May 1986

The entire history is recorded at 1 Hz, but the darker areas are when high-speed trigger data was being recorded (Gagnon, 2012). Figure A-19 is taken from the portion marked "C" in Figure A-16.



Source: Gagnon, 2012. Reprinted with permission from Elsevier

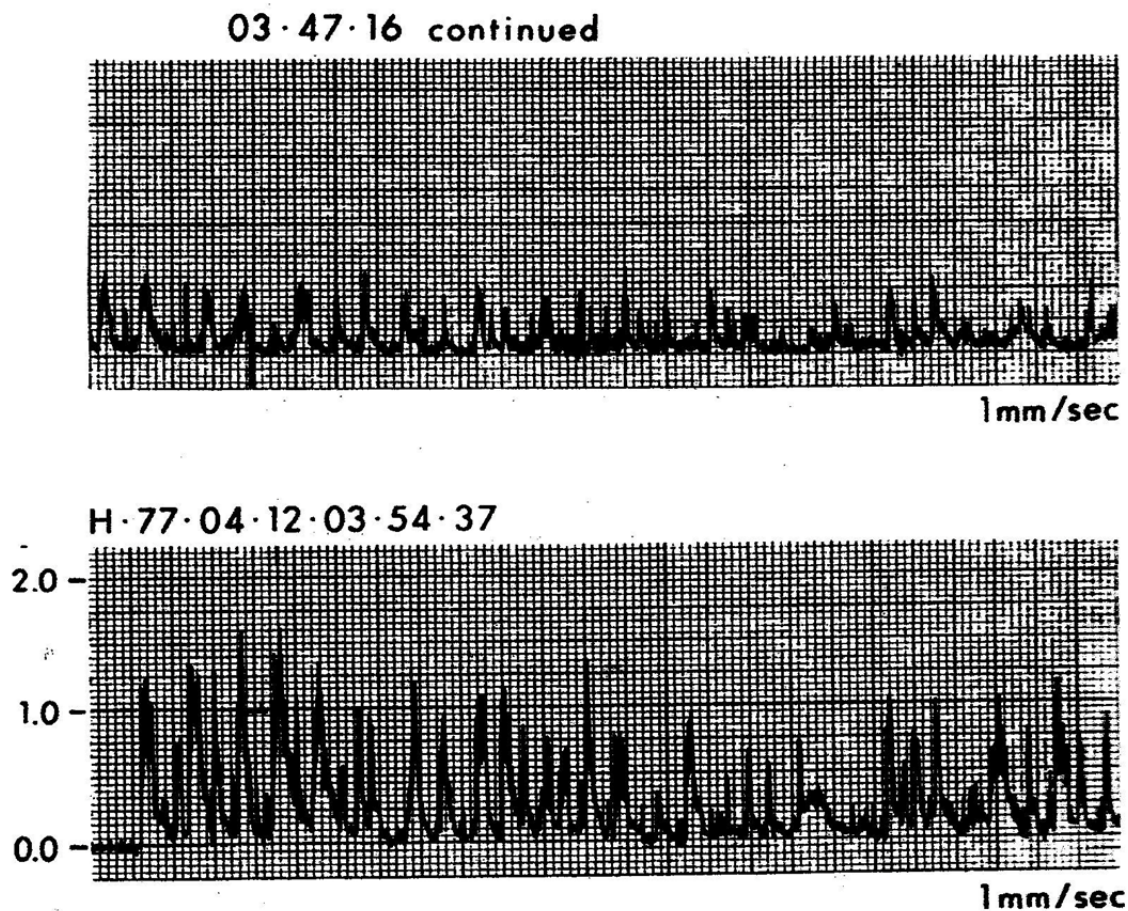
Figure A-19 Molikpaq Load History from late on 12 May 1986

Figure A-19 indicates that the load period has stretched, as the speed decreased, to between 3 and 4 seconds, from the load period of 0.7 seconds that had occurred at the beginning of the interaction, similar to

the behavior on April 12. This behavior suggests that resonance is not a requirement for this form of ice failure behavior, although clearly the consequences for the structure are more severe if there is resonance.

5.1.2.2. Hondo Bridge

Figure A-20 illustrates two load sequences recorded at the Hondo Bridge in Alberta in 1977. The upper trace corresponds to crushing failure while the lower trace corresponds to flexural failure. The pier is quite steep with an angle to the horizontal of 77° . In the case of the Hondo bridge, resonance is not occurring, so the dynamics associated with the ice force are simply due to the failure behavior of the ice.



Source: Lipsett and Gerard, 1980

Figure A-20 Hondo Bridge Load Traces

Lock-in can occur for a range of ice conditions but there are some restrictions. There must be sustained motion of the ice from one direction during which the ice is fairly homogeneous in the horizontal plane. Significant variations in thickness, and the presence of cracks and flaws will mitigate against any significant dynamics in the ice load trace and certainly mitigate against lock-in behavior.

However, lock-in can occur at any ice velocity if it provides the necessary conditions.

The ISO statement whereby the structure response velocity should be 1.4 times the ice velocity should not be given a lot of emphasis. The use of this criterion would imply an iterative process that would result in the software system being less generic. The limit on damping is more critical.

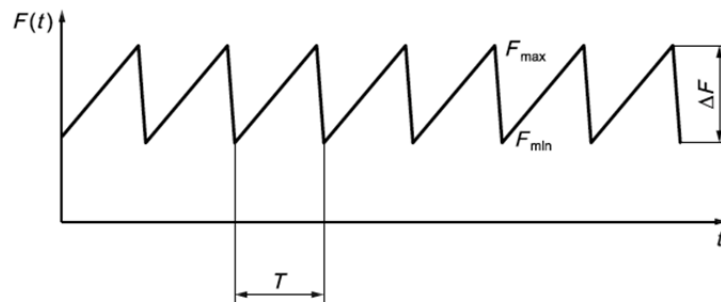
ISO 19906 has suggested that the occurrence of this behavior depends on the damping present in the structure, as well as the matching frequencies. Effectively, if there is sufficient loss of energy due to damping to offset the energy input from the ice failure process, then the lock-in behavior will not result in significant amplification of the response. It is proposed that if the damping ratio for the frequency, ξ_n , being considered is large enough, then lock-in need not be considered:

$$\xi_n \geq \frac{\phi_{nc}^2}{4\pi f_n M_n} h\theta \quad (21)$$

where:

- ϕ_{nc} is the non-normalized modal amplitude at the ice action point;
- M_n is the modal mass (in kg);
- f_n is the frequency of the eigenmode (in Hz);
- h is the ice thickness (in m);
- θ is a constant for which the suggested value is 40×10^6 kg/m-s;

On the basis that there are structural frequencies for which lock-in is possible, the analysis is carried out using an ice load function similar to that shown in Figure A-21.



Key	
t	time
F	ice action
F_{\max}	maximum value of ice action
F_{\min}	minimum value of ice action
ΔF	difference between maximum and minimum values of ice action
T	period of ice action

Source: ISO, 2010, with permission

Figure A-21 Ice load time function for lock-in conditions

The maximum ice force is that obtained from the assumption of a static ice force, and the period is selected to match the structural frequency for which the analysis is being undertaken. ISO 19906 suggests that the double amplitude (peak-to-peak range) should range from 0.1 to 0.5 of the maximum force; however, most observations of lock-in conditions have been associated with the higher end of this range, so a value of 0.4 is proposed, meaning that F_{\min} is equal to $0.6F_{\max}$.

ISO 19906 goes on to suggest that the amplitude of the load function should be adjusted such that the velocity response of the structure at the point of application of the ice load is 1.4 times the velocity of the approaching ice sheet. As this is not normally known, an equation is provided, based on observations with slender structures with natural frequencies up to 5 Hz:

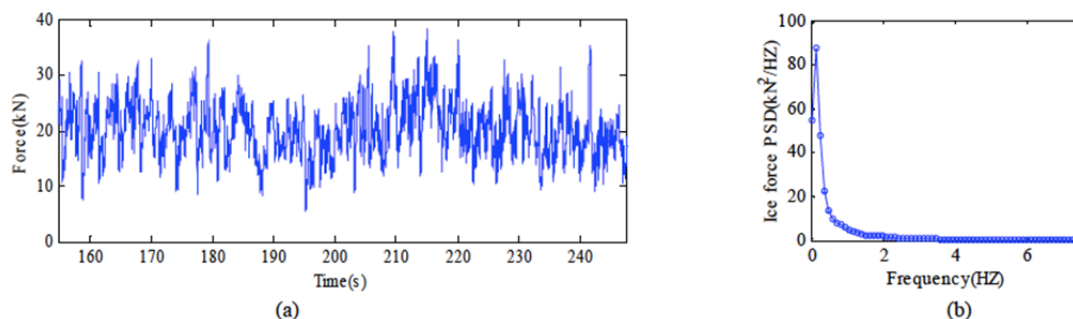
$$v = \gamma_v f_n \quad (22)$$

with γ_v taken as 0.060 m. This suggestion has not been implemented in the proposed model.

The frequency lock-in (or phase-lock) behavior clearly depends on both the characteristics of the ice and the structure. The behavior occurs because the structure reacts to the dynamic ice load in a particular manner. In some cases, a model designed to capture this behavior would include both the ice and the structure – a coupled ice-structure interaction model. This is described in more detail in Section 6 in this Appendix.

5.1.3. Continuous Crushing

Figure A-22 (Kärnä et al., 2007) provides an example of the ice load time series during continuous crushing. One can note that the average ice load is sustained for the entire duration and that the time variations tend to be random. This is further supported by the autospectral function plotted in the right hand graph, which shows no dominant frequency content to the ice load signal.



Source: Kärnä et al., 2007. Reprinted with permission from Elsevier

Figure A-22 Typical ice load time series and corresponding spectrum during continuous crushing

Karna et al. (2007) use spectral analysis based on continuous crushing data, to determine the peak ice force based on a static mean component, and a time-varying component, the maximum value of which is determined on the basis of a statistic in the form of standard deviations of the dynamic ice load. They suggest that a dynamic analysis may be required but do not provide strong guidelines as to when or how this should occur.

Analysis is carried out for a dynamic load event using an autospectral density function for the dynamic component of the load, $F(t)$. The load is then given as:

$$F_{total}(t) = F_{mean} + F(t) \quad (23)$$

The mean load is obtained from the maximum load (the limit load) and the probability of exceedance associated with the maximum load.

$$F_{max} = F_{mean} + k\sigma \quad (24)$$

Using the maximum limit load previously obtained, then k , the number of standard deviations (σ) between the mean and maximum should be in the order of 4 to 5. The standard deviation is defined from an empirically-derived intensity function:

$$I = \sigma / F_{mean} \quad (25)$$

Based on observations, the intensity, I , varies between 0.2 and 0.5, with a mean value which is in the order of 0.35 to 0.4. A value of 0.4 is recommended. Using Equations (24) and (25), the mean and standard deviation can then be obtained from the maximum limit load as:

$$\sigma = \frac{I}{1 + kI} F_{max} \quad (26)$$

$$F_{mean} = \frac{F_{max}}{1 + kI}$$

The variance in the force then defines the dynamic component. Kärnä et al. (2006) use an autospectral function to define the variance as a function of frequency, based on observations of continuous crushing on structures in both Bohai Bay and the northern Baltic Sea. In order to compare load functions from different field programs, Karna and his co-authors use a non-dimensional form of the autospectral function:

$$\tilde{G}(f) = \frac{fG(f)}{\sigma^2} \quad (27)$$

and obtain equations for the non-dimension form, $\tilde{G}(f)$ by curve-fitting to autospectral density functions of measurements of ice forces on load panels. This resulted in a relationship between the non-dimensional function and frequency as follows:

$$\tilde{G}(f) = \frac{af}{1 + k_s a^{1.5} f^2} \quad (28)$$

where:

$$a = bv^{-0.6}$$

and v is the ice velocity. Values of k_s and b are given as 3.24 and 1.34, respectively. Figure A-23 illustrates the resulting autospectral density functions.

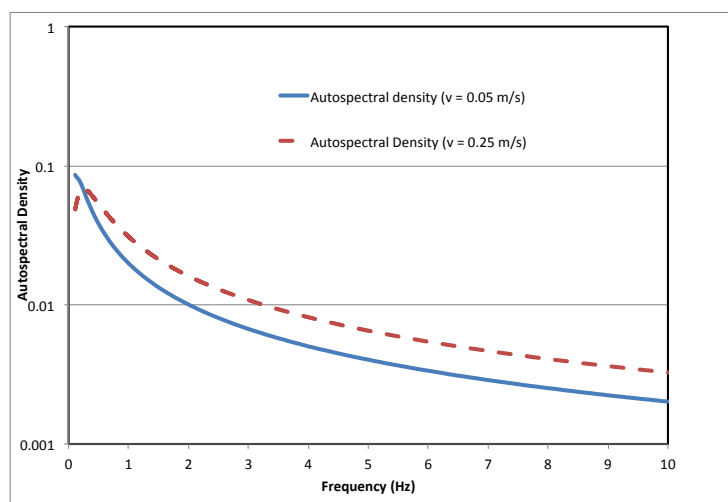


Figure A-23 Autospectral density functions for continuous ice crushing

5.2. Flexure (sloping structures)

Unlike the behavior with respect to vertical structures, in which the dynamics are governed by strain rate and the relation between the ice velocity and the structure response, dynamics during flexural failure appear to be more dependent on the ice interaction processes than any other factor, though structure flexibility may be important. Field programs (Confederation Bridge, Kemi-1, Bohai Bay jacket structures) have provided conflicting information on dynamics during flexural ice failure. The former two programs did not experience any “lock-in” dynamics similar to the form experienced with ice crushing, while the latter program did.

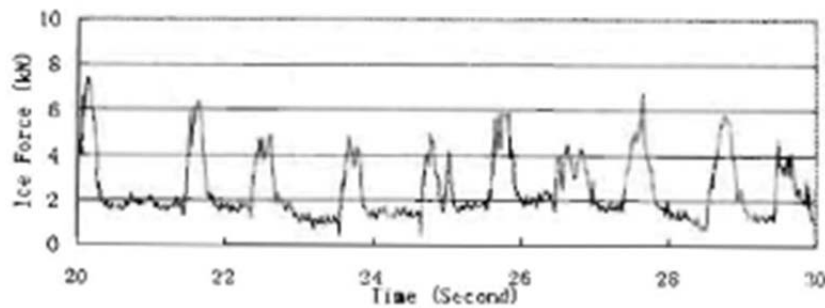
The three field programs can be summarized as follows;

- Confederation Bridge (southern Gulf of St. Lawrence): Concrete conical piers with a 52° cone angle, 14.2 m diameter at mean sea level. Level ice thicknesses range up to almost 1.0 m with consolidated layers of ridges up to 2.5 m. Ice is often snow covered so the ice/ice coefficient of friction will be relatively high (Brown and Bruce, 1997).
- Kemi-1 (Gulf of Bothnia, Baltic Sea): Steel lightpier with a 56° cone, 9.9 m in diameter at mean sea level. Ice conditions are similar to those experienced in the Gulf of St. Lawrence, with larger areas of non-deformed ice than experienced at Confederation Bridge (Tam et al., 1995).
- Bohai Bay (China): Steel jacket leg with a 60° upward breaking cone with a waterline diameter of approximately 3 m. Ice conditions are less severe than at the other two locations with thinner ice with little snow cover (Yue and Bi, 1998).

At Confederation Bridge and at Kemi-1, the ice interactions are characterized by the formation of rubble piles on the conical surface and these tend to dampen out dynamic effects. In addition, both structures are relatively stiff at the ice load point. Recently, Huang (2010) has argued with supporting laboratory tests, that the scale of the conical structures may be a major factor as defined by the ratio width to ice thickness (w/h). Thus, the larger cones did not experience dynamics because of the absence of simultaneous failure round the cone, while such failure was experienced on the Bohai Bay structures.

Figure A-24 (Yue and Bi, 1998) illustrates the dynamic characteristics of the ice failure process in Bohai Bay, whereas Figure A-23 illustrates the ice failure process on Confederation Bridge. While the plot from the Bohai Bay monitoring program shows a clear, regular, dynamic process, with the load dropping to zero to near zero between peaks, the Confederation Bridge Data shows no regular dynamic pattern, but rather, a sustained high level static load with a random dynamic pattern superimposed.

Thus, there are circumstances in which dynamics can occur during flexural failure of ice and others in which they will not occur.



Source: Yue and Bi, 1998

Figure A-24 Flexural ice failure process for Bohai Bay structure

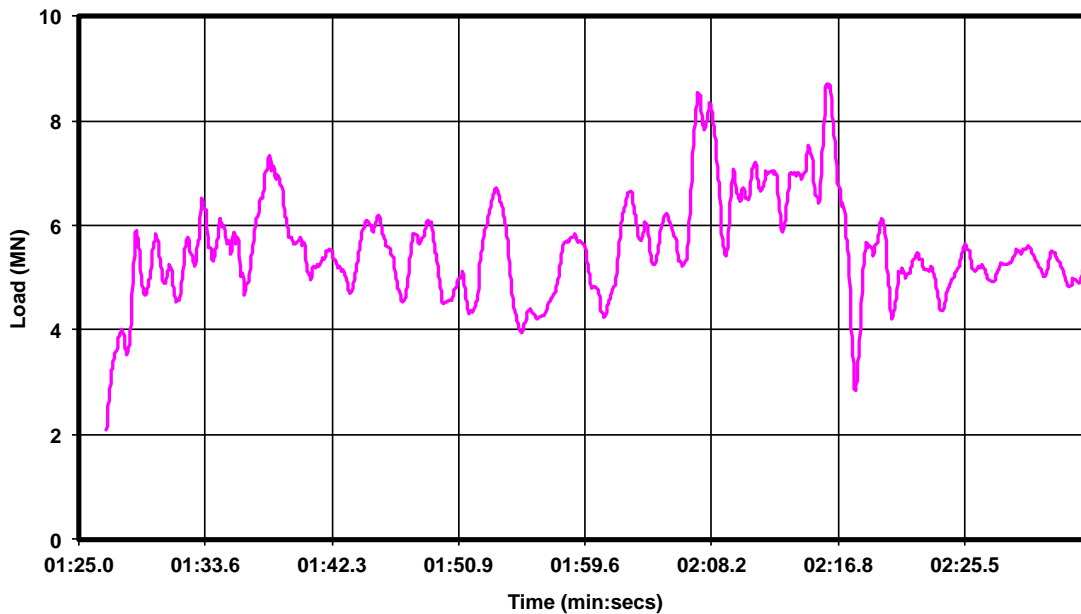
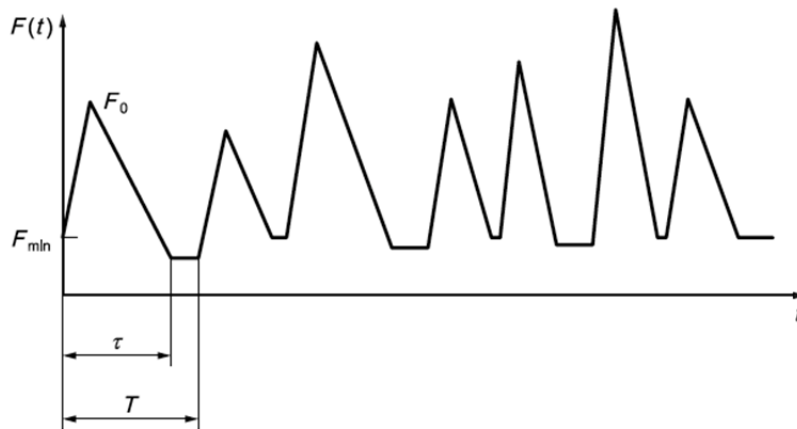


Figure A-25 Flexural failure time series at Confederation Bridge

As a consequence of the experience in Bohai Bay, ISO 19906 recommends the ice load function shown in Figure A-26 for the analysis of the dynamic effects of flexural failure of ice. In this function, both the peak ice load and the period of each load cycle are random variables. The ISO recommendations are almost entirely drawn from the work of Qu et al. (2006).



Key

- t time
- F ice action
- F_0 peak value of ice action
- F_{min} minimum value of ice action
- τ duration of loading/unloading cycle
- T period of ice action

Figure A.8-24 — Idealized time history of the horizontal action on a conical structure

Source: ISO, 2010, with permission

Figure A-26 ice failure time series for flexural failure

The experience in Bohai Bay has been that the minimum load is effectively zero ($< 0.1 F_{0,max}$), due to the complete clearing of the ice pieces between ice failure events. In the Baltic Sea, where ice-induced vibrations have not occurred, the minimum load has been measured at $0.45 F_{0,max}$. The Confederation Bridge data would support a minimum load of this level.

$F_{0,max}$ is determined as the limit load in flexural failure. Note that the 0 subscript indicates a local maximum, so $F_{0,max}$ is the highest peak. The local peak load is considered a random variable with a normal distribution. The coefficient of variation on the peak load has been assessed as between 0.2 and 0.6 for different events, and accordingly, ISO suggests that the coefficient of variation of the double amplitude, $F_0 - F_{min}$ should be 0.4. Assuming that the maximum value of the peak load, $F_{0,max}$, is the 95th percentile load, then the mean peak load is:

$$F_{0,mean} = F_{min} + 0.56(F_{0,max} - F_{min}) \quad (29)$$

The period between load peaks depends on the ice velocity, and the distance between fractures, defined as the breaking length of the ice:

$$T = \frac{l_b}{v} \quad (30)$$

The breaking length, l_b , depends on the ice thickness, strength, modulus of elasticity, structure size and ice speed. It is often given as a multiple of the ice thickness (3 to 10). ISO suggests that this ratio reduces as the thickness increases, but experience at Confederation Bridge has suggested that the ratio is at the lower range, regardless of ice thickness. The period between load peaks is also a random normal variable with a coefficient of variation that ranges between 0.4 and 0.7. A value of 0.5 is recommended by ISO.

Lastly, the duration of the load pulse can also vary, between 0.1 and 1.0 of the period between peaks. For conditions in Bohai Bay, where rubble piles do not occur, this ratio is low, close to 0.3, whereas for conditions where rubble piles do occur, the ratio should be taken as closer to 1.0.

5.3. IEC approach to ice dynamics

The IEC (2009) uses essentially the same approach to ice dynamics for both crushing and flexural failure of the ice – a shifted sine function. In each case it proposes the use of the peak load as determined using the recommended expressions for ice crushing (the Korzhavin equation) and flexure (the Ralston method).

For ice crushing, IEC recommends the equation:

$$F(t) = P(0.75 + 0.25\sin(\omega_n t)) \quad (31)$$

where P is the limit load determined using the Korzhavin equation and ω_n is the wind turbine base structural frequency. IEC recommends that this equation be checked for both the first and second modes.

The criteria for tuning (lock-in) is:

$$\frac{v}{(hf_n)} > 0.3 \quad (32)$$

where v is the ice floe speed, and h is the ice thickness.

For ice flexural failure, IEC recommends the following:

$$F(t) = P(0.75 + 0.25\sin(\omega_b t)) \quad (33)$$

where P is the limit load derived using the Ralston method, and $f_b = v / (Kh)$ where v is the ice floe speed and $4 < K < 7$. The value of K that gives the greatest response should be used.

IEC (2009) also suggests that an alternate time function may be used for both crushing and flexural failure as shown in Figure A-27.

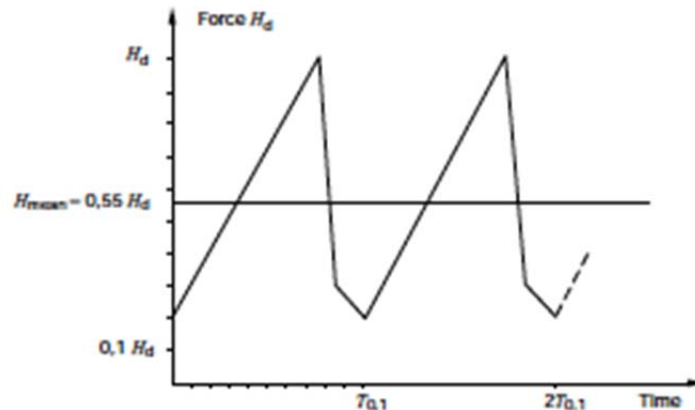


Figure A-27 Alternate saw-tooth ice load time series (IEC 2009)

where the period is either of those implied in Equations (31) and (33).

The ice load dynamic functions presented here are those used for design purposes related to Ultimate Limit States. For Fatigue Limit States, similar dynamic functions may be used, but the load levels should be reduced to correspond to those expected for normal operating conditions and should not exceed those expected as annual maxima.

6. Coupled models for dynamic ice crushing

As has been previously discussed, the interaction between moving ice and vertically-sided structures is complex, and the ice failure behavior is dependent on the relative velocity between the moving ice and the structure. ISO 19906 identifies three different behaviors; intermittent crushing, lock-in crushing, and continuous crushing. Each of these can create significant ultimate loading conditions for the structure and can be important in determining the fatigue life of a structure. However, the lock-in phenomena creates the worst conditions from a structural safety point of view, and has been known to lead to structural failure.

While the nature of the three behaviors are generally understood, the transitions from one behavior to another are less well understood, in particular the transition from intermittent crushing to lock-in. For this reason, most approaches to dynamic ice forces simply propose the application of an uncoupled time-dependent ice load function at the appropriate locations of a structural model for analysis. Nevertheless, several proposed models exist that could be used as coupled ice-structure models and which may be capable of modeling the transition from intermittent crushing to lock-in and perhaps, though less likely, to continuous crushing. The following subsections describe these models and the potential for their use.

6.1. Määttänen

Määttänen first identified the phenomenon of lock-in (self-excited vibrations) in a 1978 paper (Määttänen, 1978). Subsequently he has continued to investigate the behavior, both in the laboratory, in full-scale observations, and has developed models for the resulting ice load functions. In 1998, he published a paper that used the ice stress rate as the determinant of the strength of ice in crushing (Määttänen, 1998). The stress rate is related to the ice velocity and the velocity of the structure at the contact points. Thus there is an independent ice crushing force at each of the contact points (single tower or multiple legs) between the



ice and the structure. This results in a cyclic form of ice crushing failure (intermittent crushing) at each of these points, which will transition into lock-in, should the periods of the independent ice forces coalesce to coincide with the natural period of the structure.

Given certain limitations, the Määttänen model is relatively simple to integrate into a finite element or aeroelastic analysis system. To date the model has been integrated into one coupled ice-structure system for the analysis of offshore wind turbine foundations (Hetmanczyk, et al., 2011).

6.2. Kärnä

Kärnä has developed a series of models (labeled PSSII, Procedure for dynamic Soil-Structure Ice Interaction) (Kärnä, 1992, Kärnä et al, 1999) that also assume that the ice failure process is governed by the relative displacement and velocity at the ice/structure interface. However, the model for the ice is significantly more complicated than that of Määttänen, in that the ice model is divided into “far-field” components and “near-field” components and the near field is further divided into “elements” both in the horizontal plane and through the thickness of the ice sheet in order to model the local ice failure mechanisms of splitting and spalling. Certain assumptions are made regarding the distribution of strengths as a function of the element location. The loading and unloading phases of the near-field ice are characterized by different functions, and thus the local analysis is highly non-linear. Like the model by Määttänen, the PSSII model appears capable of modeling intermittent ice failure, and the transition to lock-in behavior. It is not able to model the continuous crushing process.

The PSSII model has been developed at VTT Technical Research Centre of Finland and is currently being integrated, by VTT, into a coupled model for the analysis of offshore wind turbine foundations (Jussila et al., 2013). Although others do appear to have had access to this model, it seems to be limited to use by VTT alone. Others have attempted to use it (e.g. John Dempsey at Clarkson University), though they have been unable to get it to execute appropriately, partly due to a lack of support materials. If this model becomes available in the future, it may be of interest to implement it in the software package.

6.3. Other models

There have been other attempts to model dynamic ice-crushing processes with the objective of understanding the transition between intermittent crushing and the lock-in behavior. Generally, none of these have been widely used or accepted. The most recent attempt was presented at the POAC-2013 conference in Finland by Andrew Palmer of the National University of Singapore on the modeling of ice-induced vibrations and lock-in (Palmer and Bjerklas, 2013, Yap and Palmer, 2013). Palmer’s model is quite simple, though may be made more complicated by selecting random values of strength and failure processes for the ice elements. The model considers a series of near-field ice elements whose behavior is independently dictated by strength and a time function for failure. It is argued that the lock-in phenomenon is associated with the synchronization of the ice failure processes. This phenomenon was observed in the Canadian Beaufort Sea with the Molikpaq structure in 1985 (Jefferies and Wright, 1988).

In summary, there are few models currently available for coupled ice-structure analysis of the effects of dynamic ice crushing (and none for the analysis for the effects of dynamic ice flexural failure). Of the two models currently in use, one (Määttänen) is relatively simple to use and is readily implemented as a coupled ice-structure model while the other (Kärnä) is overly complex and requires very extensive analysis and

interpretation to be utilized as a coupled ice-structure model and is very difficult to use as a generally available analysis tool. The simple model by Palmer is interesting as a tool to explain the transition between intermittent crushing and lock-in crushing but is not really usable as a coupled ice-structure model.

Hetmanczyk et al (2011) have developed a model for the analysis of wind-turbine dynamics caused by lock-in ice forces. Their analysis is based on the work of Määttänen (1998) using a stress-rate derivation for the ice crushing strength. Their results are interesting in that they show lock-in (resonance) for a significant range of ice velocities. The authors clearly indicate that the model cannot model the ductile behavior at low strain rates or the continuous brittle behavior at higher strain rates. The 4-term polynomial used for the ice strength/ice stress rate relation gives negative (and therefore erroneous) values for stress at higher stress rates. For this reason, the relationship is only used up to a certain value of stress rate, at which point the failure stress is taken as constant.

The Määttänen coupled ice-structure interaction model determines the current ice force as a function of the instant stress-rate in the ice. This stress rate depends on the relative velocity between the approaching ice and the local structure velocity where the ice force is applied:

$$v - \dot{x} \quad (34)$$

where v is the ice velocity, and \dot{x} is the structure velocity at the ice/structure interface.

The stress rate is then determined from:

$$\dot{\sigma} = (v - \dot{x}) \frac{8\sigma_0}{\pi D} \quad (35)$$

where σ_0 is called the reference strength, and D is the structure diameter. This definition of stress rate was originally developed by Blenkarn (1970), who specified a value for σ_0 of 125 psi (0.86 MPa) for the analysis of structures in Cook Inlet in Alaska, while Määttänen suggests a value of σ_0 of 2 MPa based on analysis of Baltic Sea structures. The equation was originally developed for narrow structures, and Määttänen cautions against using large values of D , saying that the actual diameter may be used for narrow structures, but a maximum value of $D = 1.0$ m or two times the ice thickness is recommended for wide structures. In general this model will not behave properly if the contact area ($D \cdot h$) is too high.

The actual crushing strength is given as a 4th order polynomial based on work by Peyton (1966) and plotted in Figure A-28 (ignoring minimum limits):

$$\sigma_c = [2.00 + 7.80\dot{\sigma} - 18.57\dot{\sigma}^2 + 13.00\dot{\sigma}^3 - 2.91\dot{\sigma}^4] \sqrt{1/Dh} \geq 1.0 \text{ MPa} \quad (36)$$

The force that must be applied at the loaded point on the structure is then this stress times the relevant area, where D in this case is the actual structure width:

$$F = \sigma_c D h \quad (37)$$

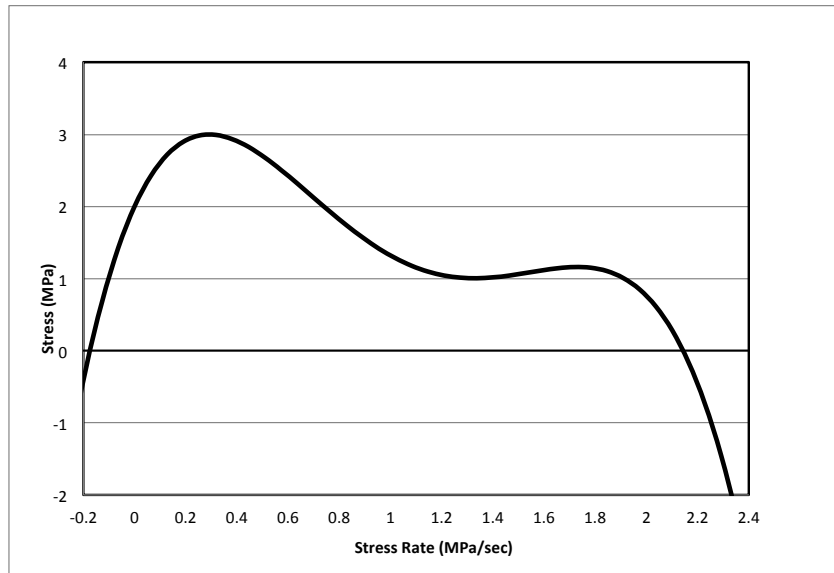


Figure A-28 Stress as a function of STRESS rate

The polynomial function in Equation (36) for the stress is capable of negative values at stress rates of greater than about 2.13 MPa/sec (Figure A-28). In the corresponding plot in Määttänen paper he shows the curve becoming asymptotic to a stress of 1.0 MPa, this is an artifact that he does not discuss, but represents the transition to continuous crushing, which cannot be modeled using this approach to lock-in. Thus in applying the equation given above, the minimum value for the stress for positive stress rates is 1.0 MPa. For negative stress rates, a low level stress is assumed (0.8 MPa).

7. Multi-legged structures

7.1. Introduction

With multi-legged structures there are several additional issues that need to be considered when determining ice loads on the structure. These are:

1. Possible interference and shielding effects between legs that depend on (Figure A-29):
 - a. The arrangement of the legs;
 - b. The ice trajectory;
 - c. The clear spacing between legs, L ;
 - d. The diameter of the legs, w ;
2. Possible non-simultaneous failure of the ice against the legs that depends on;
 - a. The compliance of the structure;
 - b. Possible dynamic effects associated with lock-in during ice crushing;

3. Possible jamming of the ice between legs resulting in increased ice force due to an increase in the effective area of the structure, depending on:
 - a. The ratio L/w ; and
 - b. The nature of the ice feature interacting with the structure.

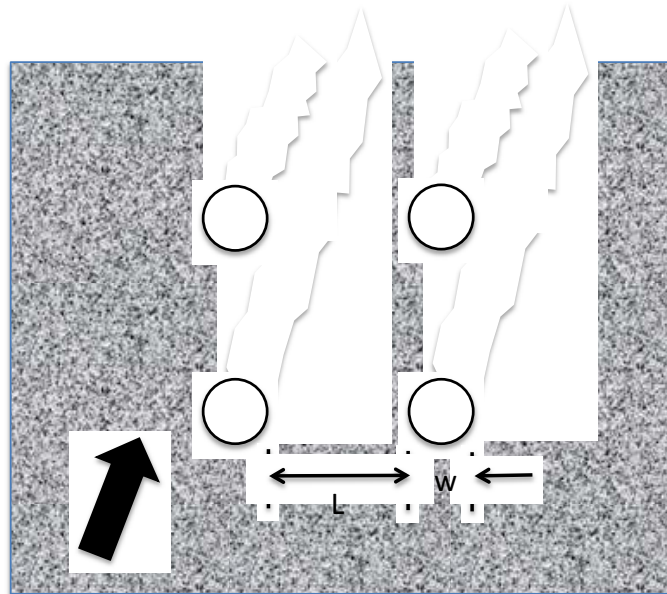


Figure A-29 Four-legged structure arrangement

7.2. Background

Although there has been relatively little recent research on the ice effects on multi-leg structures, significant work was done in the late 1980s and early 90s in response to the full-scale behaviors experienced by Chinese jacket structures in Bohai Bay. On at least one occasion, structural failure occurred as a consequence of ice-induced vibrations, and on several other occasions, the effects were severe enough to negatively impact operations on the structure.

Most of the work undertaken to understand ice forces on multi-leg structures has been small-scale modeling in ice tanks. In interpreting model results, it is important to recognize the shortcomings of model ice properties and behavior vis-à-vis full-scale ice properties and behavior. In modeling ice, the primary focus is related to modeling the thickness and strength of the model ice with respect to the full-scale thickness and strength, given a particular scaling factor. Ice model scaling is based on Froude and Cauchy scaling (Timco, 1984) although it is acknowledged that not all forces (particularly viscous effects) are scaled appropriately. The following scale factors are derived from the above scaling laws, assuming a length scale of λ .

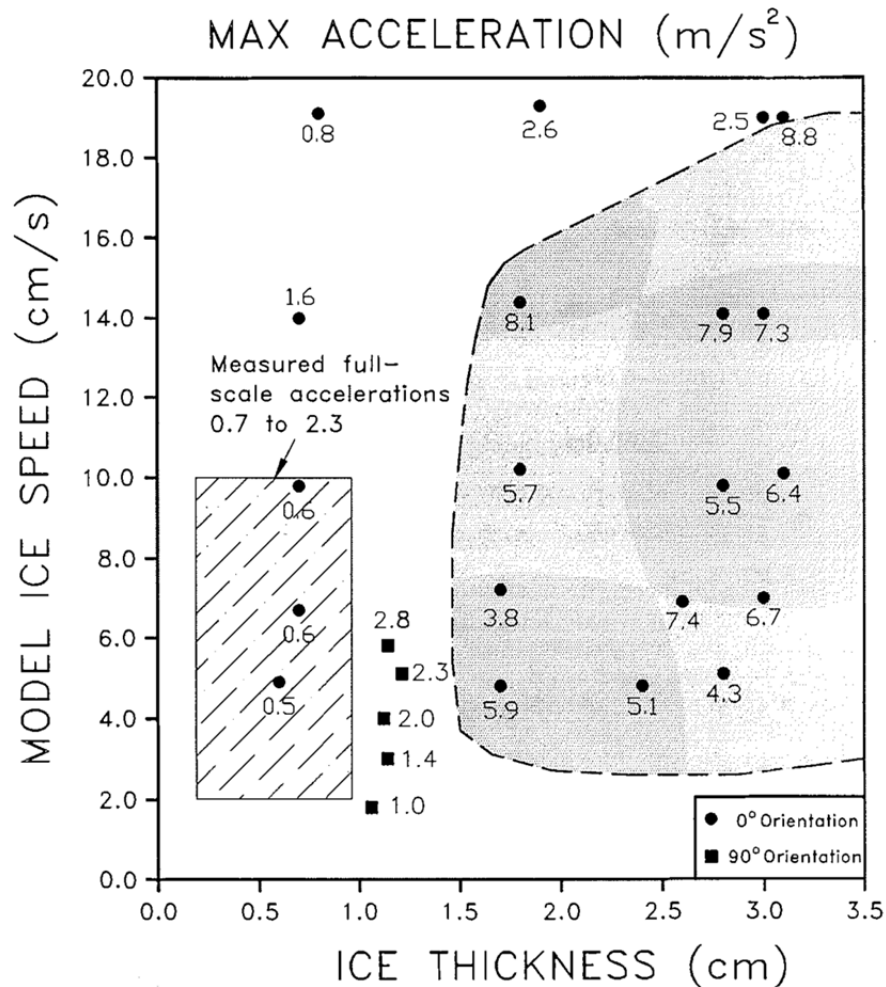
Table A-3 Scale factors for physical ice models

Property	Scale
Length	λ
Time	$\lambda^{1/2}$
Velocity	$\lambda^{1/2}$
Acceleration	1
Mass	λ^3
Force	λ^3
Density	1
Ice Strength	λ
Ice Thickness	λ
Ice Modulus	λ
Ice Fracture Toughness	$\lambda^{3/2}$
Ice-Structure Friction	1
Ice-Ice Friction	1
Structure Stiffness	λ^2
Structure Frequency	$\lambda^{-1/2}$
Damping	1
Mass	λ^3

The approach of ensuring that strength and thickness are appropriately modeled results in forces that can be scaled to full scale with some assurance. However, other parameters, particularly the modulus of elasticity and the fracture toughness are not modeled appropriately, and, while these parameters do not have a significant effect on the load, they can have a significant influence on the ice behavior. Examples of this are the excessively large pieces of model ice that result when the ice fails in flexure leading to much higher ride-up and pile-up on the model cone than is observed in full scale, and the apparent lack of fracture when model ice sheets interact with model structures.

Timco et al. (1992) carried out a series of tests on a model of the Chinese JZ20-2 jacket structure, a four-legged structure on a rectangular arrangement. The tests were designed to assess the potential for the “lock-in” form of ice crushing as a potential explanation for the severe vibrations experienced by the platform. They tested a model with a scale factor, λ , of 26. However, they were not able to determine the forces on individual legs, but rather only measured the total forces and moments on the complete structure.

Measurements of the accelerations on the structural model allowed them to assess the conditions under which the “lock-in” behavior actually occurred. Figure A-30, taken from their paper, illustrates these results. The irregular shaded area indicates results in which high deck accelerations were obtained. As expected, very low velocities and very high velocities did not result in high accelerations, nor did thin ice thicknesses.



Source: Timco et al., 1992. © 2008 Canadian Science Publishing or its licensors. Reproduced with permission.

Figure A-30 Acceleration as a function of ice velocity and thickness

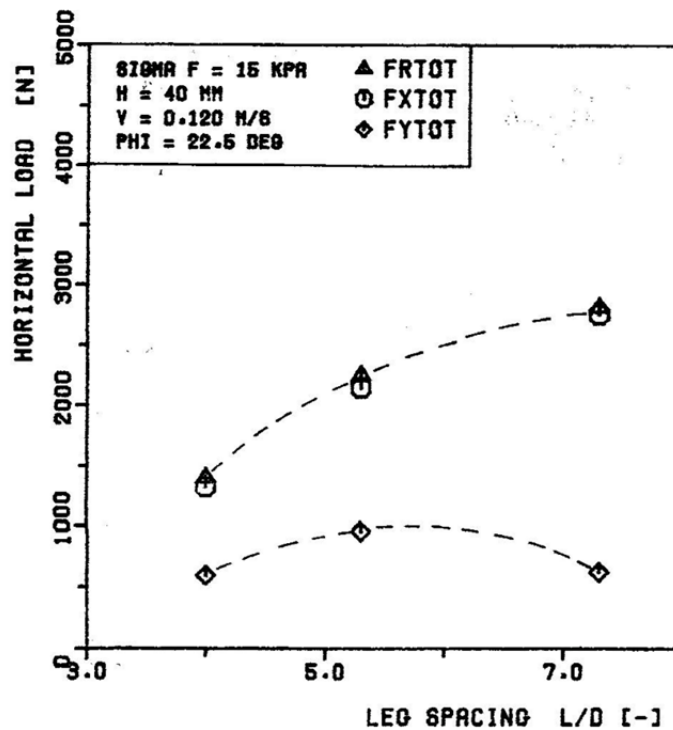
To scale these values to full scale, the ice thickness must be scaled up by the scale factor, so lock-in is occurring for ice thicknesses from approximately 40 cm to 90 cm; while velocity is scaled by $\lambda^{1/2}$, giving velocities that range from 15 cm/s to 90 cm/s.

The full-scale structure had stiffnesses (for loads applied at the waterline) ranging from 260 to 310 MN/m depending on the direction of the load, and corresponding natural frequencies of roughly 1.4 Hz. The frequency of the lock-in forces was slightly lower than the natural frequency of the structure in open water.

Evers and Wessels (1986) describe a series of tests on three- and four-legged jacket structures designed to provide some understanding of the effects of geometry and leg arrangement on the global forces on the structure. The global force was determined by summing the forces on individual legs; however, very little was reported on the relation between the forces on individual legs and the total force.

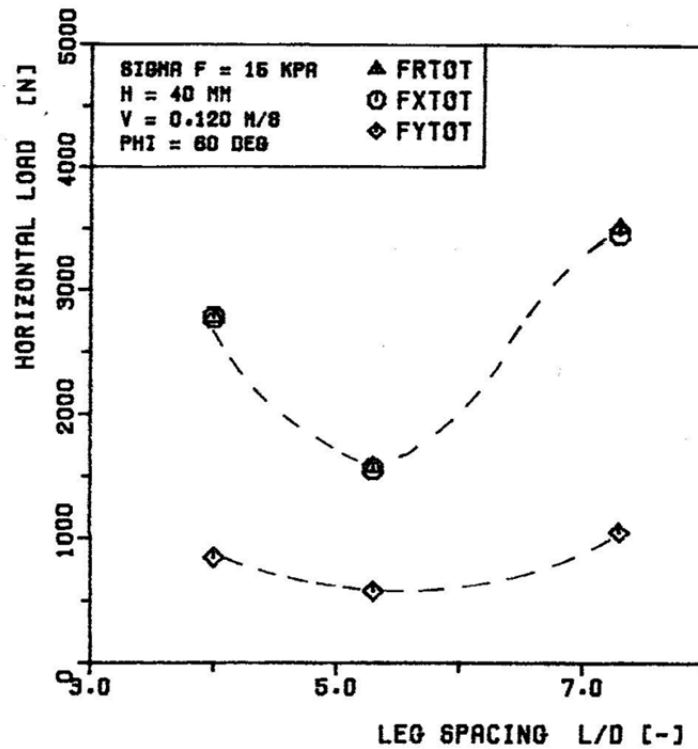
They first investigated the effect of orientation of the structure with respect to the direction of ice motion. For the four-legged structure, the maximum load was found for an ice motion 22.5° off a principal axis, while for the three-legged structure, the maximum load occurred when the ice approached two legs directly.

Their results (see Figure A-31) indicate that the effect of leg spacing on the total force is pronounced and that, for the four-legged structure the total load increases with increasing leg spacing, reaching a maximum spacing beyond which the load achieves an asymptotic value. For the three-legged structure, the minimum load was achieved at an L/D ratio of 5.3 (Figure A-32). One effect of the reduction in leg spacing is to change the direction of the resultant load on the individual legs. As the spacing reduces, a lateral load component develops in a direction towards the other leg. There is no change in the maximum resultant load, only the direction. These lateral loads tend to cancel each other out, so that the resultant total load on the structure is still in the direction of ice motion.



Evers and Wessels, 1986. With permission from author.

Figure A-31 Total load for four-legged structure

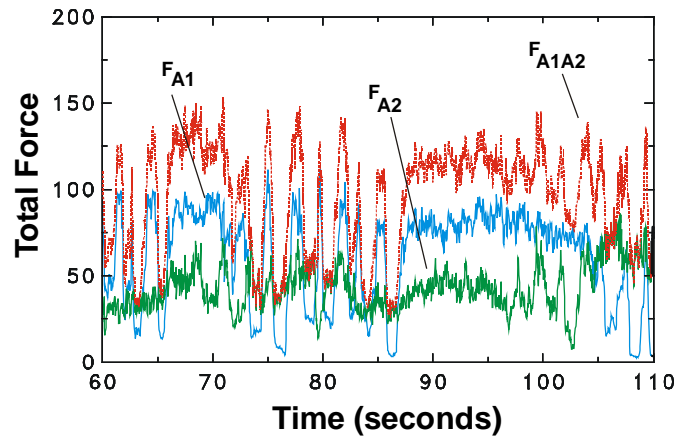


Evers and Wessels, 1986. With permission from author.

Figure A-32 Total Load for three-legged structure

Although no results are provided of the loads measured on individual legs, a comment is made in the discussion of the results that the maximum total load is only twice the maximum load on one leg.

A more recent paper by Johnston et al. (2000) describes some measurements made on a pair of legs of the same JZ20-2 platform, previously studied in model scale by Timco et al. (1992). In this paper, the measurements are taken from the full-scale structure itself. Forces were measured on two legs, in one case by a series of ice force panels installed on one leg (A1), and, in the other, by strain gauges installed in the leg structure (A2). A short (50-second) period is examined in detail, during which the ice was moving at speeds ranging from 0.35 m/s to 1.0 m/s from the southwest. This resulted in ice interacting with one of the instrumented legs before the second instrumented leg. The leg with the load panels was also provided with a camera that was synchronized with the data from the panels, meaning that the ice behavior associated with particular load effects could be identified. Figure A-33 shows the measured ice forces on both legs and the sum of the two forces.



Johnston et al, 2000. Reprinted with permission from Elsevier.

Figure A-33 Jacket Structure Load Comparisons

Of immediate interest is the character of the ice forces. The blue (middle) plot in Figure A-33 is the force trace for the A1 leg which can be seen to switch between a low-frequency signal and a high-frequency signal (the latter between 65 and 74 s and between 86 and 106 s). The second leg (green, bottom trace), however, experiences high-frequency loading throughout the load trace, except towards the end of the time trace (from 97 s onward) when it, too, experiences a few cycles of low-frequency loading. This suggests that the ice forces against the two legs are quite independent.

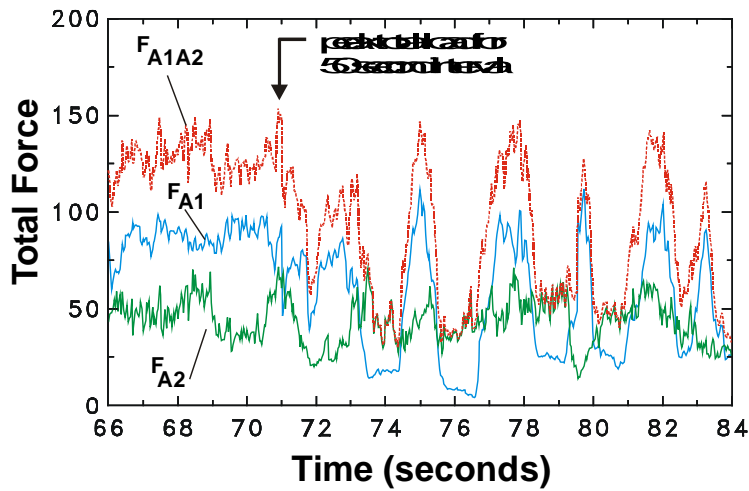
Figure A-34 illustrates the character of the load traces through a close-up of part of the time trace shown in Figure A-33. The maximum load on the structure (153 kN) was obtained in this 20-second window (at 71 s) when both legs contribute significantly to the total load. A second peak at 75 s is almost entirely derived from the load on Leg A1 which is experiencing low-frequency oscillations at this time, while Leg A2 is experiencing high-frequency oscillations.

Leg A1 was larger than A2 because the ice load panels installed on the leg increased its diameter. In their analysis, Johnston et al. have factored the load on A2 to match the diameter of the second leg, thus providing a possible comparison between the total load and the load on the individual legs. From their analysis, the peak (99th percentile) loads are presented in Table A-4.

Table A-4 Measured maximum loads

Description	99 th percentile (kN)
Leg A1	83.5
Leg A2	77
Total (A1 + A2)	130

Source: Johnston et al., 2000



Source: Johnston et al., 2000. Reprinted with permission from Elsevier.

Figure A-34 Close-up of record of Figure 33

From these results, it is fairly clear that the maximum total load as measured on the two leading legs is less than the sum of the two maxima of the loads on the individual legs. This is attributed to two reasons: the absence of simultaneity of the peak loads on the individual legs, and the different forms of ice failure on the two legs. No information is provided for the response of the platform, so there is no sense as to whether the platform was vibrating to an unacceptable level, as other papers have stated, and the load traces also support the conclusion that “lock-in” was not occurring during this period of measurements.

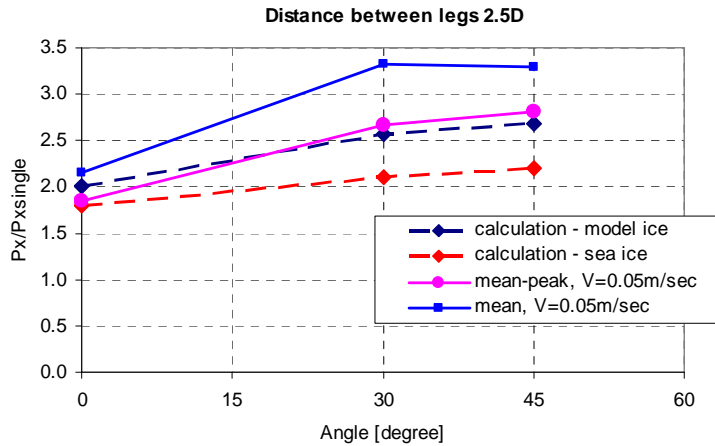
The authors emphasize that, because of the short duration of the data used for the analysis, strong conclusions regarding the design of ice forces on multi-leg platforms should not be made on the basis of the results presented. However, they note that in the earlier paper by Evers and Wessels (1986), they also found that the total load on the model platform was less than the sum of the load on the two leading legs.

More recently, Karulina et al. (2011) have presented results from a series of experiments that were carried out in St. Petersburg in support of previous numerical simulations. They tested two square four-legged structures, one with a clear leg spacing of 2.5D and a second with a leg spacing of 6D, at three different approach angles and at two different interaction velocities.

In addition to testing the four-legged structure, they also tested a single-leg structure of the same diameter in the same model ice sheets. Thus, they are able to present ratios of total force on the structure to the force on a single leg, without being concerned that the force, measured on one of the legs of the four-legged structure, might be affected by the presence of the other legs.

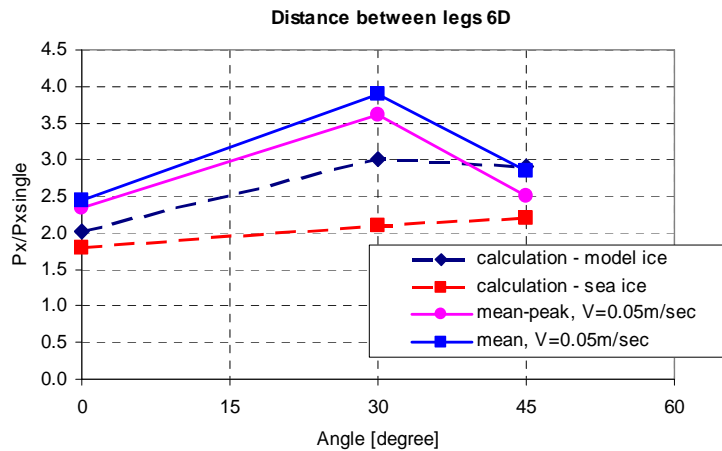
As with the model tests by Evers and Wessels, they found that the maximum force on the structure occurred at an approach angle of 30° (Evers and Wessels obtained a critical angle of 22.5°). However, they found that the total force on the structure was generally a larger multiple of the force on one leg than both the model tests by Evers and Wessels, and the full-scale observations by Johnston et al. Figure A-35 presents some of their results for a leg spacing of 2.5D, while Figure A-36 gives the corresponding results for a leg spacing of 6D. It is noted that their definition of leg spacing is slightly different from that used previously by Evers and

Wessels, who used a centre-to-centre definition of L. Thus, their leg spacing of 2.5D corresponds to a c/c spacing of 3.5D, and the clear spacing of 6, to a c/c spacing of 7D.



Source: Karulina et al. (2011), with permission of author.

Figure A-35 Results for L/D of 2.5D



Source: Karulina et al (2011), with permission of author.

Figure A-36 Results for L/D of 6D

Clearly, the results of model tests and full-scale tests have resulted in conflicting conclusions regarding the relationship between the force on a single leg of a multi-legged structure, and the total force on the structure.

Figure A-37 is also taken from the paper by Karulina et al. to illustrate the lack of fracture in front of the trailing legs. Here the ice sheet is interacting with the four-legged structure at an angle of 30°. Note the complete lack of fractures between the channels carved out by the different legs, both in the wake and in

front of the rear legs. In full scale such fractures would be common, leading to significantly lower forces on the trailing legs.



Source: Karulina et al. 2011, with permission of author.

Figure A-37 Model test behavior

On the basis of the review provided here, the ISO recommendations for the factor k_s defined below seem unduly conservative. However, the number of observations, particularly in full scale, are limited and thus recommended values of k_s have been selected on the basis of balancing the conservatism of the ISO approach, and the findings from full-scale observations.

An additional consideration for multi-legged structures is the issue of thermal forces that could develop due to a static ice sheet having grown within the confines of the legs. Thermal ice forces are an issue, particularly if the structure is placed in a region of little ice motion and static ice growth.

7.3. ISO approach

The ice force on a multi-legged structure can be obtained by determining the forces on individual legs and summing them, or by applying a formula that directly determines the total limit force on the structure. For the limit force, the latter approach is acceptable, but for dynamic forces, the former approach must be used to account for phase differences between the forces on each of the legs.

ISO 19906 suggests the following approach to determine the total limit ice force on a multi-legged structure:

$$F_T = k_s k_n k_j F_1 \quad (38)$$

where F_1 is the ice force on one leg, determined using the appropriate formulation for the limit ice force, and depending on the shape of the leg at the waterline.

k_s accounts for the interference and sheltering effects between legs. For legs in a line perpendicular to the direction of motion and with $L/w > 5$, the ice forces on the individual legs are independent. For a typical four-leg structure, in a square arrangement, a value of k_s from 3.0 to 3.5 is suggested.



k_n accounts for the non-simultaneity of the ice failure on the individual legs. Unless the structure is very compliant (and this would have to be tested for dynamic load problems), a k_n value of 0.9 is suggested. However, if forces are being determined independently for each loaded leg, then k_n is automatically accounted by the phase relationship between the forces on each leg and there is no need to further reduce the forces.

No guidance is given for the value of k_j which accounts for jamming of the ice between legs. If L/w is less than 4, the potential for jamming, especially of first-year ridges, is relatively high. ISO recommends that the loads be determined for the case of no jamming and then for the case of jammed ice. In the latter case, however, the load determination would account for the mixed forms of ice failure that is likely to occur under those circumstances, and any dynamics resulting from the ice failure process would be minimal.

Although the spacing between the legs will be small for jacket structures as wind turbine bases, jamming will be disregarded.

For dynamic analysis, the forces on each of the legs will normally act independently. However, there is the potential for the lock-in case of ice crushing to occur for all the legs interacting with ice and leading to resonance of the entire structure. This behavior will depend on the relative flexibility of the individual legs with respect to the entire structure. Similar behavior has also been observed with jacket structures in Bohai Bay in China with flexural failure of the ice. Again, this behavior will depend on the relative stiffness of the legs with respect to the entire structure.

In multi-legged structures used for offshore wind turbine bases, spacing-to-diameter ratios will be low, because there is no need for a large topside area as there is with offshore oil and gas platforms, so only low L/D ratios need be considered.

Accordingly, it may be assumed that the leading legs (with respect to the ice motion) will create broken paths in the oncoming ice sheet that will result in lower forces on the trailing legs, even if the trailing legs are not fully shielded by the leading legs.

In summary, for three-legged structures, the maximum number of loaded legs, regardless of the direction of ice motion, will be 2 (two).

For four-legged structures, the correct value for the number of loaded legs is 2.5, but this will not work with the coupled model, so values of 2 (two) or 3 (three) should be used. In this case, it does depend on the direction of the ice; if the ice is interacting directly along one of the principal axes of the structure, the number of loaded legs is 2 (as the other two are completely shielded). At other angles (30° or 45°) then the three "leading" legs are loaded and the one at the back is not.



8. Recommended implementation

The objective of the ice load analysis is the derivation of an ice load function that defines the time variation of the ice load for dynamic analysis of the wind turbine supporting structure. For this reason, ice load behavior results in purely static loads are not relevant. This includes ice loads of thermal origin, and interactions in which the dynamics are effectively dampened by the ice failure process itself (generally those interactions in which large rubble formations occur), interactions of first-year ridges, and interactions in which large rubble piles occur.

9. References

- [A-1] Ashton, G.D. (Ed.), 1986. River and Lake Ice Engineering. Water Resources Publication, Littleton, CO, USA.
- [A-2] Blenkarn K. A. (1970): Measurement and analysis of ice forces on Cook Inlet structures. Proc. 2nd Offshore Technology Conference, Houston, TX, OTC 1261, Vol. II, pp. 365-378.
- [A-3] Brown, T.G., Tibbo, S., Shrestha, N., Tripathi, D., Obert, K., Bruce, J.R., Maes, M.A., 2010, Analysis of Ice Interactions and Ice Loads on Confederation Bridge Piers, Report to Public Works and Government Services Canada, pp 373.
- [A-4] Brown, T.G., Tibbo, J.S., Tripathi, D., Obert, K., Shrestha, N., 2010. Extreme ice load events on the Confederation Bridge, Journal of Cold Regions Science and Technology, Volume 60, Issue 1, January 2010, Pages 1-14.
- [A-5] Brown, T.G., Bruce, J.R., 1997. Results for first year of ice monitoring of the Confederation Bridge. Joint Industry Report, July 1997. 120pp.
- [A-6] Cox, G.F.N. and Weeks, W.F., 1983, Equations for determining the gas and brine volumes in sea ice samples, Journal of Glaciology, Volume 29, Number 102, pp. 306-316
- [A-7] Croasdale, K.R. 1980. Ice forces on fixed, rigid structures. Special Report 80-26, US Army CRREL, Hanover, N.H. 34-106.
- [A-8] Croasdale, K.R., Cammaert, A.B., Metge, M. 1994. A method for the calculation of sheet ice loads on sloping structures. 12th International Symposium on Ice, Trondheim, Norway, 874-885.
- [A-9] Croasdale, K. R. 2012. Ice Rubbling and Ice Interaction with Offshore Facilities. Journal of Cold Regions Science and Technology; 76–77, 2012.
- [A-10] Dolgoplov, Y., Afanasiev, V., Korenkov, V. and Panfilov, D., 1975, Effect of hummocked ice on the piers of marine hydraulic structures. In Proc. IAHR Symposium on Ice, Hannover, NH, USA, pp. 469–478.
- [A-11] Evers, K-U. and Wessels, E., 1986. Model Test Study of Level Ice Forces on Cylindrical Multilegged Structures, Proc. Intl. Offshore and Navigation Conference and Exhibition, Polartech '86, Espoo, Finland, Vol. 3, pp251-275.
- [A-12] Gagnon, R.E., 2012, An explanation for the Molikpaq 12 May 1986 event, Journal of Cold Regions Science and Technology, Volume 82, January 2012, Pages 75-93.
- [A-13] Gravesen, H, Sorensen, S.L., Volund, P., Barker, A., and Timco, G., 2005, Ice loading on Danish wind turbines: Part 2. Analyses of dynamic model test results, Journal of Cold Regions Science and Technology, Vol. 41, pp. 25-47.
- [A-14] Hetmanczyk, S., Heinonen, J., 2011. Dynamic Ice Load Model in Overall Simulation of Offshore Wind Turbines. Proceedings of the 21st ISOPE International Offshore and Polar Engineering Conference, Maui, Hawaii, USA.
- [A-15] ISO, ISO 19906, Petroleum and Natural Gas Industries, Arctic Offshore Structures, International Standards Organization, Geneva, 2011, p. 465.
- [A-16] Jeffries M., and Wright W. (1988): Dynamic response of "Molikpaq" to ice-structure interaction. Proc. OMAE-88, Vol. IV, pp. 201-220. ASME. Houston, USA.
- [A-17] Johnston, M.E., Timco, G.W., Frederking, R., Jochmann, P., 2000, Simultaneity Of Measured Ice Load On Two Legs Of A Multi-Leg Platform, 19th International Conference on Offshore Mechanics and Arctic Engineering, 14-17 February, 2000, New Orleans, USA, Paper OMAE-00-1007.
- [A-18] Jussila, V., Heinonen J. 2012. Comparison of Ice-Induced Vibrations on a Conical and Cylindrical Offshore Wind Turbine Substructure. Proceedings of 21st International Symposium on Ice, Dalian China.
- [A-19] Jussila, V., Popko, W., Heinonen J. 2012. Interfacing of Ice Load Simulation Tools for Cylindrical and Conical Structure with OneWind simulation tool for offshore wind turbines, Proceedings of 22nd International Conference on Port and Ocean Engineering under Arctic Conditions 9-13 June 2013 Espoo, Finland.
- [A-20] Karulina, M., Shkhinek, K.N., and Thomas, G.A.N, 2011, Theoretical and Experimental Investigations of Level Ice Interactions with Four-Legged Structures. Proc. Of the 21st Intl. Conf. on Port and Ocean Engineering under Arctic Conditions, Montreal, Canada, paper POAC11-032.
- [A-21] Karna, T. and Masterson, D.M. 2011, Data for crushing formula, Proc. Of the 21st Intl. Conf. on Port and Ocean Engineering under Arctic Conditions, Montreal, Canada, paper POAC11-064.
- [A-22] Kärnä, T., Qu, Y., Yue, Q.J., Bi, X.J. and Kuehnlein W. (2007). A spectral model for forces due to ice crushing. Journal of Offshore Mechanics and Arctic Engineering. Vol. 129, May 2007, pp. 138-145.
- [A-23] Kärnä T. (1992): A procedure for dynamic soil structure-ice interaction. Proc. ISOPE 1992, Vol. 11, pp 764-771. International Society of Offshore and Polar Engineers, San Francisco.
- [A-24] Kärnä, T., Kamesaki, K., Tsukuda, H., 1999. A numerical model for dynamic ice–structure interaction. Computers and Structures 72, pp. 645–658.
- [A-25] Korzhavin, K.N. 1971. Action of Ice on Engineering Structures. US Army CRREL Translation TL260, Hanover, N.H., USA.
- [A-26] Lipsett, A.W. and Gerard, R., 1980. Field Measurements of Ice Forces on Bridge Piers 1973-1979. Transportation and Surface Water Engineering Department. Alberta Research Council and Alberta Cooperative Research Program in Transportation and Surface Water Engineering. Report SWE 80-3. 130 pp., Alberta, Canada.
- [A-27] Määttänen, M., 1975. On the flexural strength of brackish water in in situ tests.
- [A-28] Proceedings POAC'75, vol.1, pp. 349–359. Fairbanks, AL, USA.

- [A-29] Määttänen M. (1978): On conditions for the rise of self-excited ice-induced autonomous oscillations in slender marine structures. Finnish-Swedish Winter Navigation Board, Finland, Research Report 25, 98 p.
- [A-30] Määttänen, M., 1998. Numerical model for ice-induced vibration load lock-in and synchronization, Proceedings of the 14th International Symposium on Ice, Potsdam/New York/USA/27-31 July 1998, Vol. 2, pp. 923-930.
- [A-31] Mayne, D.C., 2007. Level Ice and Rubble Actions on Offshore Conical and Sloping Structures, Thesis submitted in Partial Fulfilment of the Requirements for a PhD Degree, University of Calgary, Canada, 215 pages.
- [A-32] Nevel, D.E. 1992. Ice forces on cones from floes. Proceedings from the 11th IAHR Ice Symposium, Banff, Canada, 3: 1391-1404.
- [A-33] Obert, K. M., 2009, Ridge Keel Geometry and Interaction with the Confederation Bridge. Thesis submitted in Partial Fulfilment of the Requirements for a MSc Degree, University of Calgary, Calgary, Alberta.
- [A-34] Palmer, A. C. and Croasdale K. R. 2012 Arctic Offshore Engineering. World Scientific Publishing Co. Ltd., Singapore.
- [A-35] Palmer, A.C., and Bjerklas, M., 2013, Synchronisation and the transition from intermittent to locked-in ice-induced vibration, Proceedings of 22nd International Conference on Port and Ocean Engineering under Arctic Conditions, 9-13 June 2013 Espoo, Finland.
- [A-36] Peyton, H.R., 1966. Sea ice strength. University of Alaska Report UAG-182. Geophysical
- [A-37] Institute, Fairbanks, AK, USA. 187 pp.
- [A-38] Qu, Yan, Yue, Qianjin, Bi, Xiangjun, Kärnä, Tuomo, 2006. A random ice force model for narrow conical structures. Cold Regions Science and Technology 45, 148–157.
- [A-39] Ralston, T.D. 1979. Plastic limit analysis of sheet ice loads on conical structures. Physics and Mechanics of Ice, IUTAM Symposium, August, Copenhagen, Denmark: 289-308.
- [A-40] Sanderson, T. J. O. 1988. Ice Mechanics - Risks to Offshore Structures. Graham and Trotman.
- [A-41] Schwarz, J., 1970, Pressure of floating ice fields on piles, Proceedings of the International Association for Hydraulic Research Ice Symposium, Reykjavik, Iceland.
- [A-42] Tam, G., Määttänen, M., Hoikkanen, J., Nortala-Hoikkanen, A., Mäkinen, E. and Kivelä, J.,
- [A-43] 1995. Ice force measurement analysis for the Kemi-I Cone — a joint industry project.
- [A-44] Volume I and II. 127 p + ~280 p Appendices + Video + Slides + Computer Program.
- [A-45] Kvaerner-Masa Inc, Vancouver, Canada
- [A-46] Tibbo, J.S., 2010, Flexural Failure of Sea Ice – Analysis of Interactions at Confederation Bridge and Assessment of Selected Prediction Techniques, Thesis submitted in Partial Fulfilment of the Requirements for a MSc Degree, University of Calgary, Calgary, Alberta.
- [A-47] Timco, G.W. and Frederking, R.M.W., 1990, Compressive Strength of Ice Sheets, Journal of Cold Regions Science and Technology, Volume 17, pp. 227-240.
- [A-48] Timco, G.W. and Frederking, R.M.W., 1982, Comparative Strengths of Fresh Water Ice, Journal of Cold Regions Science and Technology, Volume 6, pp. 21-27.
- [A-49] Timco, G.W. and Weeks, W.F., 2010, A review of the engineering properties of sea ice, Journal of Cold Regions Science and Technology, Volume 60, Issue 10, pp. 107-129.
- [A-50] Timco, G.W., Irani, M.B., Tseng, F., Lui, L.K., and Zheng, C.B., 1992, Model Tests of dynamic Loading on the Chinese JZ-20-2 Jacket Structure. Canadian Journal of Civil Engineering, Vol. 19, pp819-932.
- [A-51] Timco, G.W., 1984, Ice forces on structures: physical modeling techniques. State-of-the-Art report on ice forces on structures. Proceedings of the International Association for Hydraulic Research Ice Symposium, Hamburg, Germany, Vol. IV, pp. 117-150.
- [A-52] Timco, G.W., O'Brien, S., 1994. Flexural strength equation for sea ice. Cold Regions
- [A-53] Science and Technology 22, pp. 285–298.
- [A-54] Wadhams, P, 2000, Ice in the ocean, Gordon and Breach, London.
- [A-55] Yap, K.T. and Palmer, A.C., 2013, a model test on ice-induced vibrations: structure response characteristics and scaling of the lock-in phenomenon, Proceedings of 22nd International Conference on Port and Ocean Engineering under Arctic Conditions, 9-13 June 2013 Espoo, Finland.
- [A-56] Yue Q., Guo F., Kärnä T., 2009. Dynamic ice forces of slender vertical structures due to ice crushing, Cold Regions Science and Technology 56 (2009) 77–83.
- [A-57] Yue, Q., Qu, Y., Bi, X., Kärnä T., 2007. Ice force spectrum on narrow conical structures, Journal of Cold Regions Science and Technology, Volume 49, Issue 2, August 2007, pp. 161-169.
- [A-58] Yue, Q.J., Bi, X.J., 1998. Full-scale test and analysis of dynamic interaction between ice sheet and conical structure. Proc. 14th International Association for Hydraulic Research (IAHR) Symposium on Ice, vol. 2, pp. 939–945.

APPENDIX B – ICEFLOE USER MANUAL

1. Ice model descriptions

The IceFloe module can optionally calculate loading using one of several models of ice behavior. The models are described briefly here, with further details found in the noted references, as well as the Theory Manual in Appendix A. These models include those specified by ISO and IEC standards as well as select alternatives.

Ice loading on offshore structures generally takes one of two forms: crushing of the ice sheet against vertical or near vertical surfaces, or flexural failure (bending/snapping) of the ice against coned surfaces. These two configurations are shown in Figure B-1 and Figure B-2. The different models are listed in Table B-1.

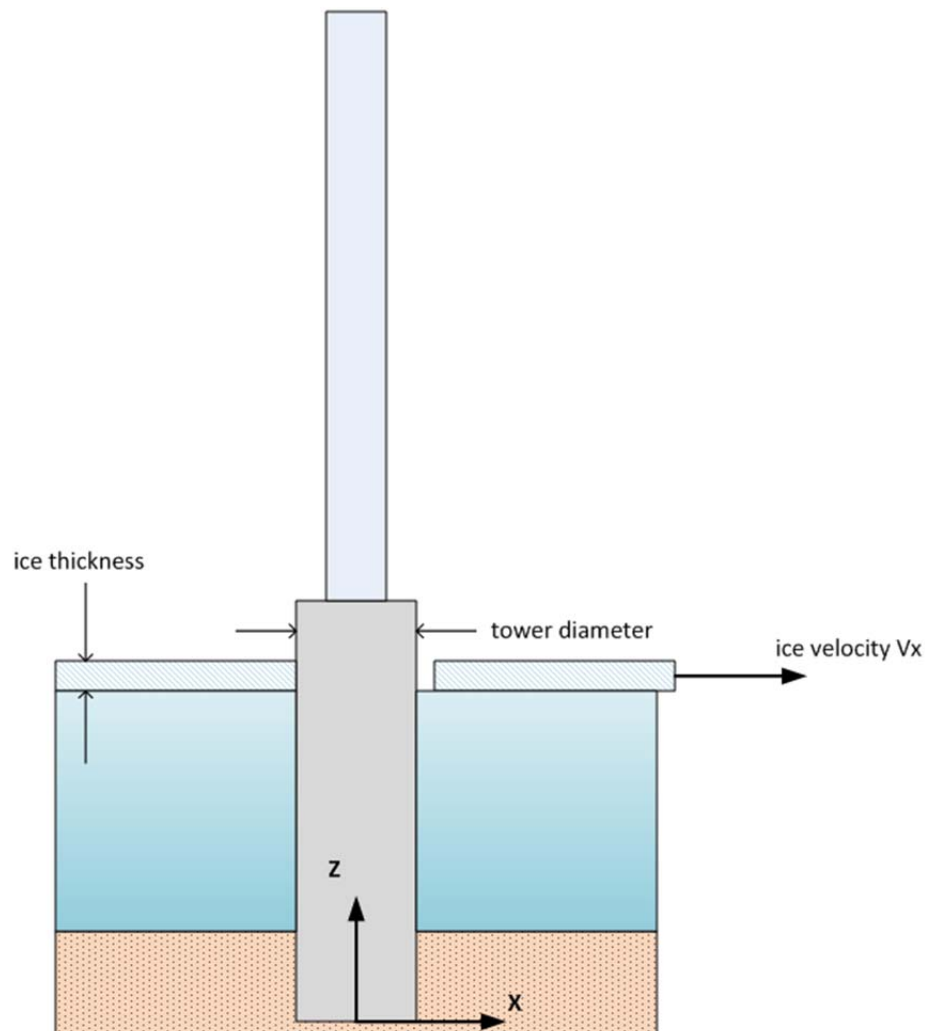


Figure B-1 Sketch of ice crushing against a vertical surface

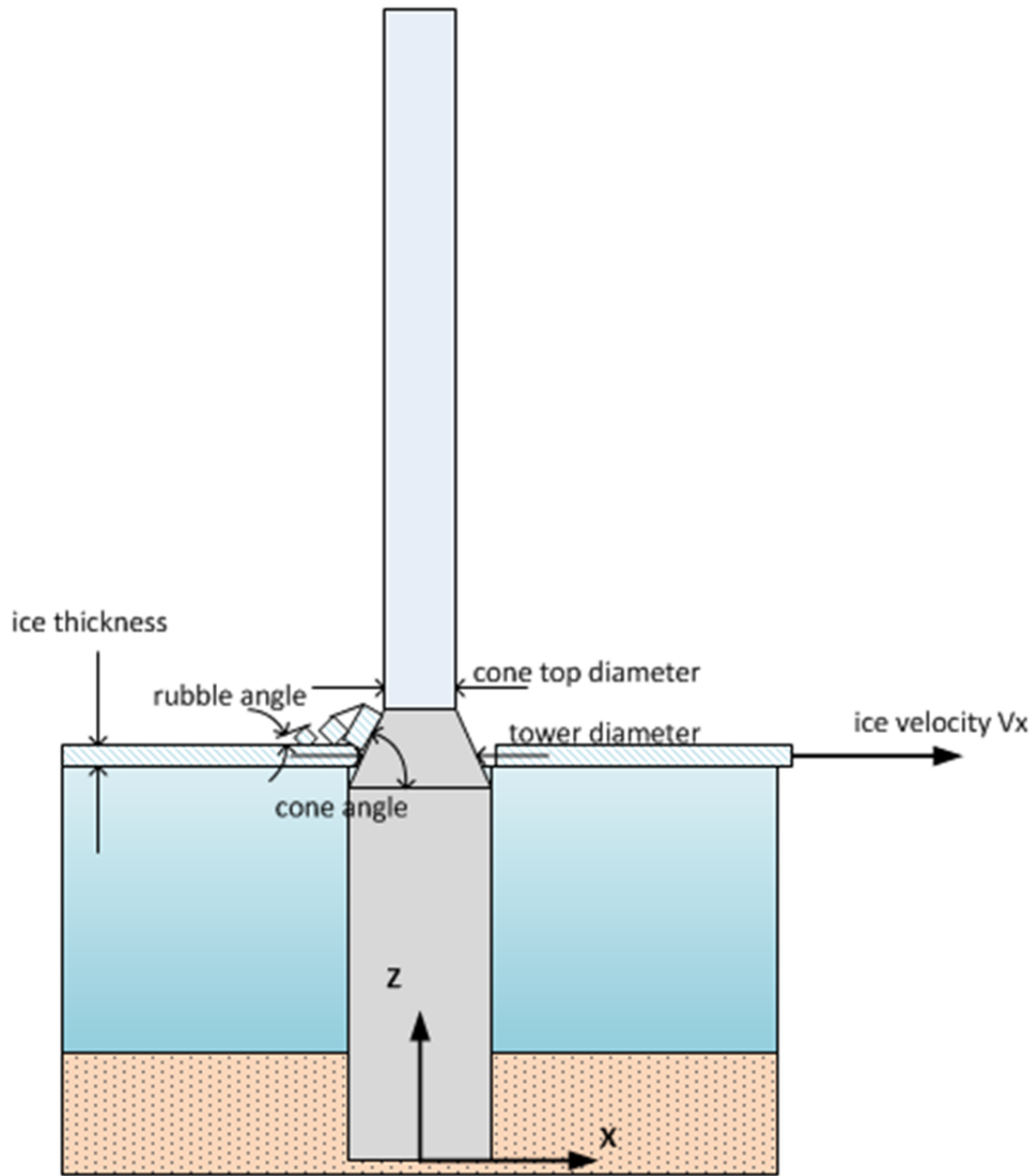


Figure B-2 Sketch of ice in flexural failure against a coned surface

Table B-1 Ice loading models available in IceFloe

Ice Load Model	Ice Type Code	Reference
Continuous random crushing	1	[6] [3], Section A.8.2.6.1.2.
Intermittent crushing per ISO	2	[3], Section A.8.2.6.1.3.
Lock-in crushing per ISO	3	[3], Section A.8.2.6.1.4.
Lock-in crushing per IEC	4	[2], Appendix E.
Coupled crushing	5	[11]
Flexural failure per ISO	6	[9] [3], Section A.8.2.6.2.
Flexural failure per IEC	7	[10] [2], Appendix E. [3], Section A.8.2.4.4.

1.1. Random Crushing

The random crushing model uses the ice sheet velocity as a parameter for a spectral distribution of the ice loading. The distribution is used to create a random time series of loads scaled by the limit crushing load as specified by ISO (a function of ice strength, thickness, and support structure width). The load time series is pre-computed in the initialization routine and interpolated in time by the update routine. For multi-legged structures, individual independent random time series are generated for each leg. An example load time series of random crushing is shown in Figure B-3 in the upper left hand corner.

1.2. Intermittent Crushing

The intermittent crushing model is an asymmetrical triangular (sawtooth) waveform with specified period separated by intervals with no load. An example load time series of intermittent crushing is shown in Figure B-3 in the upper right hand corner. For multi-leg structures the user must specify a phase angle to be used for the waveform of each leg.

1.3. Lock-In crushing

The lock-in crushing model applies a periodic waveform at the user-specified fundamental frequency of the support structure. The ISO code specifies an asymmetrical triangular (sawtooth) waveform and the IEC code specifies a sinusoidal waveform. Example load time series of lock-in crushing are shown in Figure B-3 in the middle left and right plots.

1.4. Coupled crushing

The coupled crushing model is effectively a lock-in type of model wherein the instantaneous magnitude of the load is dependent on the relative velocity between the support structure and the ice sheet. Issues to be aware of are that the structure width (tower diameter) should be less than twice the ice thickness or else the ice loading theory is invalid. The width used in the strength calculation is limited to twice the ice thickness. Further, the curves used will not be valid for excessively thick ice combined with wide structures;

8 m² is the approximate maximum area, though this somewhat depends on the minimum ice strengths chosen.

1.5. Flexural failure

There are two flexural failure models currently implemented in IceFloe. The model as specified by the ISO code is a series of triangle/sawtooth waveforms with random (although bounded) period and peak heights separated by intervals of no load. The model specified by IEC is a sinusoidal waveform at a frequency substantially below the fundamental structural frequency. The load varies from a non-zero minimum to a maximum specified peak. Example ice load time series of flexural failure are shown in Figure B-3 in the lower left and right hand corners. For the IEC model with a multi-leg structure, the user must specify a phase angle to be used for the waveform of each leg.

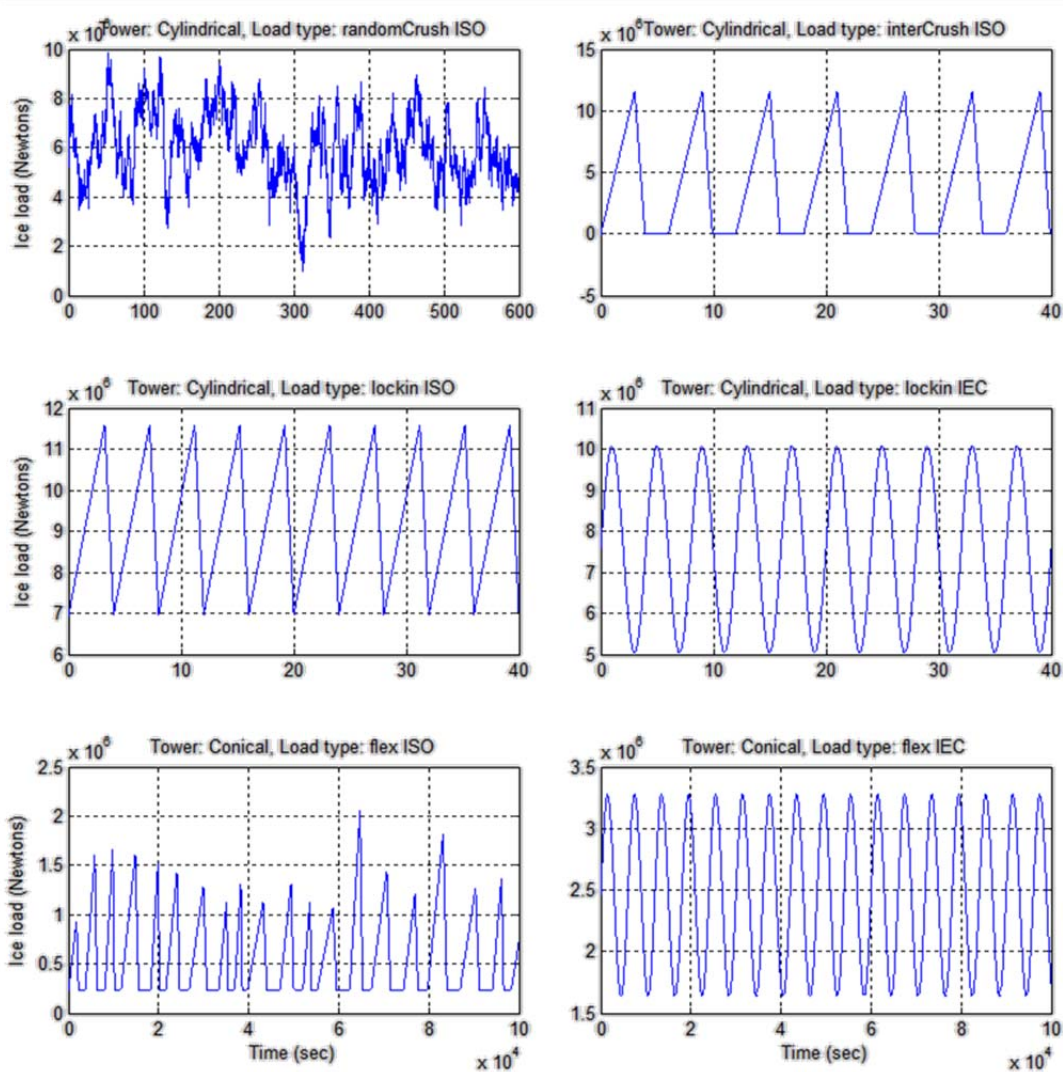


Figure B-3 Example ice load time series

1.6. Multiple-leg structures

IceFloe can calculate load time series for support structures with one, three, or four legs. When there are multiple legs, time series are calculated individually for each leg. For models with random loading, each leg load time series is independent. For models with periodic loading, the user must specify a phase angle for each leg. Additionally, the user must either specify a sheltering factor for each leg or choose the auto-calculate option for a sheltering factor. This factor accounts for the clearing of ice behind an up-floe leg which reduces the load on the down-floe leg.

For output to the calling program there is an option to provide the ice loads either individually or as a single combined set of forces plus a moment about the vertical axis. See the following section on coordinates and load components for more details.

2. Coordinate system and load components

The coordinate system used by IceFloe is shown in Figure B-4. A direction of zero means that the ice is moving and loads are applied in the positive x direction. The sense of a positive rotation of the ice direction is also shown. For a leg of a multi-leg structure, (x,y) coordinates at the waterline are required. An example cross-section at the waterline is shown in Figure B-5. Note the leg coordinates internal to the ice load routine assume that the coordinate origin is at the centroid of the legs.

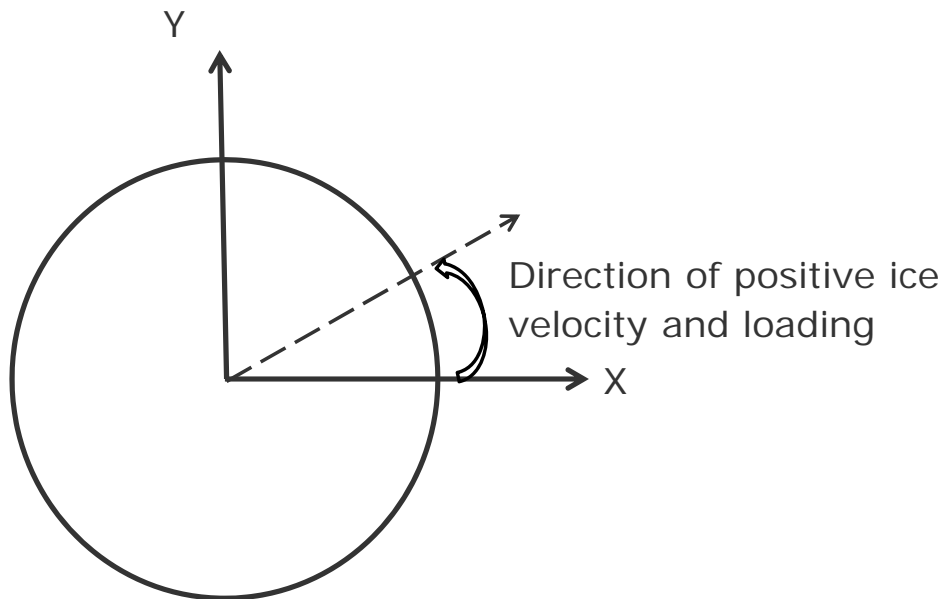


Figure B-4 Definition of ice velocity and direction coordinate system

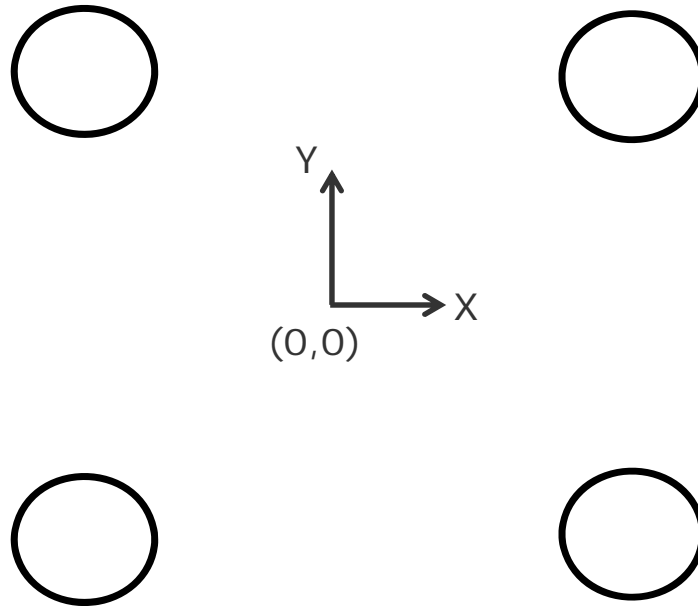


Figure B-5 Arrangement of legs

IceFloe returns force components in the x and y directions in the ground/inertial coordinate system, though it is up to the user to insure that the calling program accepts the loads this way. Vertical forces (F_z) are always zero. When loads are requested individually for a multi-leg structure, all moments are zero. However, for a single point application of equivalent loads for a multi-leg structure modeled as a single beam, a vertical moment (M_z) is returned based on a calculation using the individual leg positions and forces.

3. Console program execution

The console (DOS) executable that will calculate ice loads and save them to a file takes a single command line argument which is the name of the parameter input file. The program is run from a DOS window by issuing the following command (with the necessary path to the executable included):

file path\iceFloeConsole.exe iceFloe.inp

Two files will be created: a log file and a file with the time series of loads, both ASCII:

file path \iceFloe.log

file path \iceFloe.dat

The data file can be reformatted in Excel or MATLAB for example to match the input requirements of the structural analysis program.

4. Input file

The input file is an ASCII file that consists of comment lines and input parameter lines. Comment lines begin with an exclamation point (!) in the first column. Input parameter lines consist of a key word followed by a numeric value. See Appendix C for an example. A few points about parameter inputs:

- Key words are essentially the variable names and must be spelled correctly but are not case sensitive.
- The order of the input parameters is not important.
- Not all input parameters are required for every ice loading type; however, if a required parameter is missing a warning message will be issued to the screen and to the log file.

An alphabetical list of all possible input parameters is found in Table B-2 along with units, suggested typical values where appropriate, input checking limits, descriptive notes, and which ice loading type they are required by. Additionally, Table B-3 through Table B-5 list the input parameters specifically required for each ice loading type.

The limitations on values for the input variables currently included in the code are based on either limitations of the algorithm or a reasonable range based on experience. In the former case for example the loads on a coned structure are analyzed using an ice flexural failure model. If the coning angle is below 20 degrees or above 70 degrees the loading model is not valid. For the latter situation for example a range of tower diameters from 0.1 to 100 include all conceivable values for wind turbines while still providing a check for erroneous inputs. To defeat these limitations the code must be modified and recompiled.

Table B-2 IceFloe input parameters

Parameter Name	Typical Value ¹	Limits	Unit	Notes	Used by ice load type
coeffBreakLength	4	3 to 10	-	Multiple of ice thickness for length of ice slab between breaks	ISO flexural failure model
coeffLoadMin	0.1	0 to 1	-	Coefficient relating minimum load to peak load	ISO flexural failure model
coeffLoadPeaks	0.56	0.1 to 1.0	-	Coefficient relating mean load to peak load	ISO flexural failure model
coeffPSD_b	1.34	0.1 to 3	-	Parameter for PSD ² of random crushing load	Random crushing
coeffPSD_ks	3.24	1 to 5	-	Parameter for PSD of random crushing load	Random crushing
contactFactor_k2	-	0.1 to 2	-	Parameter for static ice crushing load	IEC crushing models
crushLoadCOV	-	0.1 to 1	-	Coefficient of variation of load	Random crushing
duration	-	>0	seconds	Length of load time series	All
fallTime	-	0.1 to 0.9	-	Fall time for sawtooth waveform – as a fraction of the period	ISO flexural and ISO and intermittent crushing models.
flexStrength	-	0 to 1E9	Pa	Ice breaking strength in flexural failure	ISO and IEC flexural failure models
freqParamK	5	4 to 7	-	Parameter for determination of the frequency of flexural loading – multiple of ice thickness	IEC flexural failure model
freqStep	-	0.001 to	Hz	Frequency resolution for	Random crushing

Parameter Name	Typical Value ¹	Limits	Unit	Notes	Used by ice load type
		0.1		PSD of random loads.	
frictionAngle	-	0 to 70	degrees	Angle at which the ice slides	ISO flexural failure model
ice2IceFriction	0.05	0 to 1	-	Friction between ice blocks	ISO flexural failure model
ice2twrFriction	0.1	0 to 0.3	-	Friction coefficient between ice and tower surface	ISO and IEC flexural failure models
iceDensity	917	>0	kg/m ³	Density of ice	ISO and IEC flexural failure models
iceDirection	0	0 to 360	degrees	Direction of ice sheet movement – see coordinate description	All
iceModulus	-	>0	Pa	Modulus of elasticity of ice	ISO flexural failure model
iceThickness	-	0.001 to 100.0	m	Thickness of ice sheet	All
iceType	1 to 7	1 to 7	-	See explanation in section B-1	All
iceVelocity		0.001 to 10.0	m/s	Speed of ice sheet	All
includeHb	1	0 or 1	-	Switch to turn breaking load term on/off	ISO and IEC flexural failure models
includeHl	1	0 or 1	-	Switch to turn ice lifting load term on/off	ISO flexural failure model
includeHp	1	0 or 1	-	Switch to turn ice pile load term on/off	ISO flexural failure model
includeHr	1	0 or 1	-	Switch to turn rubble ride-up load term on/off	ISO and IEC flexural failure models
includeHt	1	0 or 1	-	Switch to turn ice block rotation load term on/off	ISO flexural failure model
includeLc	1	0 or 1	-	Switch to turn crack length modification term on/off	ISO flexural failure model
interPeriod	-	> 1.0	s	Period of sawtooth waveform	Intermittent crushing
legAutoFactor	1	0 or 1	-	Automatically calculate the shelter factors for a multi-leg structure	All
legX#	0	None	m	X location of leg number # - need an input for each of numLegs, (0,0) is centroid	All
legY#	0	None	m	Y location of leg number # - need an input for each of numLegs (0,0) is centroid	All
loadPhase#	0	0 to 360	degrees	Phase for sinusoidal load of leg number # - need an input for each of numLegs	IEC crushing, IEC Flexural failure, ISO intermittent and lock-in crushing
minLoadFraction	-	0 to 1	-	Minimum load expressed as a fraction of the maximum load	ISO lock-in crushing
minStrength	-	0 to 1E9	Pa	Minimum ice strength in	Coupled crushing

Parameter Name	Typical Value ¹	Limits	Unit	Notes	Used by ice load type
				stress rate to strength calculation for positive tower to ice relative velocity	
minStrengthNegVel	-	0 to 1E9	Pa	Minimum ice strength in stress rate to strength calculation for negative tower to ice relative velocity	Coupled crushing
multiLegFactor_kn	0.9	0.0 to 1.0	-	Reduction in peak load to account for non-simultaneous loading of multiple legs	Lock-in crushing (IEC and ISO)
numLegs	1	1,3, or 4	-	Number of legs in support structure	All
peakLoadCOV	0.2	0.1 to 0.5	-	Coefficient of variation of peak load	ISO flexural failure model
periodCOV	-	0.1 to 0.9	-	Coefficient of variation of sawtooth waveform period	ISO flexural failure model
poissonRatio	0.3	0 to 0.5	-	Poisson's ratio	ISO flexural failure model
rampTime	10.0	>0	s	Ramp-up of forces to avoid step function and ringing	All
randomSeed	-	>0	-	Initial seed for some models	ISO flexural failure and random crushing
refIceStrength	-	0.5E6 to 50 E6	Pa	Parameter for static ice crushing load	ISO, random, and IEC crushing models
refIceThick	1	1	m	Parameter for static ice crushing load	ISO and random crushing models
rideUpThickness	2 to 3 times ice thickness	>0	m	Ice pile-up term	IEC flexural failure model
riseTime	-	0.1 to 0.9	-	Rise time for sawtooth waveform – as a fraction of the period	ISO flexural and ISO and intermittent crushing models
rubbleAngle	-	0 to 70	degrees	Angle the rubble pile makes with the horizontal	ISO flexural failure model
rubbleCohesion	0	>0	Pa	Somewhat like a breaking strength of the rubble pile	ISO flexural failure model
rubbleHeight	-	>0	m	Height of rubble pile	ISO flexural failure model
rubblePorosity	0.3	0 to 1	-	Somewhat like density of the rubble pile	ISO flexural failure model
shapeFactor_k1	-	0.1 to 1	-	Parameter for static ice crushing load	IEC crushing models
shelterFactor_ks	1	0.0 to 1.0	-	Fraction of load to be applied to legs sheltered by "up-floe" legs	All
singleLoad	0	0 or 1	-	Whether to return loads from individual legs or combined as a set of forces and a torsion	All

Parameter Name	Typical Value ¹	Limits	Unit	Notes	Used by ice load type
staticExponent	-0.16	-0.16	-	Exponent parameter for static ice crushing load	ISO and random crushing models
stdLoadMult	4	1 to 6	-	Multiplier for range of load in multiples of the stdev	Random crushing
tauMax	-	0.1 to 1	-	Maximum fraction of the sawtooth waveform period for active load change	ISO flexural failure model
tauMin	-	0.1 to 0.8	-	Minimum fraction of the sawtooth waveform period for active load change	ISO flexural failure model
timeStep	0.1	>0	s	Time step resolution of pre-calculated time series of loads	All
towerConeAngle	-	20 to 70	degrees	Angle of coned tower surface measured from horizontal	IEC and ISO flexural failure
towerDiameter	-	0.1 to 100	m	Diameter of monopole or of an individual leg	All
towerFrequency	-	0.1 to 10	Hz	Fundamental tower frequency	IEC crushing, ISO lock-in crushing
twrConeTopDiam	-	>0	m	Diameter of support structure at the top of the coned section	IEC flexural failure
waterDensity	1000	>0	kg/m ³	Density of the water	ISO flexural failure model

1 Suggested values; not assigned as default

2 Power spectral density

Table B-3 Input parameters for crushing failure models

Random Crushing (Type=1)	Intermittent Crushing (Type=2)	ISO Lock-In Crushing (Type=3)	IEC Lock-In Crushing (Type=4)	Coupled Crushing (Type=5)
randomSeed	randomSeed ¹	randomSeed ¹	randomSeed ¹	randomSeed ¹
timeStep	timeStep	timeStep	timeStep	timeStep [*]
duration	duration	duration	duration	duration ¹
rampTime	rampTime	rampTime	rampTime	rampTime
iceThickness	iceThickness	iceThickness	iceThickness	iceThickness
iceVelocity	iceVelocity	iceVelocity	iceVelocity	iceVelocity
iceDirection	iceDirection	iceDirection	iceDirection	iceDirection
refIceStrength	refIceStrength	refIceStrength	refIceStrength	refIceStrength
numLegs	numLegs	numLegs	numLegs	numLegs
towerDiameter	towerDiameter	towerDiameter	towerDiameter	towerDiameter
		towerFrequency	towerFrequency	
iceType	iceType	iceType	iceType	iceType
refIceThick	refIceThick	refIceThick	shapeFactor_k1	minStrengthNegVel
staticExponent	staticExponent	staticExponent	contactFactor_k2	minStrength
coeffPSD_b	interPeriod	riseTime		
coeffPSD_ks	riseTime	minLoadFraction		
crushLoadCOV	fallTime			
stdLoadMult				
freqStep				

¹ These parameters are not used by the specified model but are required for code compatibility.

Table B-4 Input parameters for flexural failure models

ISO Flexural Failure (Type=6)	IEC Flexural Failure (Type=7)
randomSeed	randomSeed*
timeStep	timeStep
duration	duration
rampTime	rampTime
iceThickness	iceThickness
iceVelocity	iceVelocity
iceDirection	iceDirection
flexStrength	flexStrength
iceModulus	
iceDensity	iceDensity
waterDensity	
numLegs	numLegs
towerDiameter	towerDiameter
towerConeAngle	towerConeAngle
rubbleHeight	twrConeTopDiam
ice2twrFriction	ice2twrFriction
iceType	iceType
rubblePorosity	rideUpThickness
rubbleCohesion	freqParamK
rubbleAngle	
frictionAngle	
ice2iceFriction	
poissonRatio	
peakLoadCOV	
coeffLoadPeaks	
coeffLoadMin	
periodCOV	
tauMin	
tauMax	
riseTime	
coeffBreakLength	
includeHb	includeHb
includeHr	includeHr
includeHp	
includeHI	
includeHt	
includeLc	

For multi-leg structures the parameters in Table B-5 apply for all ice load types except as noted.

Table B-5 Input parameters required for multi-leg models

legXN (one value for each leg, N=1,2,...)
legYN (one value for each leg)
shelterFactor_ksN (one value for each leg)
loadPhaseN
singleLoad
legAutoFactor
multiLegFactor_kn (Lock-In only)

5. Code structure

The following is a description of the code structure for use when attempting to understand and/or modify the code. IceFloe is written compliant with the 2003 version of the Fortran standard. The IceFloe code is set up as a number of Fortran modules with a building block approach since many of the ice load models use common variables and calculations but not all models use all of these. The modules call initialization and update functions in a cascading fashion as shown in Figure B-6 and Figure B-7. Note that the coupled crushing output routine does not use the standard output routine since it uses state information from the structure at each time step.

With the exception of the coupled crushing model, the load time series is pre-calculated in the initialization routine and interpolated with respect to time at each call to the update routine. It is noted that the coupled crushing output routine does not use the base routine since it uses state information from the structure at each time step.

Intel(R) Visual Fortran Compiler XE 14.0.0.103 [IA-32] with Visual Studio 2008 standard edition were used for compiling and linking of the code.

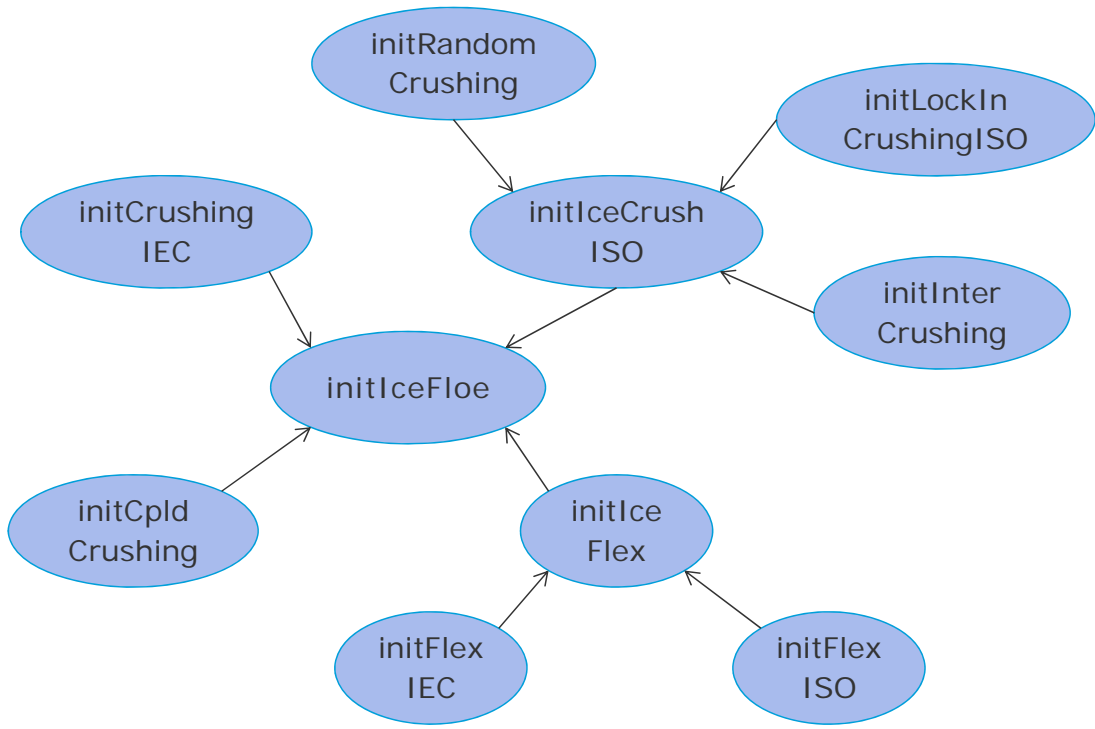


Figure B-6 Initialization hierarchy

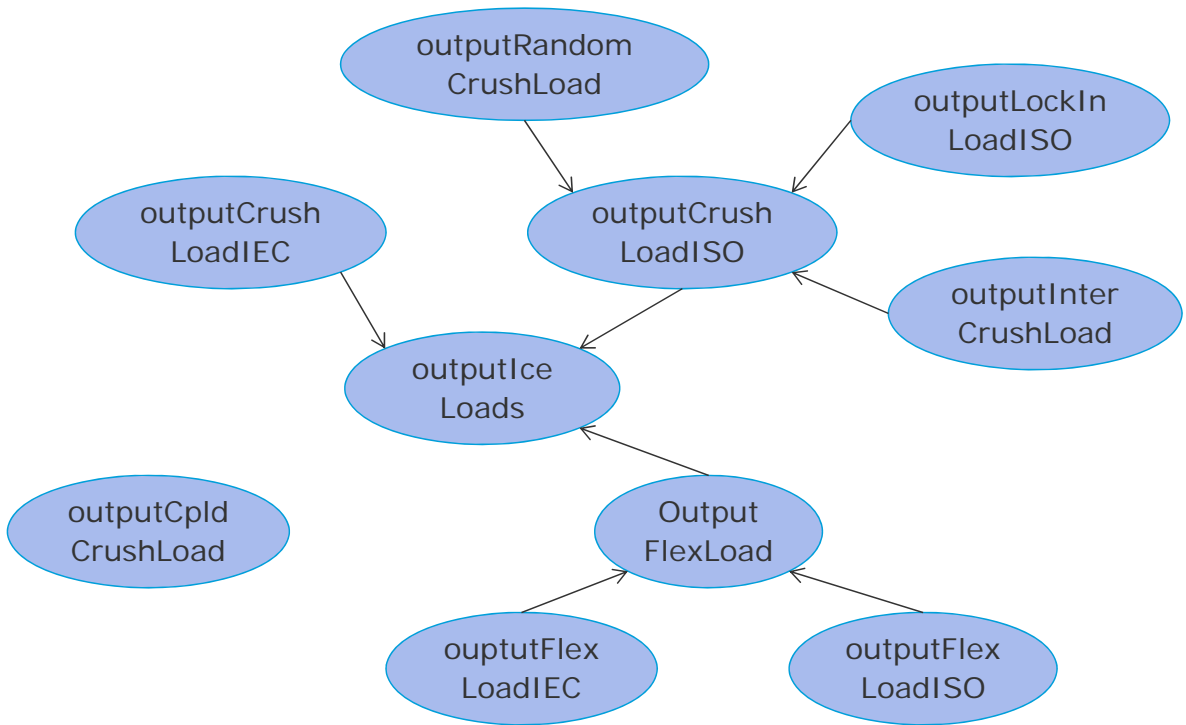


Figure B-7 Update hierarchy



5.1. Interface to other programs

In addition to the integration into FAST, interface examples are provided in the code distribution for HAWC2, Bladed, and ADAMS. For other codes the interface must be written by the user. The following are included in the distribution from the NWTC web site and can be used as examples:

- IceFloe.f90 (FAST testing);
- IceFloe.f90 for the console;
- IceFloeBladed.f90;
- HAWC2_DLL.f90; and
- IceADAMS_VFOSUB.f90.

These routines include examples of initialization and update routines.

APPENDIX C – EXAMPLE ICEFLOE INPUT FILE

```
! Sample input parameters for IceFloe
!
! Model selection and general inputs
!
timeStep          0.10
duration          600.0
randomSeed        123
rampTime          30.0
!
! General ice property inputs
!
iceThickness      0.7
iceVelocity       0.20
iceDirection      0.0
refIceStrength    1800000.0
flexStrength      800000.0
iceModulus        5500000000.0
iceDensity        927.6
waterDensity      999.0
!
! Tower configuration inputs
!
numLegs           1.0
towerDiameter     6.0
towerFrequency    0.28
towerConeAngle    55.0
rubbleHeight      1.75
twrConeTopDiam    6.00
singleLoad        1
shelterFactor_ks  0.0
!
! Inputs common to loading by ice flexural failure
!
ice2twrFriction   0.15
includeHb         1
includeHr         1
!
! Inputs for ice flexural failure via ISO method (Croasdale)
!
iceType           6
rubblePorosity    0.3
rubbleCohesion    0.0
rubbleAngle       40.0
```



frictionAngle	45.0
ice2iceFriction	0.05
poissonRatio	0.30
peakLoadCOV	0.20
coeffLoadPeaks	0.56
coeffLoadMin	0.10
periodCOV	0.50
tauMin	0.40
tauMax	0.60
riseTime	0.80
coeffBreakLength	4.0
includeHp	1
includeHl	1
includeHt	1
includeLc	1

APPENDIX D – EXAMPLE ICEFLOE OUTPUT FILE

When IceFloe is run integrated with FAST or other codes that allow for direct coupling the outputs depend on what is allowed by that code and selected by the user. When run as a standalone code IceFloe produces a time series of loads. In either cases a log file is written that will contain an echo of the inputs, version and date information, as well as any warning or error messages.

EXAMPLE LOG FILE:

Running: IceFloev1.00.00May-2014

This run started on: 16-Jun-2014 at 20:37:06

***** WARNING *****

IceFloe_init: Gravity in FAST is different than gravity in iceFloe by $-3.35026E-03$ m/s².

Parameter input file read finished.

Load time series length = 600 sec

Load ramp up time = 5 sec

Setting common ice flow input parameters

Ice type = 6

Ice thickness = 0.7 meters

Ice velocity = 0.2 m/s

Ice direction = 0 degrees

Time step = 0.1 sec

Tower diameter = 6 meters

Random seed = 123

Setting common flexural failure input parameters

flexStrength = $8.00000E+05$ Pascals

towerConeAngle = 55 degrees

ice2twrFriction = 0.15

iceDensity = 927.6 kg/m³

Breaking term, Hb term is included

Rubble pushing term, Hr term is included

Setting up flexural failure by ISO/Croasdale method

Based on the ISO 19906 standard equations for max static loads

peakLoadCOV = 0.2 (-)

coeffLoadPeaks = 0.56

coeffLoadMin = 0.1

periodCOV = 0.5

tauMin = 0.4

```

tauMax = 0.6
riseTime = 0.8
coeffBreakLength = 4
rubbleHeight = 1.75 meters
rubblePorosity = 0.3
rubbleCohesion strength = 0 Pascals
rubbleAngle = 40 degrees
frictionAngle = 45 degrees
ice2iceFriction = 5.00000E-02
waterDensity = 999 kg/m^3
iceModulus = 5.50000E+09 Pascals
poissonRatio = 0.3
Including pile up term, Hp
Including rubble lifting term, Hl
Including block rotation term, Ht
Including crack lenght modification term, Lc
** Pile up term, Hp = 593.25 Newtons
** Rubble lifting term, Hl = 43825 Newtons
** Block rotation term, Ht = 31397 Newtons
** Rubble push through term, Hr = 1.68501E+05 Newtons
** Breaking load term, Hb = 8.80005E+05 Newtons
** Maximum static load for flexural failure = 1.17809E+06 Newtons

```

ISO/Croasdale ice flexural failure loads initialized

IceFloe run complete on: 16-Jun-2014 at 21:18:29

EXAMPLE TIME SERIES FILE FROM FAST (other channels have been removed)

Predictions were generated on 16-Jun-2014 at 20:37:06 using FAST (v8.07.00b-bjj, 15-May-2014), compiled for 32-bit systems using single precision
linked with NWTc Subroutine Library (v2.03.00d-bjj, 22-Jan-2014); ElastoDyn (v1.01.06a-bjj, 2-May-2014); InflowWind (v2.00.01a-bjj, 22-Jan-2014); AeroDyn (v14.02.01b-bjj, 29-Jan-2014); ServoDyn (v1.01.02a-bjj, 31-Jan-2014); HydroDyn (v2.00.05c-gjh, 15-May-2014); SubDyn (v1.00.00c-bjj, 20-May-2014); IceFloe (v1.00.00, May-2014)

Description from the FAST input file: FAST Certification Test #19: NREL 5.0 MW Baseline Wind Turbine with Monopile RF Configuration, for use in offshore analysis

Time	VxTwrIce	VyTwrIce	IceLoadFx	IceLoadFy
(s)	m/s	m/s	kN	kN
0.0000	0.000E+00	0.000E+00	0.000E+00	0.000E+00

0.0200	-4.241E-04	-6.611E-05	4.796E-01	0.000E+00
0.0400	-1.467E-03	-7.901E-04	9.759E-01	0.000E+00
0.0600	-1.589E-03	-2.571E-03	1.489E+00	0.000E+00
0.0800	8.172E-04	-4.125E-03	2.019E+00	0.000E+00
0.1000	4.322E-03	-3.129E-03	2.565E+00	0.000E+00
0.1200	5.706E-03	1.338E-03	3.128E+00	0.000E+00
0.1400	4.918E-03	8.054E-03	3.708E+00	0.000E+00
0.1600	3.510E-03	1.500E-02	4.305E+00	0.000E+00
0.1800	1.553E-03	2.028E-02	4.918E+00	0.000E+00
0.2000	-1.515E-03	2.205E-02	5.548E+00	0.000E+00
0.2200	-4.904E-03	1.934E-02	6.195E+00	0.000E+00
0.2400	-6.603E-03	1.322E-02	6.859E+00	0.000E+00
0.2600	-5.901E-03	6.289E-03	7.539E+00	0.000E+00
0.2800	-4.133E-03	7.485E-04	8.236E+00	0.000E+00
0.3000	-2.754E-03	-2.656E-03	8.950E+00	0.000E+00
0.3200	-1.354E-03	-4.199E-03	9.680E+00	0.000E+00
0.3400	4.624E-04	-4.736E-03	1.043E+01	0.000E+00
0.3600	1.684E-03	-5.638E-03	1.119E+01	0.000E+00
0.3800	1.928E-03	-8.075E-03	1.197E+01	0.000E+00
0.4000	1.823E-03	-1.193E-02	1.277E+01	0.000E+00
0.4200	2.878E-03	-1.591E-02	1.358E+01	0.000E+00
0.4400	4.976E-03	-1.874E-02	1.441E+01	0.000E+00
0.4600	7.200E-03	-1.993E-02	1.526E+01	0.000E+00
0.4800	9.028E-03	-1.962E-02	1.613E+01	0.000E+00
0.5000	1.077E-02	-1.830E-02	1.701E+01	0.000E+00
0.5200	1.165E-02	-1.673E-02	1.790E+01	0.000E+00
0.5400	1.080E-02	-1.550E-02	1.882E+01	0.000E+00
0.5600	8.278E-03	-1.432E-02	1.975E+01	0.000E+00
0.5800	5.090E-03	-1.205E-02	2.070E+01	0.000E+00
0.6000	2.567E-03	-7.709E-03	2.166E+01	0.000E+00
0.6200	7.040E-04	-1.215E-03	2.264E+01	0.000E+00
0.6400	-6.817E-04	6.665E-03	2.364E+01	0.000E+00
0.6600	-7.357E-04	1.454E-02	2.466E+01	0.000E+00
0.6800	2.915E-04	2.070E-02	2.569E+01	0.000E+00
0.7000	1.685E-03	2.372E-02	2.674E+01	0.000E+00
0.7200	2.944E-03	2.323E-02	2.780E+01	0.000E+00
0.7400	3.931E-03	2.004E-02	2.888E+01	0.000E+00
0.7600	5.177E-03	1.552E-02	2.998E+01	0.000E+00
0.7800	6.570E-03	1.085E-02	3.110E+01	0.000E+00
0.8000	8.129E-03	6.717E-03	3.223E+01	0.000E+00
0.8200	9.790E-03	3.263E-03	3.338E+01	0.000E+00
0.8400	1.183E-02	9.287E-05	3.454E+01	0.000E+00
0.8600	1.432E-02	-3.330E-03	3.572E+01	0.000E+00

0.8800	1.617E-02	-7.123E-03	3.692E+01	0.000E+00
0.9000	1.672E-02	-1.079E-02	3.814E+01	0.000E+00
0.9200	1.599E-02	-1.360E-02	3.937E+01	0.000E+00
0.9400	1.417E-02	-1.504E-02	4.062E+01	0.000E+00
0.9600	1.152E-02	-1.500E-02	4.188E+01	0.000E+00
0.9800	8.217E-03	-1.388E-02	4.317E+01	0.000E+00
1.0000	4.720E-03	-1.244E-02	4.446E+01	0.000E+00
...				
599.0000	-3.605E-03	2.573E-04	1.178E+02	0.000E+00
599.0200	-3.264E-03	2.673E-04	1.178E+02	0.000E+00
599.0400	-2.441E-03	2.199E-04	1.178E+02	0.000E+00
599.0600	-1.316E-03	1.461E-04	1.178E+02	0.000E+00
599.0800	-3.486E-04	9.687E-05	1.178E+02	0.000E+00
599.1000	3.012E-04	1.130E-04	1.178E+02	0.000E+00
599.1200	8.874E-04	1.826E-04	1.178E+02	0.000E+00
599.1400	1.421E-03	2.740E-04	1.178E+02	0.000E+00
599.1600	1.726E-03	3.202E-04	1.178E+02	0.000E+00
599.1800	1.980E-03	2.637E-04	1.178E+02	0.000E+00
599.2000	2.107E-03	9.784E-05	1.178E+02	0.000E+00
599.2200	2.219E-03	-1.311E-04	1.178E+02	0.000E+00
599.2400	2.468E-03	-3.434E-04	1.178E+02	0.000E+00
599.2600	2.329E-03	-4.678E-04	1.178E+02	0.000E+00
599.2800	1.863E-03	-4.701E-04	1.178E+02	0.000E+00
599.3000	1.378E-03	-3.669E-04	1.178E+02	0.000E+00
599.3200	8.986E-04	-2.083E-04	1.178E+02	0.000E+00
599.3400	1.581E-04	-7.423E-05	1.178E+02	0.000E+00
599.3600	-6.475E-04	-4.272E-06	1.178E+02	0.000E+00
599.3800	-1.089E-03	4.273E-06	1.178E+02	0.000E+00
599.4000	-1.332E-03	1.351E-05	1.178E+02	0.000E+00
599.4200	-1.521E-03	7.145E-05	1.178E+02	0.000E+00
599.4400	-1.661E-03	2.174E-04	1.178E+02	0.000E+00
599.4600	-1.893E-03	4.448E-04	1.178E+02	0.000E+00
599.4800	-1.909E-03	6.846E-04	1.178E+02	0.000E+00
599.5000	-1.806E-03	8.605E-04	1.178E+02	0.000E+00
599.5200	-1.737E-03	9.081E-04	1.178E+02	0.000E+00
599.5400	-1.598E-03	8.183E-04	1.178E+02	0.000E+00
599.5600	-1.274E-03	6.355E-04	1.178E+02	0.000E+00
599.5800	-8.535E-04	4.384E-04	1.178E+02	0.000E+00
599.6000	-3.121E-04	2.784E-04	1.178E+02	0.000E+00
599.6200	-4.755E-05	1.761E-04	1.178E+02	0.000E+00
599.6400	1.184E-04	1.027E-04	1.178E+02	0.000E+00
599.6600	4.029E-04	-9.351E-06	1.178E+02	0.000E+00
599.6800	3.374E-04	-1.895E-04	1.178E+02	0.000E+00

599.7000	1.408E-04	-4.421E-04	1.178E+02	0.000E+00
599.7200	-3.304E-04	-6.959E-04	1.178E+02	0.000E+00
599.7400	-7.568E-04	-8.635E-04	1.178E+02	0.000E+00
599.7600	-1.249E-03	-8.761E-04	1.178E+02	0.000E+00
599.7800	-1.743E-03	-7.127E-04	1.178E+02	0.000E+00
599.8000	-2.071E-03	-4.196E-04	1.178E+02	0.000E+00
599.8200	-1.979E-03	-9.791E-05	1.178E+02	0.000E+00
599.8400	-1.797E-03	1.661E-04	1.178E+02	0.000E+00
599.8600	-1.614E-03	3.269E-04	1.178E+02	0.000E+00
599.8800	-1.510E-03	3.999E-04	1.178E+02	0.000E+00
599.9000	-1.184E-03	4.357E-04	1.178E+02	0.000E+00
599.9200	-6.765E-04	4.982E-04	1.178E+02	0.000E+00
599.9400	-2.600E-04	6.141E-04	1.178E+02	0.000E+00
599.9600	1.334E-04	7.654E-04	1.178E+02	0.000E+00
599.9800	8.603E-04	8.912E-04	1.178E+02	0.000E+00
600.0000	1.600E-03	9.272E-04	1.178E+02	0.000E+00



ABOUT DNV GL

Driven by our purpose of safeguarding life, property and the environment, DNV GL enables organizations to advance the safety and sustainability of their business. We provide classification and technical assurance along with software and independent expert advisory services to the maritime, oil and gas, and energy industries. We also provide certification services to customers across a wide range of industries. Operating in more than 100 countries, our 16,000 professionals are dedicated to helping our customers make the world safer, smarter, and greener.